Concrete Masonry Compressive Strength Prediction using Mechanics-based Modelling and Gaussian Process Regression with Error Evaluation based on Experimental Data

by

Wanyan Liu

A thesis submitted in partial fulfillment of the requirements for the degree of

Master of Science

in

STRUCTURAL ENGINEERING

Department of Civil and Environmental Engineering
University of Alberta

ABSTRACT

The compressive strength of masonry is an essential mechanical parameter considering its influence on structural design. Among different types of masonry, hollow concrete block masonry is the most commonly used one in North America. Over the past decades, various methods were developed to determine the compressive strength of hollow concrete block masonry, namely the physical prism testing method and the empirical method (i.e., unit strength method). Regarding the physical prism testing method, the variations and uncertainties in the testing programs lead to a need for a tool that can be used to understand the effects of different factors on masonry strength prediction. Meanwhile, the unit strength method adopted by North American masonry design standards/codes is based on research that is now outdated. Therefore, tools or models that can effectively achieve the goal of accurately predicting the compressive strength as well as the behaviour of hollow concrete block masonry need to be developed.

In this study, an automated micro-nonlinear finite-element model, using one of the most popular hard-computing techniques, is first proposed and verified to simulate the behaviour of hollow concrete block masonry prisms. Different masonry design standards/codes as well as empirical models are reviewed and compared with the proposed finite-element model over the collected experimental database. After an extensive literature review, a large database is compiled based on existing experimental studies. A global variance-based sensitivity analysis for evaluating the effect of material parameters on masonry compressive strength is then conducted based on the developed finite-element model, in which Latin hypercube sampling technique and Polynomial chaos expansions technique are adopted. Six input parameters are considered. The results show that the compressive strength of concrete masonry units is the most influential parameter, while the other

parameters have different levels of impact depending on the compressive strength combinations of concrete masonry units and mortar.

Subsequently, the experimental database previously compiled is used for developing a Gaussian Process Regression model (soft-computing model) to predict the compressive strength of hollow concrete block masonry. The whole database is divided into two groups based on mortar type (e.g., Type S, Type N), and Gaussian Process Regression models are built upon each type. A parametric study based on different covariance functions is carried out and the optimal covariance functions are selected based on mortar type. A case study based on different input parameters is also conducted and three input parameters are selected for both mortar types. The same masonry design standards/codes, which were used to compare with the finite-element model, are compared with the proposed Gaussian Process Regression model. The results indicate that the proposed Gaussian Process Regression model can provide a more accurate and reliable prediction for the compressive strength of hollow concrete block masonry, with prediction error quantified. After the proposed Gaussian Process Regression model is validated through its comparison with other models, prescribed hollow concrete block masonry compressive strength values are re-evaluated. The results indicate that the current prescribed values need to be updated and new values are proposed.

ACKNOWLEDGEMENTS

I would like to acknowledge and give my most sincere thanks to my supervisor Dr. Yong Li first. Without his help and guidance, this work presented here would not have existed.

I would also like to acknowledge the financial support provided by the Natural Sciences and Engineering Research Council (NSERC) in Canada through the Collaborative Research and Development (CRD) Grants (CRDPJ 528050-18). The financial support provided is greatly appreciated.

Special thanks go to Dr. Carlos Cruz-Noguez for introducing me to the field of masonry research and serving on my exam committee, and my other exam committee members, Dr. Victor Liu, and Dr. Nuobo Maeda. I would also like to acknowledge the help and support from my colleague, a Ph.D. student working in the same research group, Bowen Zeng, especially at the initial stage of this work.

Last but not least, I would like to thank all the family members and friends who have always been there along the journey—especially my husband and my parents, who are my biggest and strongest support.

TABLE OF CONTENTS

LIST OF TABLES

LIST OF FIGURES

CHAPTER 1: INTRODUCTION

1.1 Background

As one of the oldest construction materials, masonry has a history of over 6000 years. Masonry is commonly used for all types of structures, ranging from ancient structures like the Egyptian pyramids and Rome Colosseum to all the fascinating modern masonry buildings. Besides being aesthetically pleasing, masonry structures also have the advantages of durability, excellent thermal properties (ACI/TMS 122R-14) and most importantly, excellent properties under compression.

The compressive strength of hollow concrete masonry, which is the most commonly used one in North America, is essential for analyzing and designing masonry structures. However, its accurate prediction remains a challenging task due to inherent randomness in the composite materials as well as the uncertainties in physical prism testing. The prediction accuracy is of interest to engineers acknowledging the aphorism that all models are wrong. In the past decades, significant research efforts have been devoted in the literature. In engineering practice, two primary ways of determining the compressive strength of masonry are (1) the physical prism testing method in the laboratory or construction field and (2) the unit strength method derived empirically based on experimental testing of prisms.

As for the unit strength method, the current values listed in CSA S304-14 for hollow concrete masonry were based on the research work conducted by Maurenbrecher in the 1980s (Maurenbrecher 1980, 1983, 1985, 1986), which was developed from a linear regression analysis between the compressive strength of concrete units and the compressive strength of masonry prisms and were proved to be unduly conservative (Ip, 1999; Korany and Glanville, 2005; National Concrete Masonry Association 2008 as cited in Ross 2013). Nowadays, a much more developed database of the behaviour of masonry under compression has been formed compared to when those prescribed values were first introduced.

On the other hand, acknowledging variations in the physical prism testing methods and uncertainty in testing conditions in different experimental programs, there is a need for a tool that can be used for understanding the effects of various factors and uncertainties on mechanical behaviour or masonry strength prediction. Therefore, different computational methods (i.e., hard-computing

based on mechanics or soft-computing based on data like using machine-learning algorithms) were adopted in various research studies in the past decades as an alternative approach to determine the compressive strength of masonry or masonry assemblages/prisms.

1.2 Problem Statement

The compressive strength of masonry is a parameter that appears in multiple masonry design equations (i.e., flexural, shear and axial capacity design provisions). Although the compressive strength of masonry is a crucial characteristic when it comes to masonry design, the currently adopted unit strength method by the Canadian design standard CSA S304-14 was reported to be overly conservative in multiple studies (Ip, 1999; Korany and Glanville, 2005; National Concrete Masonry Association 2008 as cited in Ross 2013) and its level of conservatism (e.g., model accuracy) needs to be quantified for later use of reliability analysis for masonry structures. The importance of the compressive strength of masonry leads to the need for re-evaluating the prescribed values based on the unit strength method in the current design standard, and calls for a comprehensive study that can provide a more accurate and reliable prediction (i.e., accuracy and dispersion). This defines the main problem to be addressed in this thesis. Additionally, the compressive strength of masonry is often linked to the compressive strength of hollow masonry prisms via the height-to-thickness correction factors, for example, as prescribed in CSA S304-14. This needs to be re-evaluated as well.

1.3 Objectives and Methodology

Several studies have been carried out on the behaviour of hollow concrete masonry prisms under compression, and different computing methods have been proposed as an alternative approach for strength prediction. In response to physic prism testing and the unit strength method used in design standards, both hard computing (HC) and soft computing (SC) techniques can be adopted for the purposes of predicting the compressive strength of masonry. This leads to a need to develop reliable and alternative methods to predict the compressive strength of masonry or masonry prisms and assess the accuracy of compressive strength predictions.

Hard computing solutions (i.e., numerical models) are complicated due to their requirements for a series of constitutive models and the corresponding model parameters in order to describe the

failure mechanisms. However, hard computing solutions are usually more straightforward to analyze and their behaviour and stability are more predictable. These characteristics are essential in engineering designs. Hard computing has conventional intelligence and requires an analytical model. Therefore, it generally requires prewritten programs and thus acts on a fixed set of instructions. Hard computing needs predefined instructions and does not work beyond those lines. Its principle relies on certainty and flexibility.

On the other hand, the traditional soft computing solutions (i.e., data-based empirical models) developed could be negatively affected in accuracy (bias) and precision (scatter) due to the lack of systematic design of all those experiments used for the utilized database, as well as the inherent experimental uncertainties. However, artificial intelligence methods as a new form of soft-computing technique have been introduced to solve the problem. It differs from conventional hard computing in the sense that, unlike hard computing, artificial intelligence models are strongly based on intuition or subjectivity. Artificial intelligence methods are a new and modern approach that approximates systems. Therefore, artificial intelligence methods provide an attractive opportunity to represent the certitude that the human mind has the capability to store and process information that is imprecise and lacks certainty. In the current scenario, artificial intelligence methods have been developed in various domains as it solves the problem associated with current technology.

This study aims to construct prediction models for the compressive strength of hollow concrete masonry and to investigate compressive strength prediction errors. To achieve this goal, both HC and SC techniques are used to develop masonry prisms strength prediction models, and the accuracy will be assessed using the compiled experimental data. The methodology adopted is detailed as follows.

First, this study developed an automated numerical prism testing tool for hollow concrete masonry prism based on a 3D detailed mechanics-based FE model (HC method), which can further be used as a strength prediction model and for uncertainty analysis. The proposed FE model is first validated based on the experimental tests carried out by Barbosa et al. (Barbosa et al. 2009) and Mohammad et al. (Mohammad et al. 2017) in terms of stress-strain behaviour and/or damage

patterns, together with parametric studies to verify the importance of relevant micro model parameters on the masonry compressive strength prediction. After the validation, the tool developed is applied to numerical masonry prism testing of 312 groups of hollow concrete masonry prisms collected from 40 literature, including 1427 specimens in total. The accuracy in strength prediction through numerical prism testing is compared with the experimental data, together with the predictions from empirical formulas and masonry design code models. The height-to-thickness correction factors of masonry are subsequently re-evaluated. Using the tool developed for automatic numerical prism testing, the variance-based global sensitivity analysis is performed for masonry strength based on the Polynomial chaos expansion (PCE) technique, investing the influence of multiple input material property variance on the output masonry compressive strength variance.

Second, this study constructed Gaussian Process Regression (GPR) models (SC method) for the purpose of predicting the compressive strength of hollow concrete block masonry based on the aforementioned extensive experimental database. The correlation between unit compressive strength and prism compressive strength is re-evaluated because the design code proposed method, namely the prescribed values given by the current Canadian Masonry Design Standard CSA S304-2014, is based on outdated experimental studies.

To sum up, this study aims to: (1) utilize both HC and SC methods to develop accurate and reliable models that can be used to predict the compressive strength of masonry and (2) use the experimental database compiled to quantify their prediction errors and evaluate other existing methods.

1.4 Organization of Thesis

The thesis introduction, including background, problem statement, objectives and methodology, are introduced in Chapter 1. A literature review of the related literature on different aspects or methods regarding the compressive behaviour of hollow concrete block (HCB) masonry assemblages is presented in Chapter 2. Chapter 3 summarizes the detailed information on the automatic masonry prism testing for compressive strength prediction and its uncertainty analysis based on hard-computing techniques. Prediction and re-evaluation of masonry compressive

strength based on soft-computing techniques (e.g., GPR) is discussed in Chapter 4. Finally, the conclusions and recommendations are presented in Chapter 5.

CHAPTER 2: LITERATURE REVIEW

2.1 Introduction

The popularity of masonry structures can be attributed to their attractive aesthetics, excellent durability, high thermal performance (ACI/TMS 122R-14), and more importantly, great mechanical properties under compression. Among various masonry types, hollow concrete block masonry has been widely used in North America. The compressive strength of masonry is an essential mechanical property considering its important role in masonry structural design; its prediction accuracy and precision (i.e., uncertainty) affects the reliable and economical design of masonry walls. Therefore, various studies related to the compressive strength of masonry have been conducted during the past few years. Relevant work is reviewed in this chapter regarding physical testing (e.g., prism testing) in the laboratory, existing models adopted in design codes/standards (e.g., unit strength method), empirical-analytical models developed by researchers in the literature, mechanics-based finite-element models, and data-based surrogate models. Moreover, relevant work on the accuracy assessment and sensitivity study related to compressive strength prediction is also discussed. Note that a more detailed literature review, specialized for the topics in Chapter 3 and Chapter 4, is provided later in this thesis.

2.2 Physical Prism Testing in Experimental Programs

In general, the physical prism testing method requires testing on a number of prism specimens, which are usually constructed using multiple masonry units and mortar layers. The testing strength is then adjusted with a height-to-thickness correction factor, which is mainly to account for the limitation in the physical testing methods, i.e., the restraint effects of prism ends due to machine platens (CSA S304-14). During the test, masonry prism specimens are typically placed between two planks to help reduce the confinement effect of the loading machine (i.e., Khalaf 1996; Fortes et al. 2015; Ross 2013; Sarangapani et al. 2005). Capped masonry prism and the failure mechanism of masonry prisms (Fortes et al. 2013) are presented in Figure 2-1. A large number of experimental works have been conducted to study the compressive strength of masonry prisms, the height-to-thickness correction factors, and/or the compressive strength of masonry.

Barbosa (2009) tested hollow concrete block masonry prisms constructed with four different combinations of unit/mortar compressive strength. Cheema and Klingner (1984) tested 11 hollow

concrete prisms, and the experimental results were then used to calibrate linear finite element models. Drysdale and Hamid (1979) carried out an experimental study on both grouted and hollow concrete block masonry. Results indicated that a three-and-a-half-course prism could represent the failure behaviour similar to that for masonry walls. Khalaf et al. (1994) conducted an experimental investigation of a total of 57 specimens which consisted of both hollow and grouted concrete masonry prisms. Results indicated that the compressive strength of masonry was best evaluated by testing three-course high prisms. Another experimental program was carried out by Khalaf (1996), in which a total of 60 hollow and grouted prism specimens were tested. Maurenbrecher (1980, 1983, 1985, 1986) carried out extensive research on the compressive strength of hollow concrete block masonry and the results were used to develop the prescribed values in Table 4 of CSA S304-14. Ramamurthy et al. (2000) tested 306 hollow concrete block masonry constructed with both two-core units and three-core units. Sarhat and Sherwood (2014) carried out an experimental program on concrete block masonry assemblages, including both prisms and wallets. A total of 248 average compressive strength values were collected, which consisted of 1092 individual prisms. Liu (2012) tested a total of 78 prisms, including hollow concrete block prisms. Results indicated that the compressive strength decreases when the height-to-thickness ratio of prisms increases from two to five. Also, bond type and mortar joint type have an insignificant effect on concrete masonry compressive strength. More experimental tests of masonry prisms can be found in Appendix A, where some experimental data were compiled for analytical model development.

Figure 2-1: Capped masonry prism and failure of masonry prisms (Fortes et al. 2015)

2.3 Methods in Masonry Design Codes/Standards

A detailed comparison of the physical prism testing methods in the four different international standards/codes (i.e., CSA S304-14 (2014), TMS 402/602-16 (2016), Eurocode 6-2005 (2005) and AS 3700-2017 (2017)) is summarized in Table 2-1.

Table 2-1: The comprehensive overview of four masonry design standards/codes in the physical prism testing for determining concrete masonry strength

	CSA S304-14	TMS 402/602	Eurocode 6	AS 3700
Height-to-thickness ratio (*h/t*)	Close to 5	1.3-5	3-15	2-5
Number of courses	≥2	≥2	-	≥3
Correction factor	0.85-1.00	0.75-1.22	-	0.78-1.00
Reference case (*h/t*)	5.0	2.0	-	5.0
Bonding pattern	Stack/running	Stack	Stack/running	Stack
Planks	Hard	Sulfur/gypsum	Gypsum	Plywood
Bedding type	Face-shell/full	Full	Full	Face-shell
Number of specimens	5 or more	3	3 or more	3 or more
Calculation area	Effective cross-sectional area	Net mortar bedded area	Prism net area	Mortar bedded area
Post-processing	5^{th} percentile value	Mean value	5^{th} percentile value	Mean value

As seen from Table 2-1, a minimum of 2 or 3 courses is required, together with a requirement on the height-to-thickness ratio for the prism specimen. The same stack pattern as in the walls is suggested by all design codes; however, it is worth mentioning that stack pattern can be used even if it is not used in the wall. At least three specimens with face-shell bedding and/or full bedding are required to be tested in general, except for CSA S304-14, which requires at least five prism specimens. In prism compressive strength calculation, the mortar bedding area (i.e., effective cross-sectional area or the net area for full-bedding) is used. Different post-processing methods are adopted by different design standards/codes. A height-to-thickness correction factor greater than 1.0 is adopted by TMS 402/602 when the prism *h/t* is greater than 2.0. No correction is needed by Eurocode 6, as well as CSA S304 and AS 3700 when the prism *h/t* is greater than 5.0. Based on the tested specimens, the average value (mean) is used for TMS 402/602 and AS 3700, while a low percentile (e.g., 5^{th} percentile determined as 1.64 standard deviation below the mean) is used

as the specified or characteristic value for CSA S304-14 (CSA S304-14) and Eurocode 6 (BS EN 772-1-2011).

2.3.1 CSA S304.1-14

Two primary ways of determining the compressive strength of masonry are the prism testing method and the unit strength method, as mentioned in the current Canadian masonry design standards CSA S304.1-14. In the prism testing method, the specified compressive strength of masonry is determined by testing five or more small masonry specimens (prisms) and calculating the 5th percentile, determined as 1.64 standard deviation below the mean when under the Gaussian distribution assumption. The 5th percentile value is calculated as follows:

$$f_{m,5th}^{'} = \mu - 1.64 \times \sigma \qquad \text{(Eq. 2-1)}$$

The unit strength method, as the name indicates, prescribes the specified compressive strength of masonry in a table format based on unit strength and mortar type. The current version CSA S304.1-14 modified the prescribed values from the previous versions with a lower upper limit of the unit strength of 30 MPa instead of 40 MPa. The prescribed values for ungrouted hollow concrete masonry in CSA S304.1-14 are listed in Table 2-2:

Table 2-2: Prescribed compressive strength for ungrouted hollow concrete masonry in CSA S304.1-14

Net area specified compressive strength of unit (MPa)	Concrete masonry compressive strength (MPa)	
	Type S Mortar	Type N Mortar
10	6.5	6
15	10	8
20	13	10
30 or more	17.5	12

Note that linear interpolation may be used for other values of the compressive strength of the unit. For concrete units with a specified compressive strength greater than 30 MPa, the masonry compressive strength can also be determined by the physical prism testing method instead of the unit strength method according to CSA S304.1-14 - Clause 5.1.2.

2.3.2 TMS 402/602-16

Both the unit strength method and prism testing method are adopted by the American masonry design standard TMS 402/602-16. As for the prism testing method, the compressive strength of masonry is determined by calculating the mean prism strength based on three specimens and then corrected by the height-to-thickness correction factor specified in TMS 402/602-16. The prescribed values (TMS 402/602-16) are developed based on the test results collected from decades ago and since then, studies (NCMA 2012) about maximizing the usage of concrete unit strength have been carried out. Compared to the prescribed values of masonry compressive strength proposed by the CSA S304.1-14, TMS 402/602-16 suggested some higher values of masonry compressive strength when it comes to the same concrete masonry units; one of the reasons causing this is the prescribed values are mean values, while in CSA S304.1-14 5th percentile is used. The prescribed values for ungrouted hollow concrete masonry in TMS 402/602-16 are listed in Table 2-3:

Table 2-3: Prescribed compressive strength for ungrouted hollow concrete masonry in TMS 402/602-16

Net area compressive strength of concrete masonry (MPa)	Net area compressive strength of concrete masonry unit (MPa)	
	Type S or M Mortar	Type N Mortar
11.72	-	13.10
13.10	13.10	14.82
13.79	13.79	18.27
15.51	17.93	23.44
17.24	22.41	28.96
18.96	26.89	-
20.69	31.03	-

2.3.3 Eurocode 6-2005

Eurocode 6-2005 for the design of masonry structures in Europe proposes using the following equation to calculate the compressive strength of masonry:

$$f_m^{'} = K f_b^{\alpha} f_m^{\beta} \quad \text{(Eq. 2-2)}$$

where $f_m^{'}$ is the characteristic compressive strength of masonry in MPa; f_b is the mean compressive strength of the concrete units in MPa, f_m is the compressive strength of mortar layers in MPa; K, α and β are constants defined according to Eurocode 6-2005. Note that the characteristic compressive strength of masonry is taken as the smallest compressive strength of an individual masonry prism specimen or the 5th percentile determined as 1.64 standard deviation below the mean under the Gaussian distribution assumption, whichever is the greater (BS EN 772-1-2011). According to Ferguson (Ferguson 1995), the method of measuring the compressive strength of mortar is based on the flexural strength specimens, which is 1.28 times the compressive strength of normal mortar cubes. Thus, when using Equation 2-1, the compressive strength of mortar layers is increased by 1.28 times by the strength increase factor. Regarding values for constants K, α and β, they are 0.52, 0.7 and 0.3, respectively (for masonry made with hollow concrete units which have vertical cavities of more than 25% but no more than 60%, as well as general purpose mortar and lightweight mortar) according to Eurocode 6-2005.

The normalized mean compressive strength of the concrete units f_b is converted from the average concrete unit compressive strength $f_u^{'}$ to the air-dried compressive strength of an equivalent 100 mm wide × 100 mm high masonry unit, see as follows:

$$f_b = k_c \delta f_u^{'} \quad \text{(Eq. 2-3)}$$

where k_c is a material factor taken as 1.0 for air-dried blocks and δ is a shape factor accounting for the masonry unit height and thickness according to BS EN 772-1-2011.

2.3.4 AS 3700-2017

The current Australian masonry design standard AS 3700-2017 provides an equation for masonry constructed with clay, concrete or calcium silicate units based on the compressive strength of masonry units and two correction factors, including a bedding type factor and a joint thickness factor. For hollow concrete masonry unit prisms, the following Equations are adopted:

$$f_m^{'} = k_h f_{mb}^{'} \quad \text{(Eq. 2-4)}$$

$$k_h = 1.3(h_u / 19 t_j)^{0.29} \quad \text{(Eq. 2-5)}$$

$$f_{mb}^{'} = k_m \sqrt{f_{uc}^{'}} \quad \text{(Eq. 2-6)}$$

where f_m' is the compressive strength of masonry; k_h is the mortar joint thickness factor but not to exceed 1.3; f_{mb}' is the compressive strength of masonry specimens for masonry units whose ratio of height to mortar bed joint thickness is 7.6; h_u and t_j are the height of concrete unit and thickness of mortar joint, respectively; k_m is a compressive strength factor, which is provided as 1.4 and 1.6 for hollow concrete masonry unit with full bedding and face shell bedding respectively; f_{uc}' is the 28 day unconfined compressive strength of masonry units in MPa.

2.4 Empirical Formulas for Prism and/or Masonry Compressive Strength

When it comes to strength prediction models for hollow concrete masonry, a variety of empirical formulas have been developed (i.e., Mann 1982; Köksal et al. 2005; Fortes et al. 2015 etc.) using masonry prism testing data generated from physical prism testing. Multiple parameters have been considered in the reported empirical models in order to predict the compressive strength of masonry. The two most well-known parameters are the compressive strength of masonry units and the compressive strength of mortar. Mann (Mann 1982) tested masonry prism specimens constructed with a variety of masonry units, including hollow concrete masonry units and proposed the following equation to predict the compressive strength of masonry:

$$f_m^{'} = 0.83 f_b^{0.66} f_m^{0.18} \quad \text{(Eq. 2-7)}$$

Guo (Guo 1991) carried out an experimental study which consisted of a total of 356 concrete block prisms and, subsequently, a finite element analysis to study the relationship between the prisms and the constituent materials. Finally, the following empirical equation was proposed to predict the compressive strength of masonry:

$$f_m^{'} = f_b(0.85 - 0.004 f_b - 0.7 / f_m) \quad \text{(Eq. 2-8)}$$

Köksal (Köksal et al. 2005) proposed an analytical equation based on data generated from nonlinear three-dimensional finite element analyses that were validated based on hollow concrete block experimental studies. The results of the applied finite element analyses were reported to agree with the experimental data. The proposed empirical equation to predict the compressive strength of masonry is as follows:

$$f_m^{'} = 1.57 \ln(f_m) + 0.75 f_b \quad \text{(Eq. 2-9)}$$

Fortes (Fortes et al. 2005) combined eight different compressive strengths of concrete masonry units with five different mortar mixes to construct a total of 96 hollow concrete block masonry prisms. Subsequently, an empirical equation was proposed to predict the compressive strength of hollow concrete block masonry:

$$f_m^{'} = 18.46 \ln(f_b) - 37.71 \quad \text{(Eq. 2-10)}$$

Note that for all the formulas above, $f_m^{'}$ is the compressive strength of masonry, f_m is the compressive strength of mortar and f_b is the compressive strength of concrete masonry units.

Other than the two well-known parameters mentioned above, some studies suggested that the height-to-thickness ratio of the prisms is also an influential parameter for masonry prism compressive strength prediction when the prism testing method is used. Sarhat (Sarhat 2014) compiled a database of hollow concrete masonry compressive test results and proposed an empirical equation based on the collected database. Three parameters were included in the proposed equation as follows:

$$f_m^{'} = 0.8(1.107 C_b C_h f_b^{0.75} f_m^{0.18}) \quad \text{(Eq. 2-11)}$$

$$C_h = \begin{cases} (1 - 0.05(5 - \frac{h}{t}))^{-1} & \frac{h}{t} < 5 \\ 1 & \frac{h}{t} \geq 5 \end{cases}$$

where C_b is a mortar bedding type factor whose value is taken as 1.0 when masonry prism is built with face shell bedding and 0.91 when masonry prism is built with full bedding; C_h is a correction factor for the height-to-thickness ratio of masonry prisms.

However, due to the lack of systematic design of all those experiments used for the utilized database, as well as the inherent experimental uncertainties, the models developed could be negatively affected in accuracy (bias) and precision (scatter).

2.5 Mechanics-based Finite-element Methods

Being a less expensive yet reasonably accurate approach, detailed mechanics-based finite element (FE) modelling is an attractive alternative to physical prism testing for predicting the masonry compressive strength. Compared to the semi-empirical formulas, mechanics-based finite element (FE) models consider the underlying physics and are thus usually considered a more accurate approach, especially for researchers specializing in computational modelling. Previous studies (Guo 1991; Suwalski and Drysdale 1986) suggested three different approaches for finite element modelling of masonry prisms: plane-stress (PS) modelling, plane-strain (PE) modelling, and three-dimensional (3D) modelling. Pina-Henriques and Lourenço (Pina-Henriques and Lourenço 2003) suggested that the simplified methods (i.e., PS, PE) can lead to different compressive strengths and different failure mechanisms from 3D modelling, and a 3D modelling approach was recommended as more adequate for small-scale prisms as in physical prism testing. Similar conclusions were given by Barbosa et al. (Barbosa et al. 2009): the PS modelling approach largely underestimated the masonry strength, while the PE modelling approach overestimated the capacity of masonry under compression. In these studies, the 3D FE models were typically calibrated and/or validated with a few physical prism tests. Note that the modelling process typically involves time-consuming pre-processing and prior knowledge of software for modelling, theoretical knowledge of constitutive material models, and empirical knowledge of determining some model parameter values. This prevents its wide use from being accepted by engineers as an effective method for compressive strength determination.

No existing studies aimed to automate the FE modelling, which typically involves a good knowledge of the material constitutive models, quality FE meshing, and contact/interaction definition, to develop a numerical prism testing as a readily used tool for masonry strength perdition. More importantly, some model parameters have to be assumed due to a lack of information (Hamid and Chukwunenve 1986). The FE model accuracy for masonry strength prediction was not well assessed or quantified with comparison to a large experimental database of prism testing available in the public literature. The only study that assessed the prediction accuracy using an experimental database is the one carried out by Hamid and Chukwunenve (Hamid and Chukwunenve 1986), which proposed a detailed micro-FE model in DIANA for

predicting the compressive strength of solid (i.e., clay brick and stone) masonry prisms and used a total of 50 cases with different bonding patterns.

2.6 Data-based Surrogate Models

The accuracy of masonry compressive strength has a significant effect on the design and reliability assessment of masonry walls. Therefore, studying masonry compressive behaviour is the fundamental part of studying masonry. However, it is very challenging to determine the compressive strength of masonry because of its complicated composite characteristic, which is caused by the anisotropic nature of masonry. In the field of modern civil engineering, numerical models have grown to be increasingly complicated and therefore become overly time-consuming.

In general, numerical models are more complex due to their requirements for a series of constitutive models and the corresponding model parameters in order to describe the failure mechanisms. In contrast, based on the data generated from prism tests, various empirical models have been proposed, which include the compressive strength determination methods proposed by different masonry design codes and other models proposed in the literature. The empirical models developed based on a limited dataset by assuming the explicit parametric model form assumed in the empirical functions could be problematic in accuracy or generalization. Alternatively, as a new form of data-based modelling method, soft-computing techniques using artificial intelligence (AI) or machine learning (ML) can be used to take advantage of large datasets and the interpolation capabilities of AI or ML models. AI or ML models can be an inexpensive yet efficient approximation of the actual numerical models and largely reduce computational costs.

Compared to the above-mentioned traditional methods (i.e., empirical formulas), artificial intelligence (AI) or machine learning (ML) models have been proven to be more powerful. For example, Artificial Neural Networks (ANN) and Gaussian Process Regression (GPR) models have been commonly used, due to their great flexibility in function approximations, in studying the mechanical properties of concrete, including compressive strength and elastic modulus of concrete (Tayfur et al. 2014; Ahmadi-Nedushan 2012; Duan et al. 2013; Asteris et al. 2021; Dao et al. 2020).

Specific to the field of masonry, Zhou et al. (Zhou et al. 2016) adopted multilayered feed-forward networks for predicting the compressive strength of hollow concrete block masonry prisms. In that study, a total of 90 datasets, consisting of 308 prism specimens, were collected and used to develop predictive models based on three input variables (i.e., masonry unit compressive strength, mortar compressive strength, and prism height-to-thickness ratio). The network developed consisted of 3 neurons in the input layer, 12 neurons in the 1 hidden layer and 1 neuron in the output layer as shown in Figure 2-2.

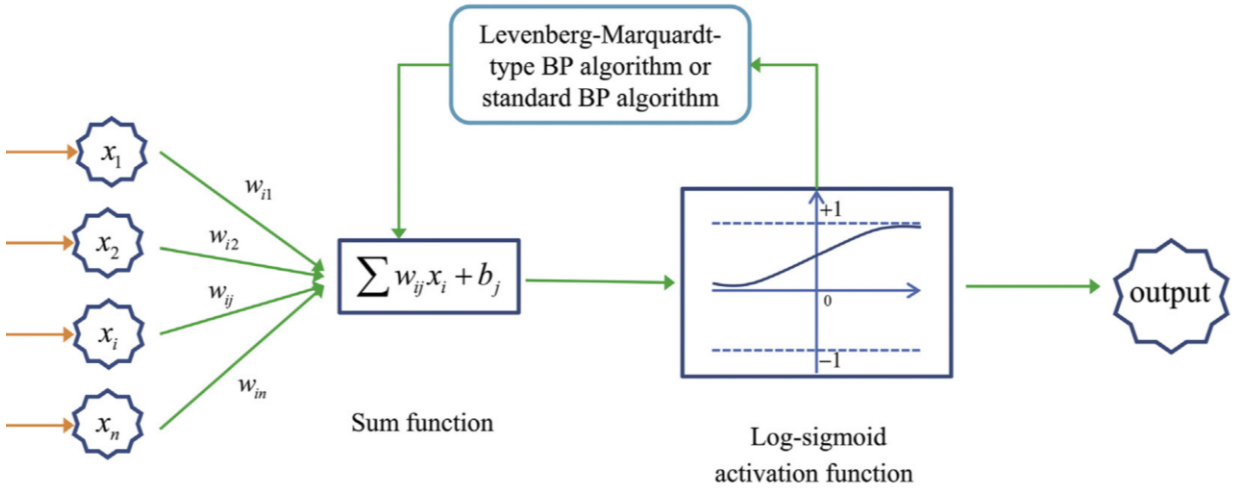

Figure 2-2: Architecture of typical ANN. A typical ANN without input, sum functions, log-sigmoid activation function, and output (Zhou et al. 2016)

Similarly, Asteris et al. (2021) used multilayered feed-forward networks for predicting the compressive strength of masonry prisms with various brick materials, including earth bricks, clay bricks, concrete bricks, silicate bricks, based on a total of 232 specimens collected from the literature. The development of the proposed network was based on hidden layers ranging from 1 to 2 with the number of neurons ranging from 1 to 30 for each hidden layer. The results proved that the optimum network consisted of 3 neurons in the input layer, two hidden layers with 8 and 28 neurons, respectively and 1 output neuron. Lan et al. (2020) utilized a three-layer neural network to predict the compressive strength of earth block masonry based on three input parameters: compressive strength of bocks, compressive strength of mortar, and prism height-to-thickness ratio, with a total of 72 groups of datasets (348 specimens). The model consisted of 3 neurons in the input layer, one hidden layer with the number of neurons ranging from 3 to 12 and

1 output neuron. Garzón-Roca et al. (2013) also used a three-layer neural network to determine the compressive strength of clay brick masonry using the compressive strength of clay brick and cement mortar based on a total of 19 experimental studies (96 specimens).

However, the aforementioned ANN model developed depended on the pre-selected configuration (e.g., number of layers and nodes for multilayered feed-forward neural network) and is typically more suitable for problems with large datasets, requiring a relatively large number of data samples for training, validation, and testing. When the sample size of data collected is relatively limited, it can potentially lead to overfitting and a lack of generalization for the model developed.

In contrast, GPR, as a nonparametric probabilistic ML algorithm, is superior when small-data problems occur. It has the advantage of leveraging or integrating prior knowledge with data observed, which allows it to be less dependent on the data and, thus, more suitable when limited data exist. Furthermore, GPR, as a nonparametric ML Algorithm, has the biggest advantage of no assumptions (or weak assumptions) about the form of the underlying functions. Therefore, Gaussian Process Regression model is flexible and capable of fitting a large number of functional forms and can result in higher performance models for prediction, and the GPR-based model can be continuously updated when more data is observed. This makes it easy to accommodate new data, for example, when more prism tests are completed if it is used for masonry prism strength prediction. Additionally, the prediction uncertainty or error can be provided after the model training process in GPR model development due to its probabilistic feature.

Gaussian Process modelling was adopted under the form of surrogate modelling by Sacks et al. (Sacks et al. 1989), in which Gaussian Process modelling was used to replace the time-consuming computational model with an input-output mapping. Later, it was used in the masonry field as well. Chisari et al. (2018) adopted GPR as the surrogate of the detailed FE model and conducted a sensitivity analysis of a brick-masonry mesoscale model. Moravej et al. (2019) used Gaussian Process to reduce the calculation burden in their work using the modular Bayesian approach to replicate the undamaged to damaged states of real masonry structures. Peng et al. (2020) proposed a new method based on Gaussian Process Regression to calculate the reliability index for the in-plane shear failure of unreinforced masonry walls. The results indicated that the proposed GPR

model was very efficient. In a related study, Peng et al. (2019) used the deterministic shear model as the prior GPR model and then updated the prior model with the collected test results. The surface of the prior mean function of different models is presented in Figure 2-3. The GPR models were proven to be very efficient and very convenient to improve with the new data.

Additionally, applications of other commonly used artificial intelligence models for studying masonry behaviour, including pattern recognition, strength prediction, seismic analysis etc. can also be found (i.e., García-Macías et al. 2020; Towashiraporn 2004; Mishra et al. 2019; Liu et al. 2017; Sharafati et al. 2021; Spiridonakos and Chatzi 2015).

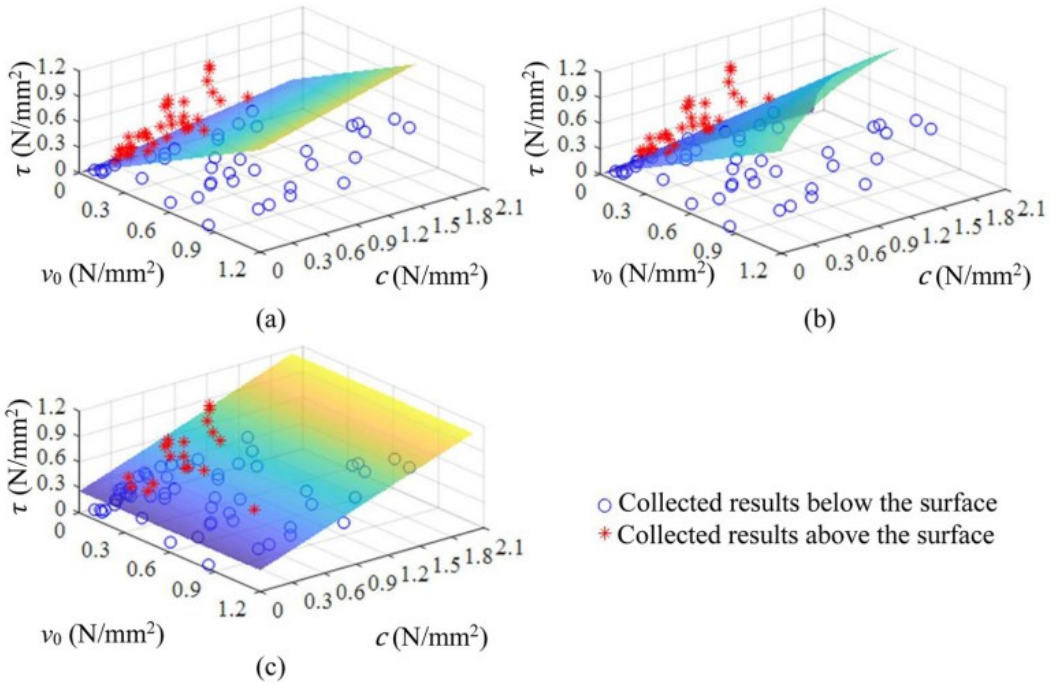

Figure 2-3: Surface of the prior mean function: (a) Model 1, (b) Model 2 and (c) Model 3 (Peng et al. 2019)

2.7 Model Accuracy Assessment and Sensitivity Analysis

In the past decades, various research studies were carried out to investigate the effect of different parameters on the compressive strength of masonry either experimentally or numerically, and a few of them focused on hollow concrete masonry for which the failure mechanism can be different

from brick masonry (Berto et al. 2005). Barbosa et al. (2009) conducted compressive tests on three-course hollow concrete masonry prisms with four different unit-mortar strength combinations, indicating that the failure mode of masonry prisms is associated with the mechanical properties of masonry components. Mohamad et al. (2017) tested hollow concrete masonry prisms constructed with weak units and strong mortar, and the results indicated that mortar governs the prism failure process. Based on the conclusion, it is suggested that masonry design codes should take masonry failure due to the behaviour of mortar into account. As shown in Appendix A, such experimental studies have been carried out by Chahine et al., Drysdale et al., Gayed et al., etc. However, only a few prisms can be tested in each study due to financial and time limitations.

Compared to the ones carried out based on experimental programs, those sensitivity analyses that are based on FE models have more flexibility. Hamid and Chukwunenye (Hamid and Chukwunenye 1986) used 3D elastic FE models developed in commercial software ANSYS to study the elastic compressive behaviour of hollow concrete masonry prisms. Köksal et al. (Köksal et al. 2005) conducted a nonlinear three-dimensional finite element analysis. The effect of the value of cohesion, the friction angle of the Drucker-Prager yield criterion and model parameters for the constituent material model were discussed, then adequate values were proposed. In a study conducted by Zahra and Dhanasekar (Zahra and Dhanasekar 2016), a series of sensitivity studies were carried out based on the proposed analytical model, and the results indicated that the unit strength has a significant effect on the masonry strength while the mortar strength only has a marginal effect. The thickness of mortar joint, on the other hand, was proven to have a profound effect on the masonry strength. Note that the proposed model considered masonry as a continuum and thus was unable to capture the local responses. Abasi et al. (2020) proposed a simplified micro finite element modelling method to study the height-to-thickness correction factors for solid concrete masonry prisms proposed by the current international masonry design codes.

Thus, it can be concluded that most of the previous research on the effect of different parameters on masonry compressive strength was based on deterministic finite element models. While in actual tests and constructions, the material properties of different masonry components are usually normally distributed (Moradabadi et al. 2015). Therefore, a deterministic analysis may result in a large prediction error and affect the prediction accuracy. Meanwhile, different input variables may

have different levels of influence on the prediction results. That is to say, it is important to calculate the significance level in order to further quantify the contributions of all the input variables. A systematic global sensitivity study of masonry prism was only carried out by very limited previous studies (Zhu et al. 2017; Álvarez-Pérez et al. 2020). Hence, an automatic FE model is developed in this study to carry out a sensitivity analysis, which is aimed at quantifying the contribution of different input parameters to the output variance. However, one major limitation is that most of the previous research on the effect of different parameters on masonry compressive strength was based on deterministic finite element models.

2.8 Summary

The compressive strength of hollow concrete block masonry is an essential mechanical parameter considering its influence on structural design. Different methods can be used as witnessed in previous work carried out on the behaviour of masonry prisms under compression. Acknowledging the importance of the compressive strength of masonry, discrepancy of existing models and methods, and the lack of probabilistic prediction error assessment, this thesis will contribute to developing more reliable models and assessing prediction model accuracy for masonry compressive strength. To accomplish this, this work will leverage the mechanics-based finite element and probabilistic ML (i.e., GPR) with an extensive experimental database compiled for masonry prism testing.

CHAPTER 3: AUTOMATIC NUMERICAL PRISM TESTING FOR HOLLOW CONCRETE MASONRY COMPRESSIVE STRENGTH PREDICTION WITH ERROR ASSESSMENT AND VARIANCE-BASED SENSITIVITY ANALYSIS

3.1 Introduction

Compressive strength of hollow concrete masonry (HCM) is essential for analysis and design of masonry structures. However, its prediction remains a challenging task due to inherent randomness in the composite materials as well as the uncertainties in physical prism testing. The prediction accuracy is of interest to engineers acknowledging the aphorism that all models are wrong. In the past decades, significant experimental research efforts have been devoted in the literature. In engineering practice, two primary ways of determining the compressive strength of masonry are the physical prism testing method in the laboratory or construction field and the unit strength method derived empirically based on experimental testing of prisms (e.g., Maurenbrecher (1980, 1983, 1985, 1986)).

Regarding physical prism testing, different masonry design standards/codes have different testing specifications and ways to define the compressive strength of masonry using testing statistics (e.g., mean or 5^{th} percentile). A comprehensive review of four design standards or codes, namely, CSA S304-14 (2014) in Canada, TMS 402/602-16 (2016) in the United States, Eurocode 6-2005 (2005) in Europe, and the AS 3700-2017 (2017) in Australia, is summarized here to emphasize the differences and similarities in the masonry strength determination, as well as relevant limitations. In general, the physical prism testing method requires testing a number of prism specimens, which are usually constructed using multiple masonry units and mortar layers. The tested prism strength is then adjusted to obtain the compressive strength of masonry with a height-to-thickness correction factor, which is mainly to account for the limitation in the physical testing methods, i.e., the restraint effects of prism ends due to machine platens (CSA S304-14). During the test, masonry prism specimens are typically placed between two planks to help reduce the confinement effect of the loading machine (i.e., Khalaf 1996, Fortes et al. 2015, Ross 2013, Sarangapani et al. 2005).

In view of variations in the physical prism testing methods and uncertainty in testing conditions in different experimental programs, there is a need for a tool that can be used for understanding the effects of various factors and uncertainties on the mechanical behavior or masonry strength

prediction. A digital twin or copy of physical prism testing, such as mechanics-based detailed FE models of the prisms tested, can play a complementary role, and can potentially provide an alternative approach for strength prediction.

When it comes to strength prediction models, a variety of semi-empirical formulas have been developed (i.e., Mann 1982, Köksal et al. 2005, Fortes et al. 2015 etc.) using masonry prism testing data generated using the physical testing methods aforementioned. However, due to the lack of systematic design of all those experiments used for the utilized database, as well as the inherent experimental uncertainties, the models developed could be negatively affected in accuracy (bias) and precision (scatter).

Compared to the semi-empirical formulas, mechanics-based FE models consider the underlying physics and are thus considered a more accurate approach. Previous studies (Guo 1991, Suwalski and Drysdale 1986) suggested three different approaches for FE modeling of masonry prisms: plane-stress (PS) modelling, plane-strain (PE) modelling, and three-dimensional (3D) modelling. Pina-Henriques and Lourenço (2003) suggested that the simplified methods (i.e., PS, PE) can lead to different compressive strengths and different failure mechanisms from 3D modelling, and the 3D modeling approach was recommended as more adequate for small-scale prisms as in physical prism testing. Similar conclusions were given by Barbosa et al. (2009): the PS modelling approach largely underestimated the masonry strength, while the PE modelling approach overestimated the capacity of masonry under compression. In these studies, the 3D FE models were typically calibrated and/or validated with a few physical prism tests. No existing studies aimed to automate the FE modelling, which typically involves a good knowledge of the material constitutive models, quality FE meshing, and contact/interaction definition, to develop a numerical prism testing as a readily used tool for masonry strength perdition. More importantly, some advanced model parameters, which are typically not readily available for masonry units/mortar, have to be assumed due to a lack of information (Hamid and Chukwunenve 1986). The FE model accuracy for masonry strength prediction was not well assessed or quantified with comparison to a large experimental database of prism testing available in the public literature. The only study that assessed the prediction accuracy using an experimental database is (Hamid and Chukwunenve 1986), which proposed a detailed micro-FE model in DIANA for predicting the compressive strength of solid

(i.e., clay brick and stone) masonry prisms and used a total of 50 cases with different bonding patterns. Thus, this study will develop such a tool that will facilitate systematic accuracy assessment using a large experimental database complied for this study and variance-based sensitivity analysis, i.e., investigating the effect of different parameter uncertainties on the uncertainty of the compressive strength of hollow concrete masonry.

In the past decades, various research studies were carried out to investigate the effect of different parameters on the compressive strength of masonry either experimentally or numerically, and a few of them focused on hollow concrete masonry for which the failure mechanism can be different from brick masonry (Berto et al. 2005). Barbosa et al. (2009) conducted compressive tests on three-course hollow concrete masonry prisms with four different unit-mortar strength combinations indicating that the failure mode of masonry prisms is associated with the mechanical properties of masonry components. Mohamad et al. (2017) tested hollow concrete masonry prisms constructed with weak units and strong mortar and the results indicated that mortar governs the prism failure process. It was suggested that masonry behaviour due to the failure of mortar should be considered (Drysdale et al. 1979, Gayed et al. 2012, Chahine et al. 1989, etc). Note that only few prisms were tested in each study to study the effect of different parameters on the compressive strength of masonry, and thus numerical models are more appropriate for parametric studies.

Hamid and Chukwunenye (1986) used 3D elastic FE models developed in commercial software ANSYS to study the elastic compressive behavior of hollow concrete masonry prisms. Köksal et al. (2005) conducted a nonlinear three-dimensional FE analysis. The effect of the value of cohesion, friction angle of the Drucker-Prager yield criterion and model parameters for constituent material model were discussed, then adequate values were proposed. In a study conducted by Zahra and Dhanasekar (2016), a series of sensitivity study was carried out based on the proposed analytical model and the results indicated that the unit strength has a significant effect on the masonry strength while the mortar strength only has a marginal effect. The thickness of mortar joint, on the other hand, was proven to have a profound effect on the masonry strength. Note that the proposed model considered masonry as a continuum and thus was not able to capture the local responses. Abasi et al. (2020) proposed a simplified micro-FE modelling method to study the

height-to-thickness correction factors for solid concrete masonry prisms proposed by the current international masonry design codes.

Thus, it can be concluded that most of the previous research studied the effect of different parameters on masonry compressive strength without considering the model accuracy or other pertinent uncertainties (Moradabadi et al. 2015; Zhu et al. 2017). While in real tests and constructions, the material properties of different masonry components are usually random (e.g., normally distributed (Ganesan and Ramamurthy 1992)). Therefore, a deterministic analysis may be associated with prediction error and inaccuracy. Meanwhile, different input variables may have different levels of influence on the prediction results. That is to say, it is important to calculate the significance level in order to further quantify the contributions of all the input variables. Hence, an automatic FE model is developed in this study to carry out a variance-based sensitivity analysis, which aims to quantify the contribution of different uncertain input parameters to the output variance.

To sum up, this chapter aims to develop a detailed mechanics-based 3D FE model for automatic numerical prism testing of hollow concrete masonry, which can further be used as a strength prediction tool for uncertainty analysis. The proposed FE model is first validated based on the experimental tests carried out by Barbosa et al. (2009) and Mohammad et al. (2017) in terms of stress-strain behaviour and/or damage patterns, together with parametric studies to verify the importance of relevant micro model parameters on the masonry compressive strength prediction. After the validation, the tool developed is then applied to numerical masonry prism testing of 312 groups of hollow concrete masonry prisms collected from 40 literatures, including 1427 specimens in total. The accuracy in strength prediction through numerical prism testing is assessed using the experimental data and compared with the predictions from empirical formulas and masonry design code models. Using the tool developed for automatic numerical prism testing, the variance-based global sensitivity analysis is performed for masonry strength based on Polynomial chaos expansion (PCE) technique (Marelli and Sudret 2014, Marelli et al. 2021), investigating the influence of multiple input material property variance on the output masonry compressive strength variance.

3.2 Numerical Prism Testing Tool

A numerical prism testing tool is developed based on a detailed mechanics-based 3D FE model, in which the modeling and simulation process is completely automated. Modeling strategies are discussed, followed by validation and verification studies based on parametric analysis to study the importance of the model parameters using this tool.

3.2.1 Detailed micro-FE modeling strategy for prisms

In this section, hollow concrete masonry prisms under uniaxial compressive loading are modeled using three-dimensional (3D) detailed micro-FE techniques in commercial finite element software ABAQUS. The schematic view of FE modeling strategy for prism testing is presented in Figure 3-1 for a representative 3-course hollow concrete block masonry prism.

The masonry prism components (i.e., concrete units and mortar layers) as well as the unit-mortar interfaces are modeled explicitly. To be specific, concrete units and mortar layers are represented by C3D8R elements (eight-node linear brick elements with reduced integration). The unit-mortar interfaces, representing the interactions between units and mortar layers, are modeled by "surface-to-surface" contacts with the normal behavior defined as a "hard" contact to avoid penetration and the tangential behavior defined assuming Coulomb friction with finite sliding (Moradabadi et al. 2015). In addition, to mimic the physical prism testing, the two end platens (or planks) are also modeled explicitly by rigid elements with the prism-platen interfaces described by "surface-to-surface" contacts in the same manner as for the unit-mortar interfaces but with different properties (e.g., frictional coefficients). Displacement-control loading method is employed, and the displacement is applied though the top steel platen represented by the red arrows as indicated in Figure 3-1. The top loading platen is restrained in the lateral directions while the bottom loading platen is restrained in all degrees of freedom.

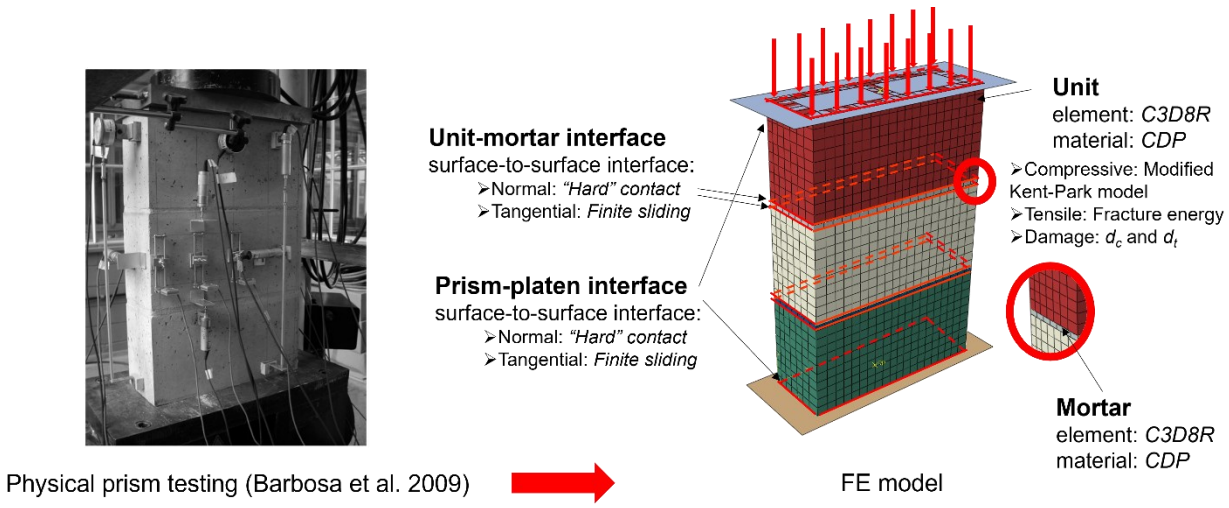

Figure 3-1: Schematic view of FE modeling strategy for prism testing

Both concrete units and mortar are represented by the concrete damage plasticity (CDP) model (Álvarez-Pérez et al. 2020s), which is able to capture both compressive crushing failure and tensile cracking failure. The elasticity parameters for CDP (i.e., Young's modulus for concrete units and mortar) are required and readily obtained from material coupon tests of units and mortar. The Poisson's ratio of 0.2 is used for concrete units (Hamid and Chukwunenye 1986) and cement/lime mortar (Hamid and Chukwunenye 1986). The plasticity parameters for CDP include the dilation angle Ψ (e.g., typically 30° – 40° for concrete), the ratio between the initial values for equi-biaxial compressive yield stress f_{b0} and the uniaxial compressive yield stress f_{c0} (=1.16), the flow potential eccentricity ε (= 0.1), the second stress invariant ratio K (ranging from 0.5 to 1.0) (Santos et al. 2017), and the viscosity parameter μ (Abasi et al. 2020).

Additionally, the uniaxial compressive behavior and tensile behavior need to be defined. In this study, the well-established Kent-Park model (σ-ε) modified by Chaudhari and Chakrabarti (2012) is adopted to describe the compressive behaviors of concrete and mortar with different material parameters. The adopted model consists of a parabolic ascending segment and a linear descending segment, as described as follows:

$$\begin{cases} \dfrac{\sigma}{\sigma_{cu}} = 2\dfrac{\varepsilon}{\varepsilon_0'}(1-\dfrac{\varepsilon}{2\varepsilon_0'}),\ \varepsilon \le \varepsilon_0 \\ \dfrac{\sigma}{\sigma_{cu}} = 1-0.15(\dfrac{\varepsilon-\varepsilon_0'}{\varepsilon_{cu}-\varepsilon_0'}),\ \varepsilon > \varepsilon_0 \end{cases} \quad \text{(Eq. 3-1)}$$

where σ and ε are the stress and strain of concrete and mortar under compression; σ_{cu} is the peak compressive strength of concrete and mortar, provided in the material coupon tests of units and mortar; ε_0' is the strain corresponding to the peak compressive strength, which is assumed as 0.002 (Martin et al. 1991) for concrete masonry units and 0.003 for mortar (Harsh et al. 1990); ε_{cu} is the ultimate strain, which is assumed as 0.003 (Martin et al. 1991) and 0.005 for mortar (Harsh et al. 1990).

The tensile behavior is described by a linear pre-cracking segment before reaching the uniaxial tensile strength σ_t followed by post-cracking tension stiffening, which is characterized by the fracture energy cracking criterion. The fracture energy criterion ($G_f = 0.073\sigma_{cu}^{0.18}$) proposed by CEB-FIP model code is adopted in this study due to its mesh independence (Tao and Chen 2015). The tensile strength for concrete, if not available from material coupon tests, an empirical relationship (Arıoglu et al. 2006) can be used to calculate the tensile strength, see as follows:

$$\frac{\sigma_t}{\sigma_{cu}} = 0.387\sigma_{cu}^{-0.37} \quad \text{(Eq. 3-2)}$$

Damage parameters are used in the CDP model as numerical indicator of material degradation in the post-peak range. To accurately predict the prism behavior under compression, damage parameters are included to better predict the failure patterns. The following equations (Obaidat 2017, Birtel and Mark 2006) are adopted to compute the compressive and tensile damage parameter d_c and d_t, respectively:

$$\begin{aligned} d_c &= (\sigma_{cu} - \sigma_c)/\sigma_{cu} \\ d_t &= 1 - \frac{\sigma_t E_c^{-1}}{0.9\varepsilon_t^{in} + \sigma_t E_c^{-1}} \end{aligned} \quad \text{(Eq. 3-3)}$$

where σ_{cu} is the peak compressive strength, σ_c is the compression stress along the descending stress-stain curve, σ_t is the tensile strength, E_c is the modulus of elasticity and ε_t^{in} is the tensile inelastic strain.

To ensure computational efficiency and accuracy, a mesh sensitivity analysis is performed for the representative 3-course hollow concrete block masonry prism with unit dimensions of 140 mm in depth, 190 mm in height and 390 mm in length, as well as mortar thickness of 10 mm. Different mesh sizes are employed to examine the mesh influence. The masonry stress-strain results are presented in Figure 3-2, which indicates that a mesh size of less than 20 mm does not notably affect the compressive behaviour; while the compressive strength and the corresponding strain are more sensitive to the mesh size when a mesh size is greater than 20 mm. Thus, the adopted mesh size is 20 × 20 × 20 mm and 20 × 20 × 10 mm for concrete units and mortar layers, respectively.

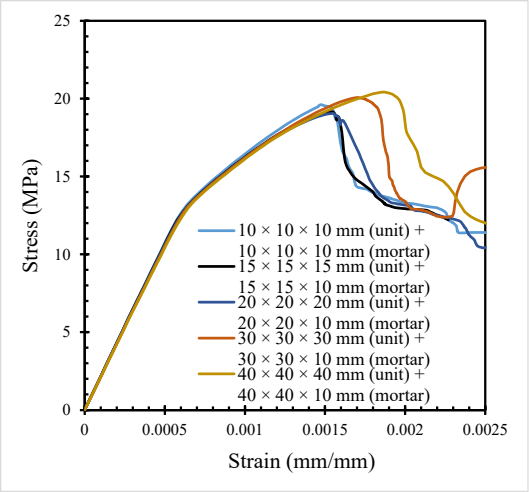

Figure 3-2: Mesh sensitivity analysis of a three-course hollow concrete masonry prism

3.2.2 Finite element modeling automation

In order to achieve the goal of numerical prism testing, the FE modeling and analysis of prism is automated through python in this study. The architecture of the Python tool for numerical prism test based on automatic 3D finite element modeling is illustrated in Figure 3-3. All prism related parameters can be defined in an input file ("Input_Variables.txt"), including both geometric and material property or model parameters. These input parameters are fed into ABAQUS through "Prism_Generation.py", which is called by "Submit_Jobs.py". In the prism generation process,

automatic FE meshing, 3D constitutive material model definition including the concrete unit and mortar compressive stress-strain curve generation using the models defined earlier, and the contact interaction, loads, as well as the boundary conditions. Note that this is typically a burden for engineers as it requires good knowledge of the model (e.g., meshing, CDP models, contact) but the automation process removes such a barrier in the numerical prism testing. Furthermore, more than one job for different prisms can be created and submitted. After the analysis of submitted jobs are finished, "Post-Processor.py" will be called to extract the compressive stress-strain curve for masonry, the compressive strength, and/or the damage or failure pattern of the prism as well as the equivalent plastic strain (PEEQ). The entire process is streamlined in Python, rendering ready application of the tool for numerical prism testing and masonry compressive strength prediction.

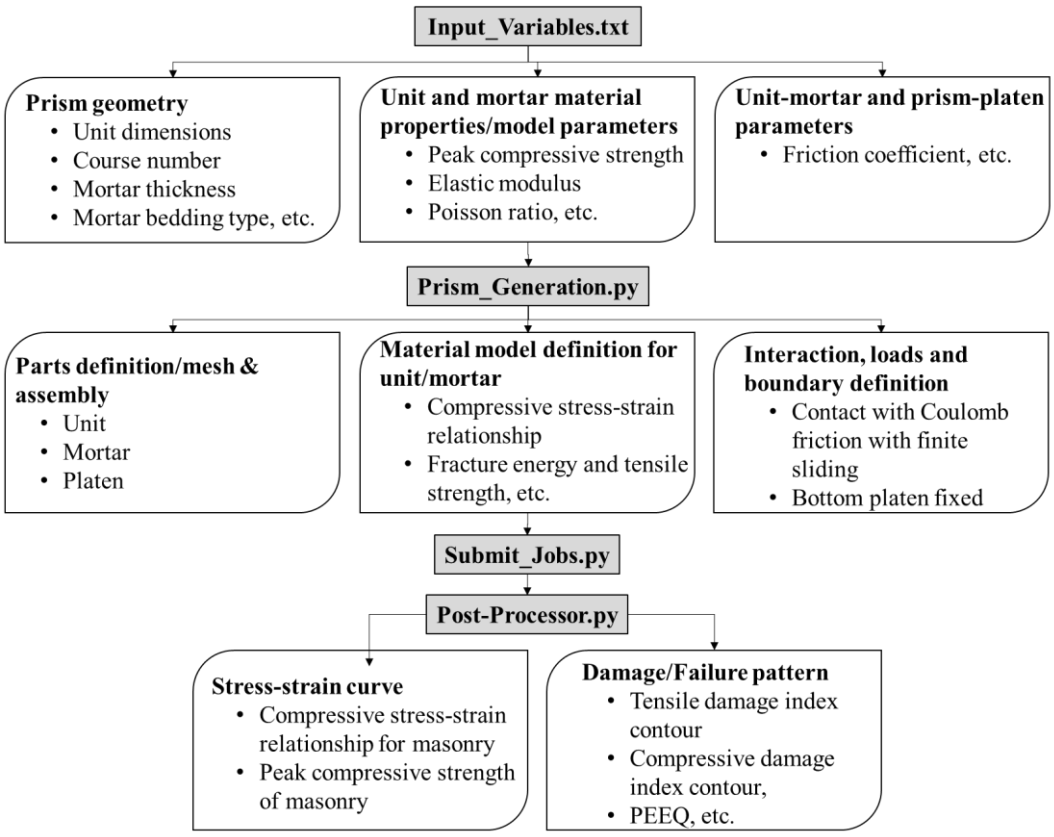

Figure 3-3: Python tool for numerical prism test based on automatic 3D finite element modeling

3.2.3 FE model verification and validation

One of the challenges of validating mechanics-based 3D micro-FE models is the lack of information on all the material properties or model parameters needed, especially when the FE model prediction is to be compared with a large experimental database. Typically, the most important properties such as compressive strength and modulus of concrete units and mortar are readily available from the experimental reports. However, the other material model parameters required in 3D micro-FE models are missing, including common material properties such as the strain corresponding to the compressive strength, the tensile strength, the fracture energy, the Poisson ratio, and other advanced model parameters such as dilation angles of concrete unit and mortar. For the common material properties, their values are assumed based on the literature, as mentioned in the previous section, except Poisson ratio and the dilation angles which are typically assumed. These advanced model parameters are studied through parametric analysis below, which helps justify the choice of typical values based on their sensitivity.

Specifically, the prism behaviour is firstly studied using a representative 3-course HCM prism, with respect to the dilation angle Ψ and Poisson's ratio v of both units and mortar layers. The dilation angle varies from 30° to 40° for concrete units while 35° is recommended for HCB (Nasiri 2017, Darmayadi 2019, Dere 2017, Genikomsou 2014, Kmiecik 2011 and Michal 2015) and 5° to 40° for mortar depending on the type and constitution: 5.7° for mud mortar, 7.4 ° to 8.1° for lime-mud mortar, 7.8° to 8.0° for lime-sand mortar, 35.8° for cement-sand mortar and 38.8° for cement-lime mortar (Rahgozar 2017). Figure 3-4 a and b show how the dilation angle (Ψ) utilized in the material model of HCM units and mortar affects the compressive stress-strain behavior of HCM: the ultimate compressive strength increased when Ψ increased. The compressive stress-strain curve is not significantly affected by the dilation angle of HCB when its between 30° to 40° and thus the recommended value 35° is adopted. Poisson's ratio of concrete units varies from 0.18 to 0.21 while 0.2 is recommended in many literatures (Klun et al. 2021). The value of Poisson's ratio of mortar, however, ranges from 0.07 to 0.25 depending on the type of mortar (Klun et al. 2021): 0.25 for weak lime mortar, 0.2 for cement/lime mortar, 0.15 for Portland cement mortar etc. It is shown in Figure 3-4 c and d that the Poisson's ratio (v) of both HCM units and mortar have little impact over the compressive stress-train curve. Therefore, 0.2 is adopted for the Poisson's ratio of

both HCM units and mortar. Note that the value of viscosity parameter μ, a common technique that is often adopted to solve the convergence issues due to the use of concrete damage plasticity model (Álvarez-Pérez et al. 2020, Arıoglu et al. 2006), is also studied in a similar manner. To suppress the numerical instabilities due to convergence issues and to speed up the calculation time, a relatively large value of μ is recommended but a noticeable increase can be observed on the compressive strength prediction if μ is too large. Thus, the relatively small value of $\mu = 0.01$ is used since it does not affect the strength prediction much.

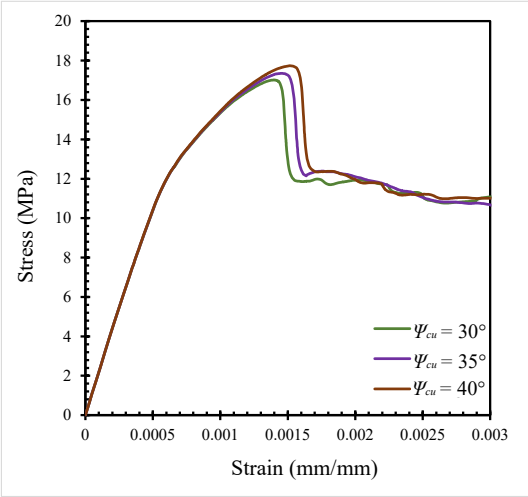

(a) Dilation angle (CMU)

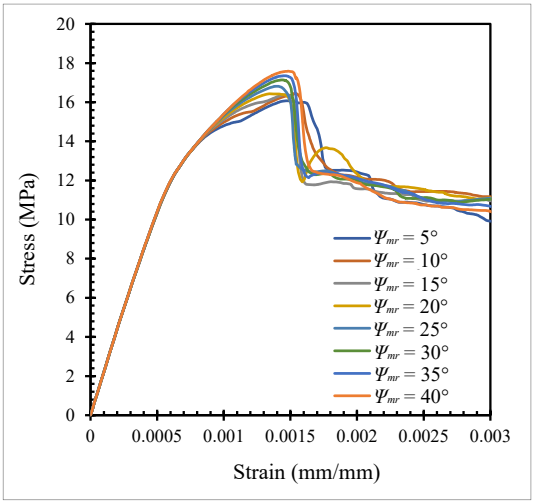

(b) Dilation angle (mortar)

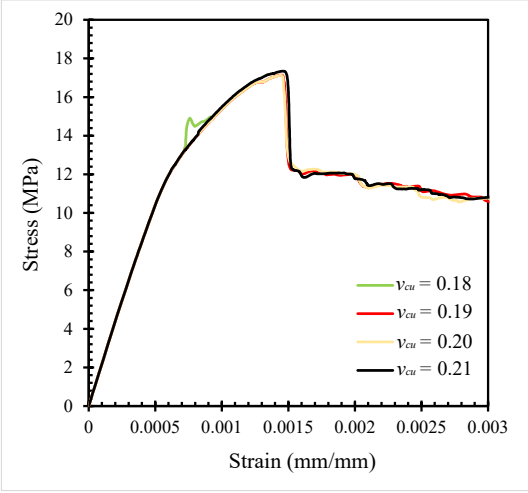

(c) Poisson ratio (CMU)

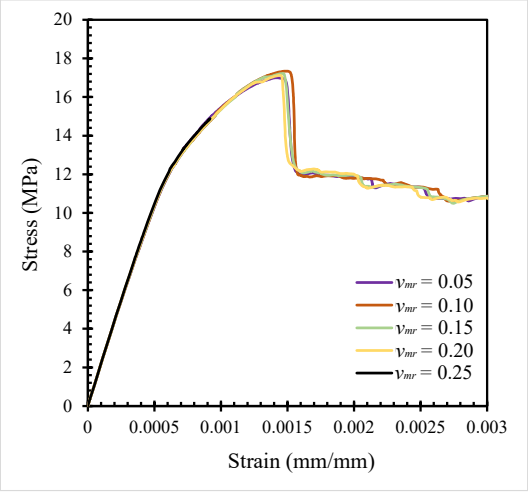

(d) Poisson ratio (mortar)

Figure 3-4: Parametric study of the proposed FE model with respect to advanced material model parameters in CDP: a) Dilation angle (CMU), b) dilation angle (mortar), c) Poisson ratio (CMU), and d) Poisson ratio (mortar)

After determining these advanced material model parameters, the developed model is first verified by running a series of parametric studies to confirm its capability of capturing the effects of important factors affecting the masonry strength. The examined factors include the compressive strength of unit f_b and mortar f_m and the thickness of mortar layer h_m. The stress-strain curves obtained using different values h_m, f_m and f_b, are presented in Figure 3-5.

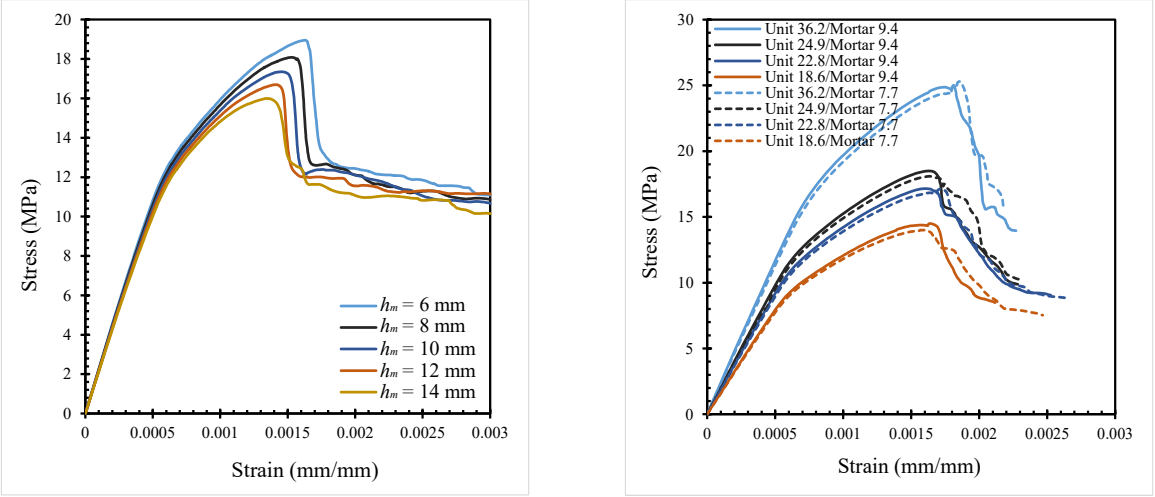

(a) Mortar thickness

(b) Compressive strength (MPa) of unit and mortar

Figure 3-5: Parametric study of the proposed FE model with respect to factors affecting the masonry strength in CDP: a) Mortar thickness and b) compressive strength of unit and mortar

The examined h_m values differ from 6 mm up to 14 mm, see Figure 3-5 a. When the mortar layer became thicker, the ultimate compressive strength decreased. This phenomenon can be explained by the equilibrium between the total tensile force on the concrete unit and the total compressive force on the mortar joint along the vertical direction. When the thickness of mortar joint increases, the vertical tensile stress increases in the concrete unit which result in an early failure on the

masonry prism. Thus, it can be said that workmanship (i.e., the thickness of mortar layers) plays an important role when it comes to the compressive strength of masonry. The examined concrete unit compressive strength values differ from 18.6 MPa through 22.8 MPa and 24.9 MPa up to 36.2 MPa, while the examined mortar joint compressive strength values differ from 7.7 MPa to 9.4 MPa. According to Figure 3-5 b, the compressive strength of concrete units can significantly affect the masonry compressive strength. The masonry compressive strength increased with the increasement of unit strength. While on the other hand, the compressive strength of mortar showed much less impact on the masonry compressive strength. Considering that only two sets of mortar strength are compared here, a more systemic sensitivity analysis is carried out and discussed in section 3.4 and the results indicate that the compressive strength of mortar still has minor impact other than the most influential parameter compressive strength of CMU.

In order to validate the methodology used in the proposed FE model, the prisms tested on two groups of experimental programs are simulated. The first validation is based on the experimental program carried out by Barbosa et al. (2009), in which a total of four groups of prisms, with three specimens in each group except group 4 with an exceptional of two specimens. Full bedding mortar is adopted as so in the experiment. The dimensions (mm) of the hollow concrete blocks and the lay-out of the prisms tested are shown in Figure 3-6 a and b. The compressive and tensile strength of concrete masonry units and mortar are presented in Figure 3-6 c. Note that f_c and f_t mentioned in Figure 3-6 c were reported based on gross area (Barbosa et al. 2009) and thus their values need to be converted using net area when defining the material properties of concrete unit and mortar in the FE model. All the concrete blocks used in the experiment are cast together with the exact same geometry. All prism specimens are built with three blocks staked together and 10 mm bed mortar joint. Four sets of prisms are subjected to uniaxial compressive load using the same loading machine under displacement control. The difference is the ratio between the compressive strength of concrete units and mortar, and the ratio between the elastic modulus of concrete units and mortar. Group 1 and 2 have a relatively higher ratio between the compressive strength of concrete unit and mortar of 2.4, while the same ratio in Group 3 and 4 is relatively lower of 1.6. The same trend can be observed for the elastic modulus ratio between the concrete units and mortar. Group 1 and 2 have a relatively higher ratio of 2.1, while on the other hand, Group 3 and 4 have a lower

ratio of 1.65. The different ratios of elastic modulus can explain the different failure modes. When the ratio of elastic modulus between unit and mortar is relatively higher (Group 1 and 2), mortar crushing occurred as the dominant failure mode, in comparison with Group 3 and 4 which no mortar joint crushing was observed.

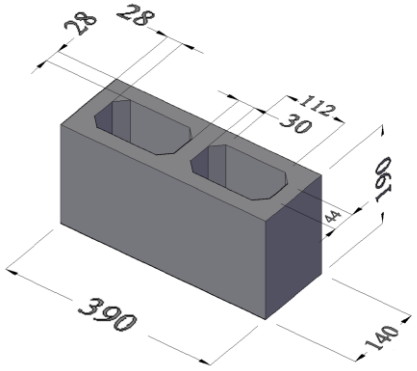

(a) Hollow concrete unit

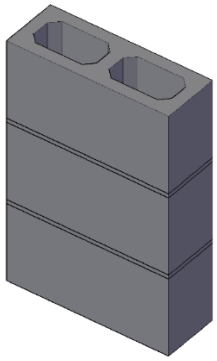

(b) Three block stack-bond prism

Group	Material	f_c (MPa)*	f_t (MPa)*
Group 1	Concrete	9.4	1.1
	Mortar	22.8	2.2
Group 2	Concrete	7.7	0.9
	Mortar	18.6	1.7
Group 3	Concrete	15.5	1.8
	Mortar	24.9	2.4
Group 4	Concrete	22.2	2.6
	Mortar	36.2	3.1

* Note that here f_c and f_t are calculated based on gross area [4].

(c) The compressive and tensile strength of concrete units and mortar (Barbosa et al. 2009)

Group	Material	f_c (MPa)	f_t (MPa)
Group1	Concrete	23.1	2.28
	Mortar	20.3	-
Group2	Concrete	7.7	0.9
	Mortar	7.4	-
Group3	Concrete	15.5	1.8
	Mortar	4.5	-

(d) The compressive and tensile strength of concrete units and mortar (Mohamad et al. 2017)

Figure 3-6: Dimensions (mm) and lay-out of masonry specimens: a) hollow concrete unit, b) three block stack-bond prism, c) CMU and mortar properties (Barbosa et al. 2009) and d) CMU and mortar properties (Mohamad et al. 2017)

The comparisons of the stress-strain curves between the FE-predictions and the experimental results are presented in Figure 3-7 for Group 1, 2, 3 and 4. It can be observed that the nonlinear behaviour of prisms is well captured by the FE model, with a slight underestimate of the compressive strength. The most common failure mechanism for weak mortar-strong unit combination in prism testing, i.e., tensile splitting failure, is observed in the FE prediction results as shown by the contour plots of the tensile damage parameter (DAMAGET) for the tested specimens (e.g., for specimen # as shown in Figure 3-8). According to the test results, the cracks first occurred in the face shell of the concrete unit near the center line and in the center of the transverse side web at the peak load. The vertical cracks across the face shell and the transverse webs propagated and led to failure with significant strength drop at the ultimate state. This is consistent with the evidence reported in the test (Barbosa et al. 2009).

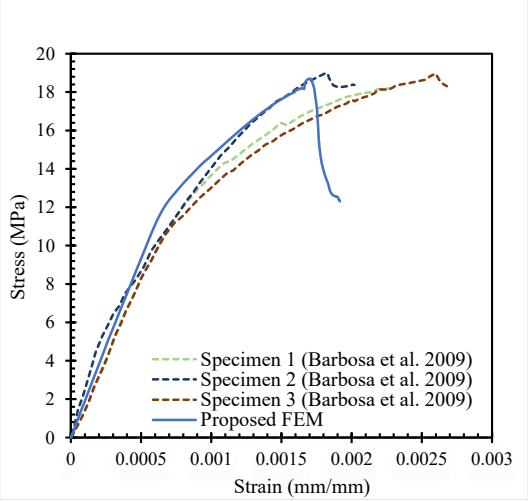

(a) Group 1

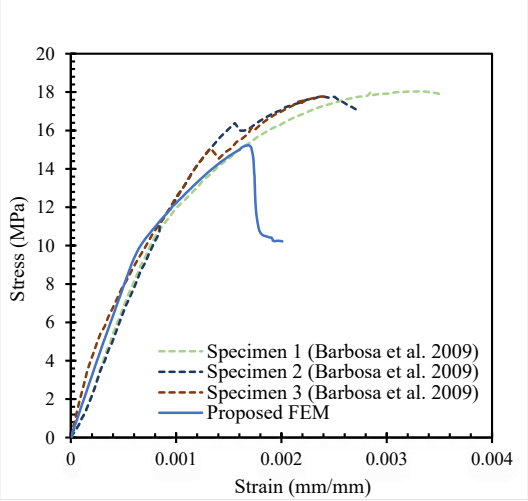

(b) Group 2

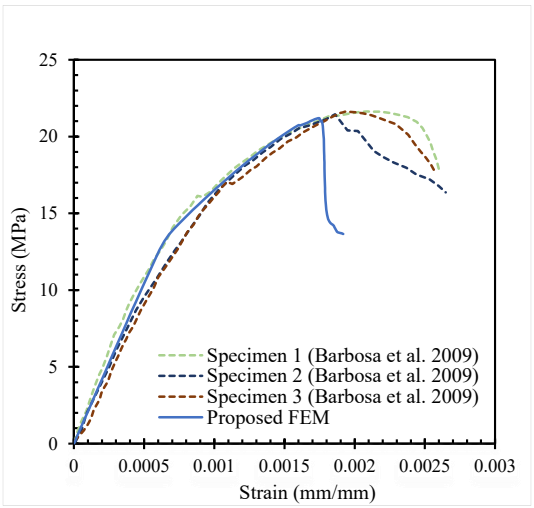

(c) Group 3

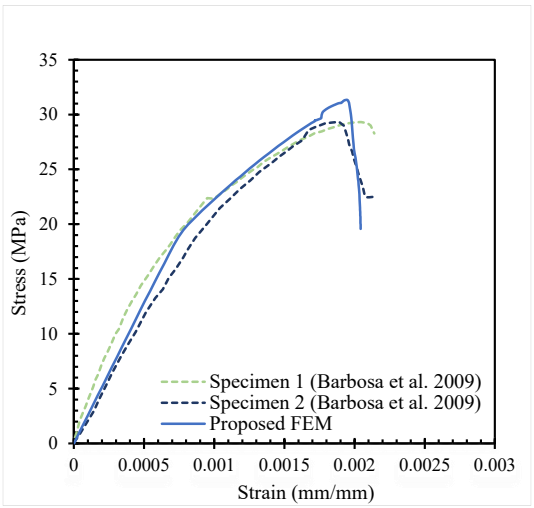

(d) Group 4

Figure 3-7: Comparison of stress-strain curves between FE predictions and experiment: (a) Group 1, (b) Group 2, (c) Group 3 and (d) Group 4

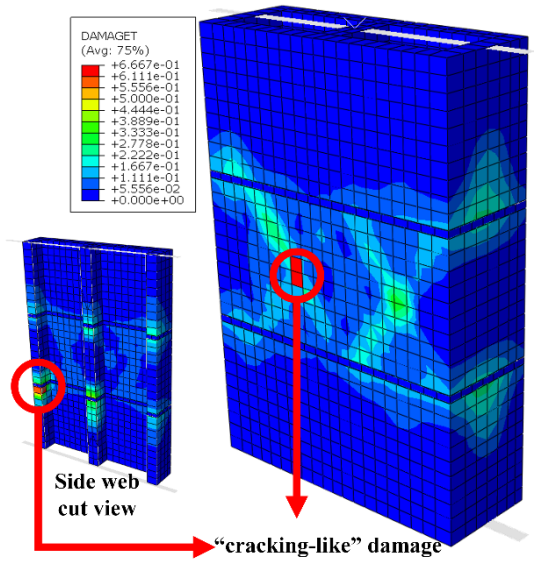

(a) Peak load

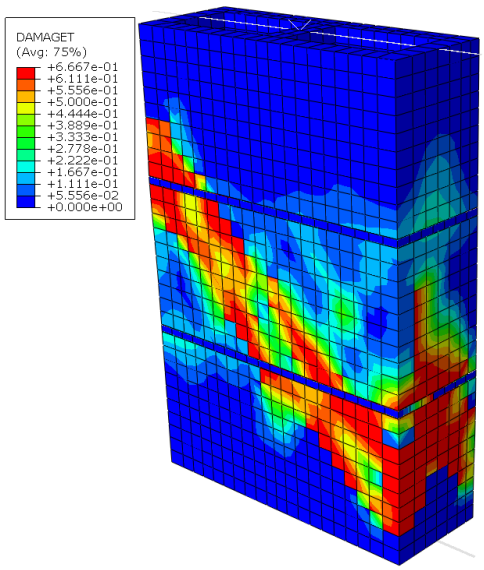

(b) Ultimate state

Figure 3-8: The failure mechanism in the FE model: (a) peak load and (b) ultimate state (Group 1)

The comparison of the masonry prism strength predicted by the FE models and experiment are summarized in Table 3-1 for all the four groups of prism testing. The prediction errors for Group 1, Group 3, and Group 4 are relatively small (less than 4%), while the prediction error for Group 2 is larger (14.61%). The same trend can be observed in the FE model prediction in (Barbosa et al. 2009). The proposed FE model showed an overall consistent prediction based on the prediction error.

Table 3-1: The summary of FE and experimental compressive strength (Barbosa et al. 2009)

	Group 1		Group 2		Group 3		Group 4	
	Value (MPa)	Error (%)	Value (MPa)	Error (%)	Value (MPa)	Error (%)	Value (MPa)	Error (%)
Experimental (Barbosa 2009)	18.2	-	17.8	-	21.4	-	30.1	-
FE Model (Barbosa 2009)	16.4	-9.80	14.2	-20.00	19.7	-7.94	30.4	+1.18
FE model (Present study)	18.7	+2.75	15.2	-14.61	21.2	-0.09	31.3	+3.99

The second validation is based on the experimental program carried out by Mohamad et al. (2017), in which a total of three groups of prisms, with three specimens in Group 1 and four specimens in Group 2 and 3. All of them have the same geometry as shown in Figure 3-6 a and b. The compressive and tensile strength of concrete masonry units and mortar are also included in Figure 3-6 d. The comparisons of the stress-strain curves between the FE-predictions and the experimental results are presented in Figure 3-9 for Group 1, 2 and 3, respectively.

Similarly, it can be observed in Figure 3-9 that the proposed FE model is able to well capture the average behaviour of hollow concrete masonry prisms under compression, but the maximum compressive strength was overestimated (see Table 3-2). Considering the large variation in the experimental tests, the FE prediction is considered acceptable. Note that no effort was made to calibrate the empirical model parameters to achieve a nearly perfect match for each individual specimen. In contrast, the same set of parameters and rules as described earlier, e.g., see Equations (3-1) – (3-3), is used for advanced model parameters. This naturally will lead to model inaccuracy, which needs to be assessed.

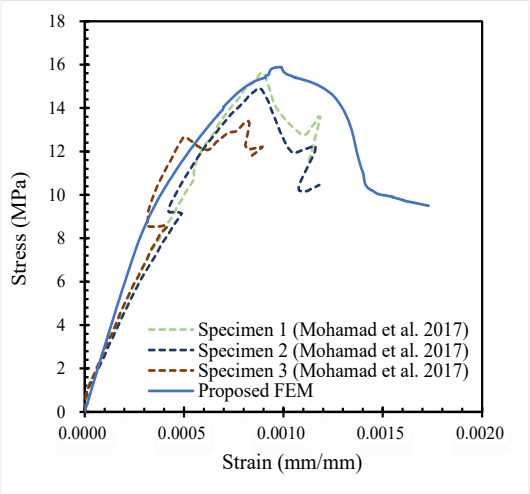

(a) Group 1

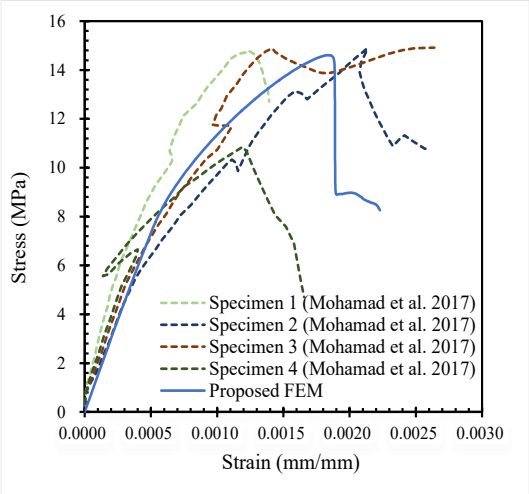

(b) Group 2

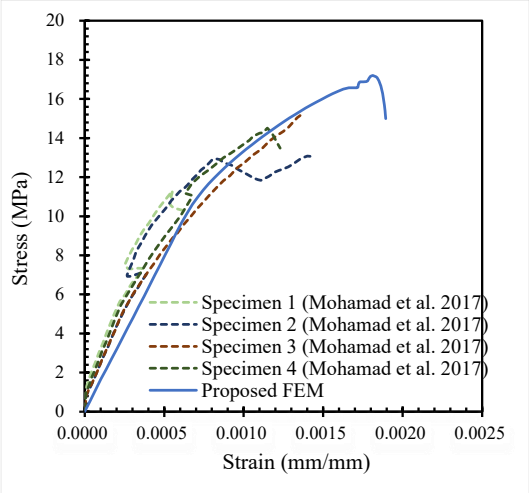

(c) Group 3

Figure 3-9: Comparison of stress-strain curves between FE predictions and experiments: (a) Group 1, (b) Group 2, (c) Group 3

The full results of the second validation are listed below in Table 3-2. The validation error of group 1 is 6.3%, which is the largest among all. While the validation error for group 2 and 3 are very close around 2%. The average validation error is 3.49%. Based on the validation error, the proposed FE model can provide an accurate prediction of the prism compressive strength.

Table 3-2: The summary of FE and experimental compressive strength (Mohamad et al. 2017)

	Group 1		Group 2		Group 3	
	Value (MPa)	Error (%)	Value (MPa)	Error (%)	Value (MPa)	Error (%)
Experimental (Mohamad 2017)	14.9	-	14.3	-	13.9	-
FE model (present study)	15.9	+6.30	14.6	+2.05	14.2	+2.11

3.3 FE-based Masonry Prism Strength Prediction and Accuracy Assessment

After an extensive literature review of hollow concrete masonry prism tests, a large database is compiled based on HCM prisms compressive tests. The database consists of 312 groups of HCM prisms, leading to 1427 individual prism specimens, which are collected from 40 literatures. Hollow concrete blocks with a void ratio ranging from 25% to 60% are studied here as "hollow" blocks as per CSA standard, in which the voids pass through the entire depth of concrete masonry blocks completely. Solid, semi-solid (void ratio < 25%) blocks are not considered for consistence. With reference to typical masonry prism testing, the course number of prisms selected is limited to be in the range between two and six in the database. The complete list of the collected database is presented in Appendix A, where the material properties tested for concrete units and mortar within each group are included.

The numerical prism testing tool developed in this study is used to predict the compressive strength of HCM prisms in the large experimental database mentioned above. Numerical prism testing is performed for the entire database with masonry strength prediction compared for masonry prisms with type S mortar and type N mortar, respectively. Note that the mortar is classified in accordance with the masonry design codes (CSA S304-14): mortar with compressive strength of 5 – 12.5 MPa is classified as type N (161 groups), and mortar with compressive strength of 12.5 – 17.6 MPa was classified as type S (151 groups). The comparison between FE-predicted and experimental strengths through numerical and physical prism testing is presented in Figure 3-10. It is shown that the proposed numerical prism testing provided an overall good prediction without a systematic bias.

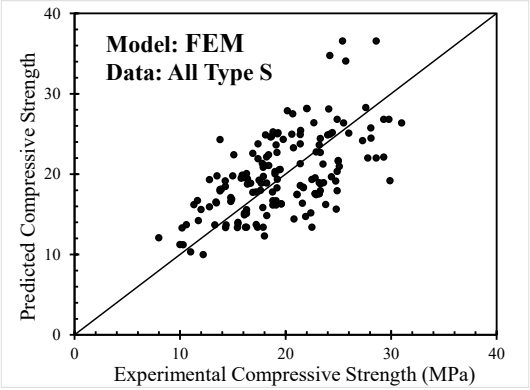

(a) Type S

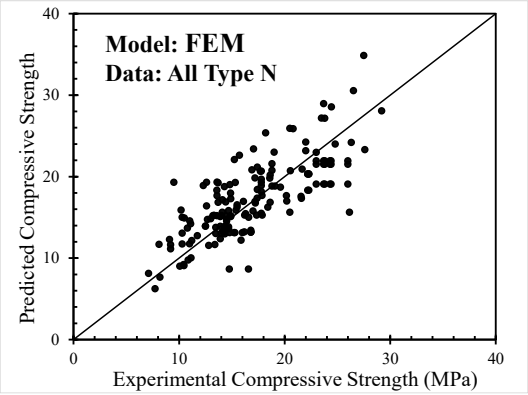

(b) Type N

Figure 3-10: Comparison of between FE-predicted and experimental masonry strength through numerical and physical prism testing: a) type S mortar, and b) type N mortar

To quantify the prediction error, the histograms of the test-to-prediction ratio for prisms with type S mortar and type N mortar are presented in Figure 3-11. The mean values of the prediction error of type S and N mortar are 1.01 and 1.02, respectively. The coefficient of variations of the prediction error of type S and N mortar are 22.1% and 17.5%, respectively. Normal distribution is adopted for the probability density function to fit the distribution of the prediction error.

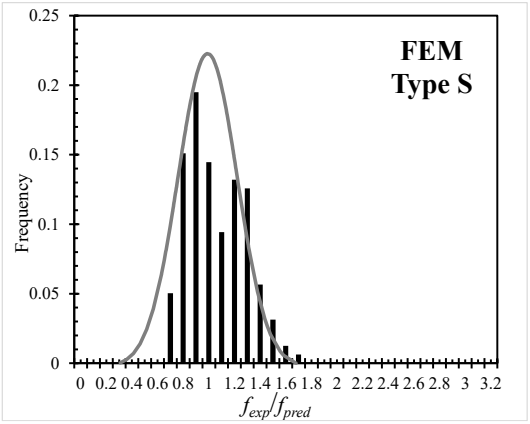

(a) Type S

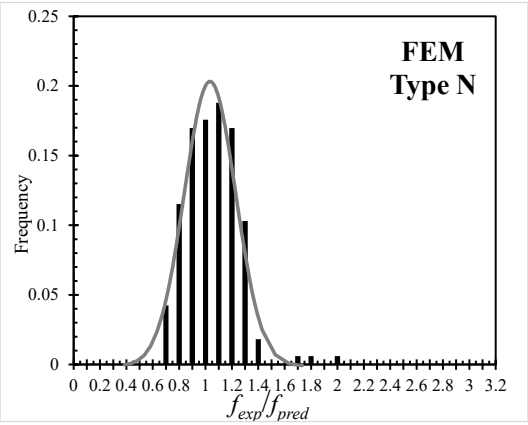

(b) Type N

Figure 3-11: Histogram for prediction error of the numerical prism testing: a) type S mortar, and b) type N mortar

3.3.1 Accuracy comparison with empirical formulas

In this section, the most representative empirical formulas from literature for the compressive strength of masonry are selected and assessed with the experimental database compiled from physical prism testing, with their accuracy compared to that of the proposed numerical prism testing. In order to compare with the test results for the compressive strength of masonry prisms, the calculated values for the compressive strength of masonry based on empirical formulas should be converted to the masonry prism strength, by dividing the masonry strength with the corresponding correction factor for a certain height-to-thickness ratio (*h/t*) (see Table 3-3 (CSA S304-14)). Note that linear interpolation is used for other values of *h/t*. The selected empirical models are summarized in Table 3-4, including four models proposed by Mann (1982), Guo (1991), Köksal et al. (2005), and Fortes et al. (2015), respectively. Note that the units in Equation (3-4) – (3-7) are MPa.

Table 3-3: Summary of height-to-thickness correction factors (CSA S304-14)

Height-to-thickness ratio	Correction factor
2	0.85
3	0.90
4	0.95
5 to 10	1.00

Table 3-4: Empirical equations for the prediction of masonry compressive

	Formula	Equation	Reference	Unit type
1	$f_m' = 0.83 f_b^{0.66} f_m^{0.18}$	(Eq. 3-4)	Mann (1982)	HCB
2	$f_m' = f_b(0.85 - 0.004 f_b - 0.7 / f_m)$	(Eq. 3-5)	Guo (1991)	HCB
3	$f_m' = 1.57 \ln(f_m) + 0.75 f_b$	(Eq. 3-6)	Köksal et al. (2005)	HCB
4	$f_m' = 18.46 \ln(f_b) - 37.71$	(Eq. 3-7)	Fortes et al. (2015)	HCB

Note that for all the formulas above, f_m is the compressive strength of mortar and f_b is the compressive strength of concrete masonry units.

The comparison of prediction ability of different empirical models and the proposed FE model is shown in Figure 3-12 for type S and type N mortar, respectively.

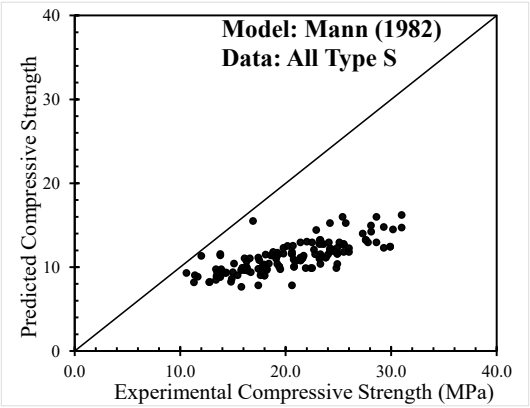

(a)

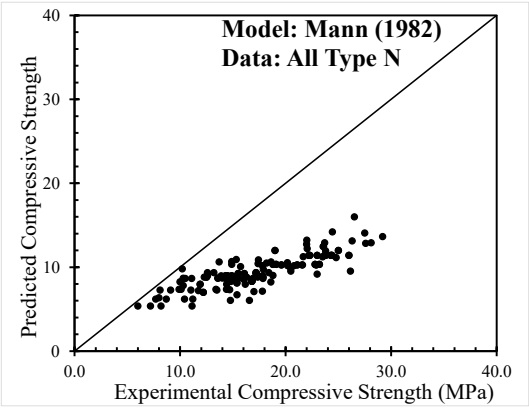

(b)

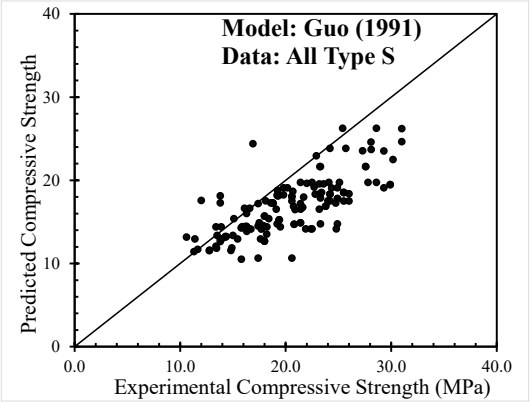

(c)

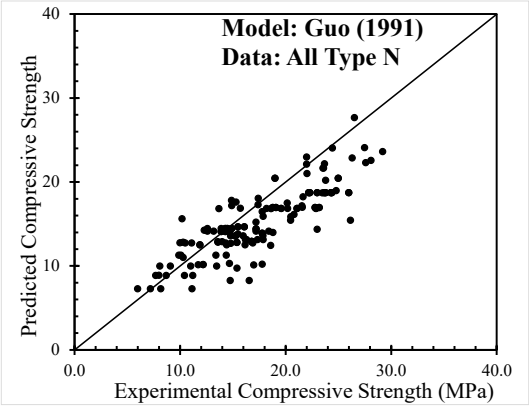

(d)

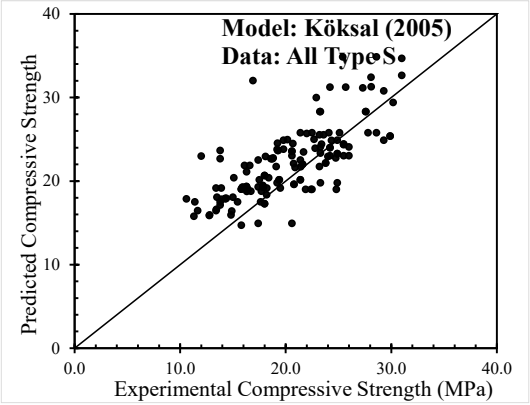

(e)

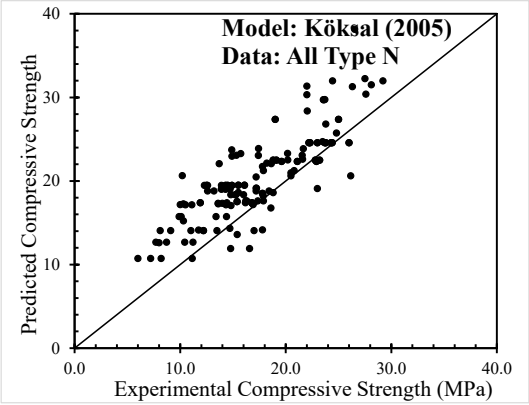

(f)

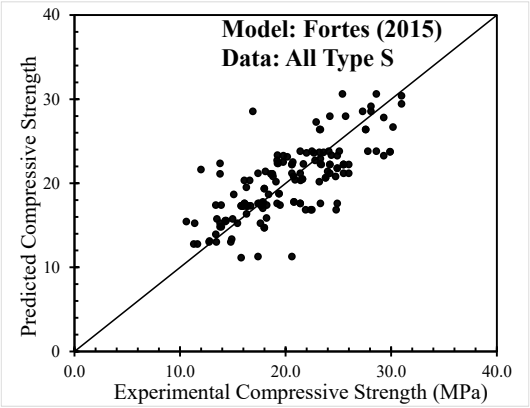

(g)

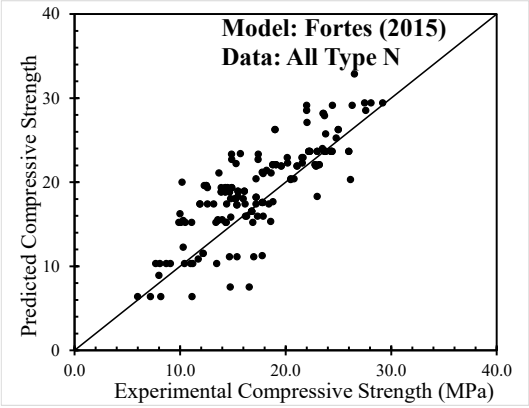

(h)

Figure 3-12: Comparison of prediction ability of: a) & b) Mann (1982), c) & d) Drysdale & Guo (1990), e) & f) Köksal et al. (2005), g) & h) Ernesto et al. (2015) for type S & N mortar

The prediction error is evaluated by the test-to-prediction ratio, defined as the experimental compressive strength f_{exp} divided by the model predicted compressive strength f_{pred}. The statistics of the prediction error for the proposed FE model and different empirical formulas proposed by Mann, Guo, Köksal et al., Fortes et al. are summarized in Table 3-5. It is shown that the proposed FE model has the best prediction results on average in terms of the mean value of the f_{exp}/f_{pred} ratio. The models by Mann (1982) and Guo (1991) tend to underpredict the prism strengths, while the models by Köksal et al. (2005) and Fortes et al. (2015) tend to overpredict the prims strengths. All models appear to have better prediction performance for type S mortar (i.e., lower coefficient of variation and mean value closer to 1). It is worth pointing out that the model proposed by Fortes et al. (2015), has a remarkable performance when it comes to HCM prisms with type S mortar, but its performance for type N mortar is much worse. Considering the average performance, both models by Fortes et al. (2015) and FEM is acceptable. However, the proposed FE model has accurate and more consistent prediction results regardless of the mortar type with negligible bias and stable COV (i.e., 17.5% for type N and 22.1% for type S).

Table 3-5: Descriptive statistics values of f_{exp}/f_{pred} for different empirical formulas and the proposed FE model

Test-to-prediction ratio	Mortar Type						Overall Database		
	Type S			Type N					
	Mean	STD.	COV (%)	Mean	STD.	COV (%)	Mean	STD.	COV (%)
Mann (1982)	1.81	0.28	15.6	1.82	0.32	17.6	1.82	0.30	16.7
Guo (1991)	1.21	0.20	16.2	1.15	0.21	17.9	1.18	0.20	17.2
Köksal et al. (2005)	0.91	0.15	15.9	0.85	0.15	17.9	0.88	0.15	17.2
Fortes et al. (2015)	1.01	0.17	17.3	0.93	0.22	24.0	0.97	0.21	21.1
FEM	1.01	0.22	22.1	1.02	0.18	17.5	1.02	0.21	20.2

3.3.2 Accuracy comparison with methods specified in masonry design codes and standards

As mentioned earlier, different statistics are used in these models by the design codes for additional safety margin. In particular, in CSA S304.1-14 and Eurocode 6-2005, the predicted compressive strength is the 5th percentile ($f_{m,5th}^{'}$), which can be calculated through the following equation assuming a normal probability distribution:

$$f_{m,5th}^{'} = \mu - 1.64 \times \sigma \qquad \text{(Eq. 3-8)}$$

where μ is the arithmetic mean and σ is the standard deviation. Thus, for a fair comparison, instead of using the average value of the prism tests, the 5th percentile value estimated from Equation 3-8 is used as the experimental strength f_{exp} for CSA S304.1-14 and Eurocode 6-2005. In contrast, the average value of the prism tests within each group is used as f_{exp} for TMS 402/602-16 and AS 3700- 2017. The comparison and the corresponding prediction error of different mortar types are presented in Figure 3-13. To quantify the prediction error, the histograms of the test-to-prediction ratio for prisms with type S mortar and type N mortar are presented in Figure 3-14 with the descriptive statistics values summarized in Table 3-6.

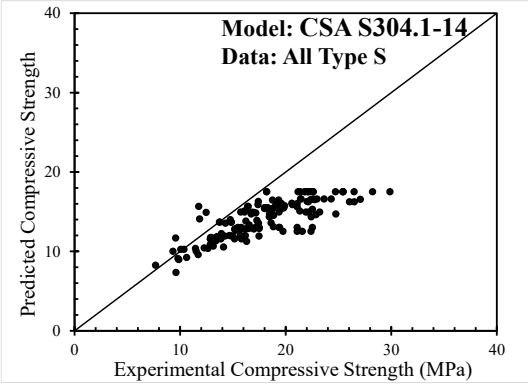

(a) CSA S304-14

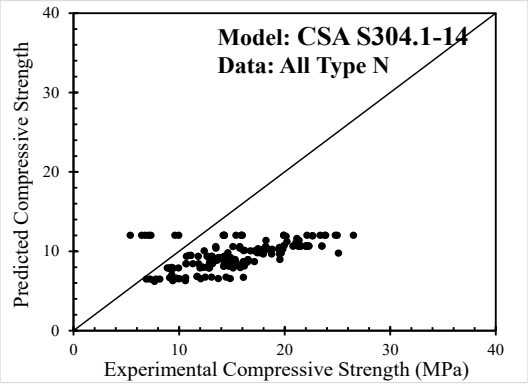

(b) CSA S304-14

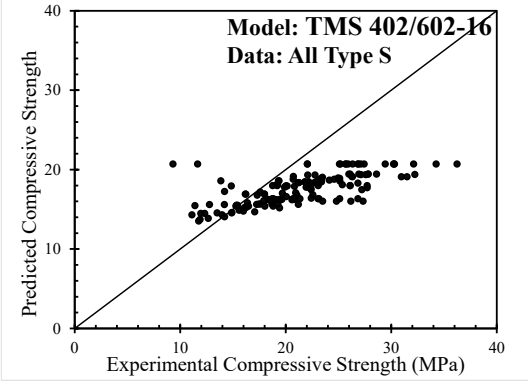

(c) TMS 402/602-16

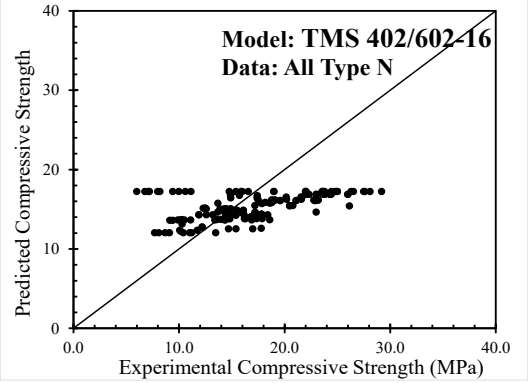

(d) TMS 402/602-16

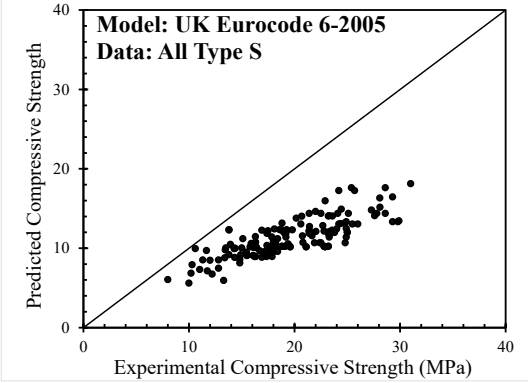

(e) Eurocode 6-2005

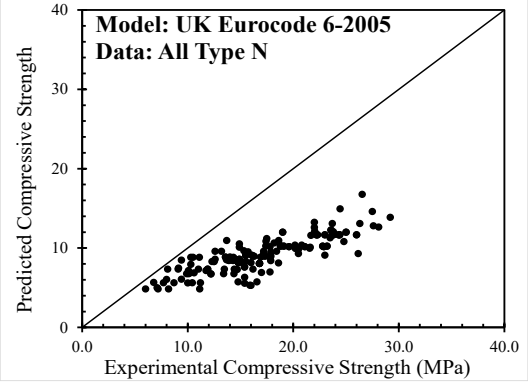

(f) Eurocode 6-2005

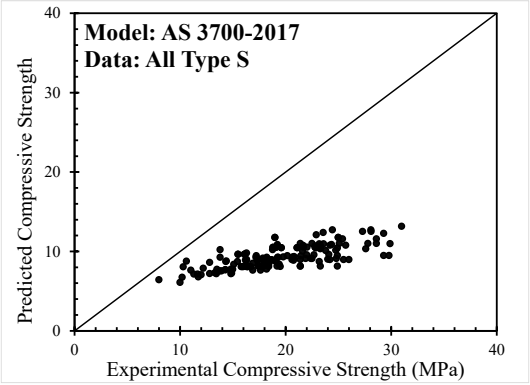

(g) AS 3700-2017

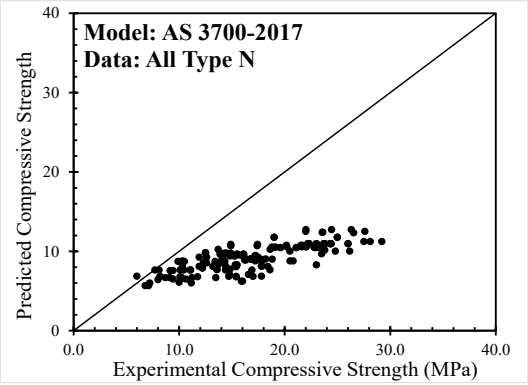

(h) AS 3700-2017

Figure 3-13: Comparison of prediction ability of a) & b) CSA S304.1-14, c) & d) TMS 402/602-16, e) & f) Eurocode 6-2005, g) & h) AS 3700-2017 for type S & N mortar

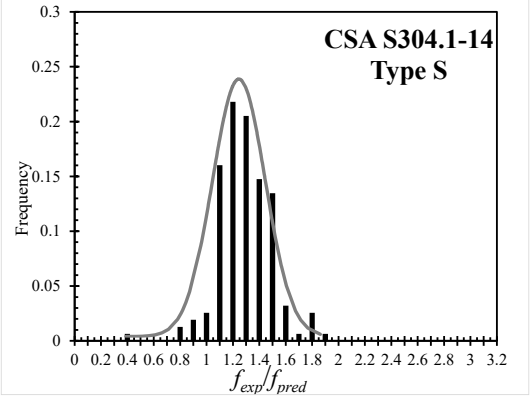

(a) CSA S304-14

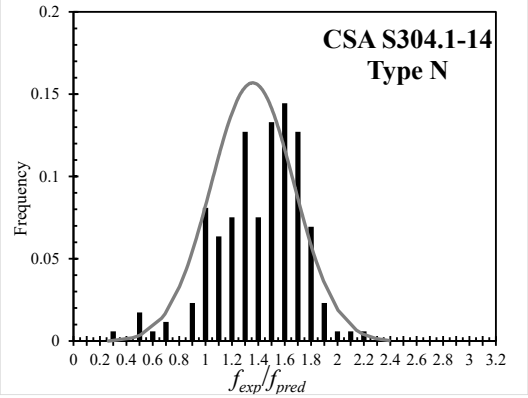

(b) CSA S304-14

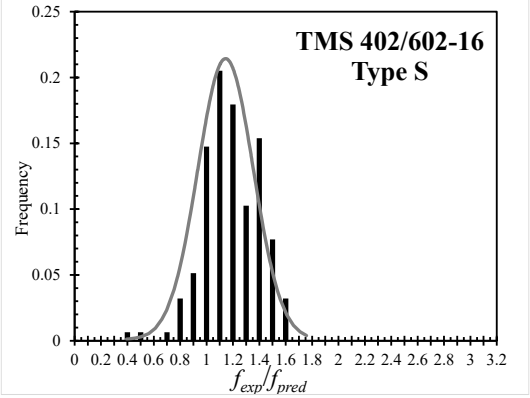

(c) TMS 402/602-16

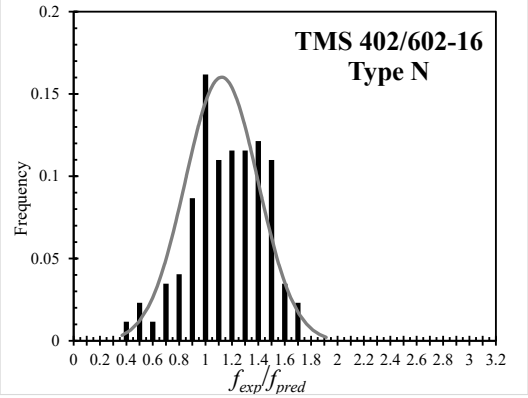

(d) TMS 402/602-16

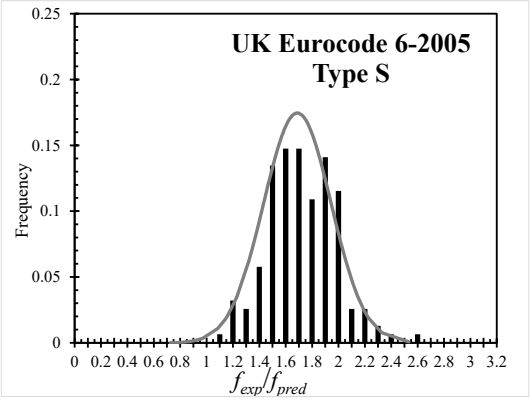

(e) Eurocode 6-2005

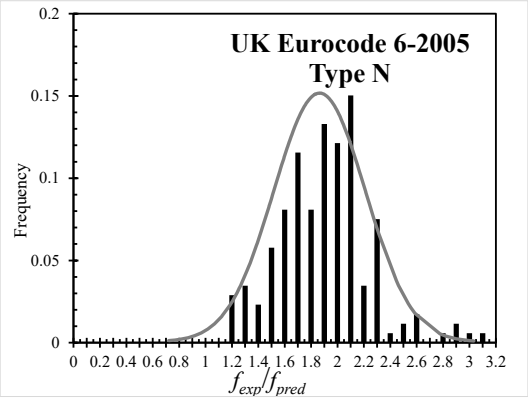

(f) Eurocode 6-2005

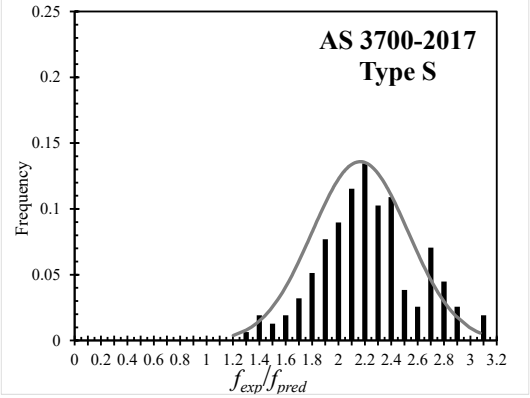

(g) AS 3700-2017

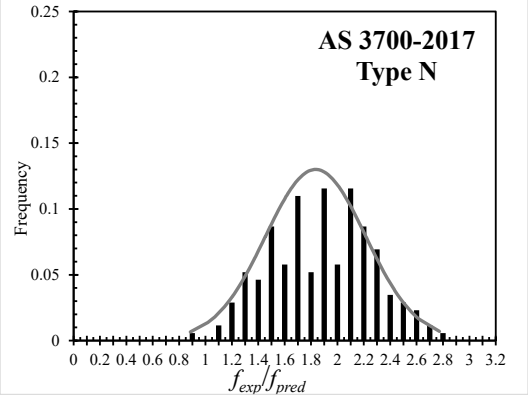

(h) AS 3700-2017

Figure 3-14: Histogram for overall prediction error of a) & b) CSA S304.1-14, c) & d) TMS 402/602-16, e) & f) Eurocode 6-2005, g) & h) AS 3700-2017 for type S & N mortar

Table 3-6: Descriptive statistics values of f_{exp}/f_{pred} for the international masonry design codes and the proposed FE model

Test-to-prediction ratio	Mortar Type						Overall Database		
	Type S			Type N					
	Mean	STD.	COV (%)	Mean	STD.	COV (%)	Mean	STD.	COV (%)
CSA S304.1-14	1.24	0.20	16.2	1.36	0.32	23.2	1.30	0.27	21.1
Eurocode 6-2005	1.67	0.26	15.5	1.85	0.35	18.9	1.77	0.32	18.2
TMS 402/602-16	1.13	0.21	18.6	1.11	0.28	25.1	1.12	0.25	22.2
AS 3700-2017	2.17	0.37	16.8	1.83	0.38	20.9	1.99	0.41	20.7
FEM	1.01	0.22	22.1	1.02	0.18	17.5	1.02	0.21	20.2

It is shown in Table 3-6 that the proposed FE model has the best correlation between prediction results and experimental results, while Eurocode 6 and AS 3700 both have over-conservative prediction results with an average f_{exp}/f_{pred} ratio of 1.77 and 1.99, respectively. As for different types of mortar, the Eurocode 6 performed well regarding the coefficient of variance, while the average f_{exp}/f_{pred} ratio is 1.67 and 1.85 for type S and type N mortar respectively, which is significantly over-conversative. The CSA S304-14 performed well for type S mortar with an average f_{exp}/f_{pred} ratio of 1.24 and a coefficient of variation of 16.2%. The proposed FE model, on the other hand, provides a better prediction result with an average f_{exp}/f_{pred} of 1.02. When it comes to type N mortar, the CSA S304-14 shows a more conservative prediction comparing to the proposed FE model which performed well with an average f_{exp}/f_{pred} ratio of 1.36. Overall, the TMS 402/602-16 shows the most accurate prediction with an average of 1.1 which can be insufficient sometimes (i.e., the compressive strength is over-predicted when the unit strength is smaller than 20 MPa, while it is under-predicted when the unit strength is greater than 20 MPa). The CSA S304-14 is still more conservative than the proposed FE model when type N mortar is adopted even a 95% confidence lower limit is applied to the proposed FE model, which shows the over-conservative of CSA S304-14 of some types of prisms. Both Eurocode 6-2005 and AS 3700-2017 are way over-conservative and significantly underestimated the compressive strength of masonry. In contrast, the proposed numerical prism testing method provided an overall good prediction without a systematic bias.

Histograms of the f_{exp}/f_{pred} ratio are presented in Figure 3-14. It can be observed that the proposed FE model has the most consistent prediction values and the f_{exp}/f_{pred} ratio is concentrated around 1.0. The histogram of the f_{exp}/f_{pred} ratio of AS 3700-2017 has the heaviest tail and will significantly over-estimate the compressive strength of masonry.

3.3.3 Height-to-thickness correction factors re-evaluation

Using the proposed FEM, the height-to-thickness correction factors of masonry compressive strength are re-evaluated. The re-evaluation of height-to-thickness correction factors are based on different mortar types. The height-to-thickness correction factor is taken as 1 when the masonry prism height-to-thickness ratio is 5. Based on the database (Appendix A) previously mentioned,

the height-to-thickness correction factors are re-evaluated by modifying the CMU course number. The summary of the re-evaluated height-to-thickness correction factors are presented in Table 3-7:

Table 3-7: Summary of height-to-thickness correction factors based on the proposed FEM

Height-to-thickness ratio	Type S & N	Type S Mortar			Type N Mortar		
	CSA	Mean	Std	COV	Mean	Std	COV
3	0.9	0.946	0.036	0.039	0.959	0.033	0.034
4	0.95	0.976	0.038	0.039	0.995	0.022	0.022
5	1	1.014	0.028	0.028	1.005	0.013	0.012
6	1	1.008	0.042	0.041	1.002	0.026	0.026
7	1	1.001	0.045	0.045	1.009	0.027	0.027
8	1	0.998	0.051	0.051	1.009	0.033	0.033

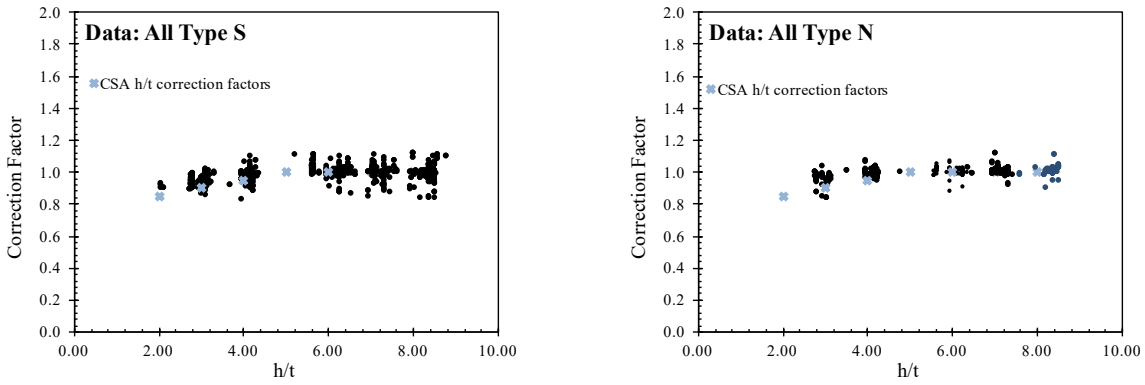

(a) (b)

Figure 3-15: Comparison of the height-to-thickness correction factor for CSA S304 and the proposed FEM: (a) type S mortar, (b) type N mortar

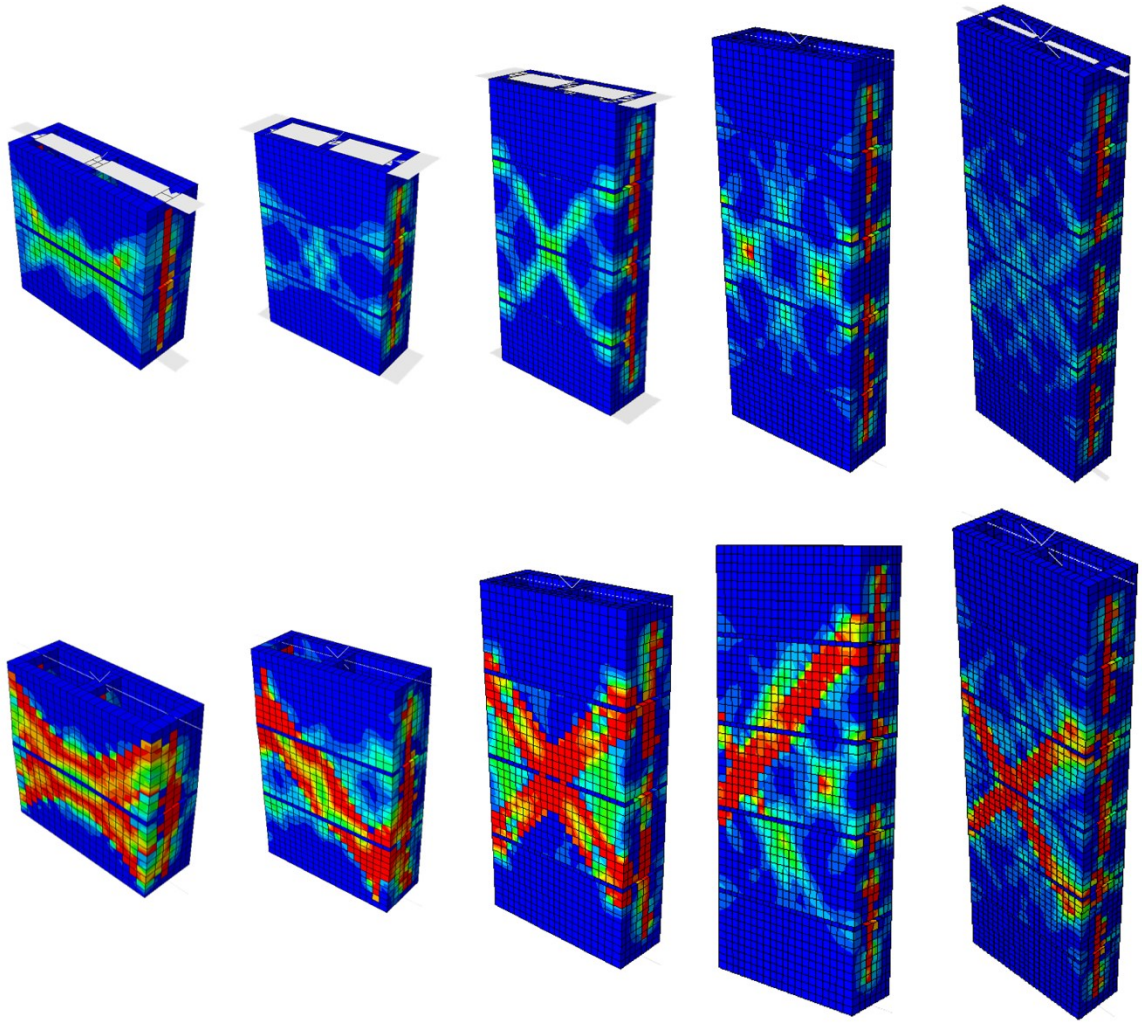

Figure 3-16: The failure mechanism occurred in FE models based on different height-to-thickness ratios (top row: peak load; bottom row: ultimate load)

The comparison of the CSA S304 proposed and re-evaluated height-to-thickness correction factors based on the database mentioned is presented in Figure 3-15. The failure mechanism occurred in FE models based on different height-to-thickness ratios at peak and ultimate load is presented in Figure 3-16. It can be observed in Figure 3-15 and Table 3-7 that the height-to-thickness correction factor stays at 1.0 when the height-to-thickness ratio of masonry prism is equal to or greater than 4, which can be explained by the failure mechanism presented in Figure 3-16. It can be observed that when CMU course number increases, tensile splitting occurs on the webs along the entire prism while the face-shell damage only occurs in the center of the prism. Based on the FEM result,

it is found that increasing the course number has no effect on the compressive strength of masonry due to the localized damage occurred at the mid-span of the prism, which is consistent with CSA S304.

3.4 FE Model-based Global Sensitivity Analysis (GSA)

Uncertainty quantification has become more and more important over time in the engineering field. Comparing with deterministic modeling, stochastic modeling accounts for the inevitable uncertainties existed in the physical world. However, to collect the large amounts of information needed for the uncertainty quantification, repetitive runs of expensive computational models (i.e., FE model) are required. Thus, metamodeling offers a convenient and inexpensive surrogate. A sensitivity analysis is developed over different concrete masonry units and mortar combinations. Multiple approaches are available for conducting sensitivity analysis. Namely three methods that are commonly used including correlation-based measures, linearization methods and global methods. Comparing with the first two methods, global methods take into account the whole input domain. Both the individual variables and the effects of the interactions between multiple variables are considered (Zhu et al. 2017).

Thus, global sensitivity analysis method is adopted for the sensitivity analysis in this study. An uncertainty quantification framework (Marelli and Sudret 2014) implemented in MATLAB is adopted to carry out the analysis. First, input samples and their distribution can be obtained from experimental studies. Then the simulation model is chosen. The most used models include Monte Carlo and polynomial chaos expansion. After that an uncertainty analysis is conducted. Finally, the sensitivity indexes can be calculated and the sensitivity level of different input parameters can be depicted in a pie chart.

3.4.1 Methodology

The modeling scheme of global sensitivity analysis is presented here in Figure 3-17. First, Latin hypercube sampling (LHS) method is adopted to generate the input values in MATLAB. The experimental design (ED) size is 500. Then the numerical analysis is run through the FE computational model using the developed automated tool, and the compressive strength is collected as the output variable. After finishing the input-output experimental design, a PCE-based

Sobol' indices global sensitivity analysis is performed to decompose the variance of the output into indices that can be attributed to the input variables. Leave-one-out (LOO) cross-validation is used to obtain a compromise between estimation and reasonable computational cost. The size of the validation set is 10^4.

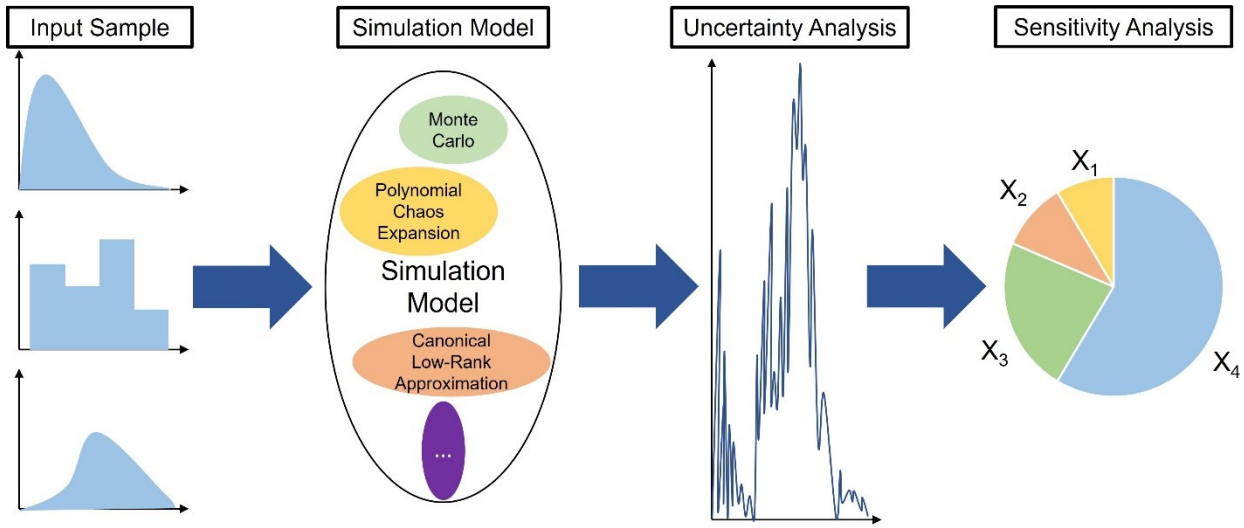

Figure 3-17: Modeling scheme of global sensitivity analysis

3.4.1.1 Sensitivity indices

Sobol' indices method, also referred to as Analysis of variance (ANOVA), is based on the idea describing the total variance in terms of the decomposition of independent input variables. The index regarding one single input variable is the so-called first-order Sobol' index, which represent the individual effect. Interaction indices with respect to multiple variables and the interaction effects between them are called the higher-order indices, which cannot be decomposed into individual variables. The total Sobol' indices are the total contribution concerning every single variable.

3.4.1.2 PCE-based estimation

Polynomial chaos expansions (PCE) are a surrogate modeling technique that approximate computational models through polynomial functions. Sobol' indices are typically evaluated using

Monte Carlo simulation. In order to evaluate the Sobol' indices with the computationally costly models (i.e., FE models), metamodeling approach can be adopted as an effective surrogate.

3.4.2 Results and discussion

Both strong unit-weak mortar prisms and weak unit-strong mortar prisms are studied. For the former combination, numerical prisms are built using concrete masonry units with a nominal strength of 20 MPa and both type S and type N mortar. As for the latter combination, numerical prisms are built using concrete masonry units with a nominal strength of 10 MPa and both type S and type N mortar. Both the concrete block unit compressive strength and the mortar compressive strength are adopted from the experimental program carried out by Gayed et al. (2012) and Ross (2013) (represented by G and R in Table 3-8), which the average measured unit strength is 29.87 MPa for U20 and 8.15 MPa for U10. The statistics of the input variables adopted in the experimental design and the PCE validation set are summarized in Table 3-8. Six random variables are considered in total, which five of them are normally distributed including compressive strength of concrete unit, compressive strength of mortar, elastic modulus of concrete unit, elastic modulus of mortar and thickness of mortar layer. The Poisson's ratio of mortar is the sixth variable with a uniform distribution ranging from 0.05 to 0.25 (Hamid and Chukwunenye 1986, represented by H in Table 3-8).

Table 3-8: Input parameters used in GSA

Nr.	Variable	Mean	Cov (%)	Reference	Distribution
1	Unit compressive strength U10	8.15 MPa	10.41	G and R	Normal
2	Unit compressive strength U20	29.87 MPa	16.04	G and R	Normal
3	Unit elastic modulus U10	9325.9 MPa	17.82	G and R	Normal
4	Unit elastic modulus U20	37075.9 MPa	4.82	G and R	Normal
5	Mortar compressive strength Type S	15.72 MPa	21.7	G and R	Normal
6	Mortar compressive strength Type N	8.59 MPa	30.99	G and R	Normal
7	Mortar elastic modulus Type S	19160 MPa	12.5	Appendix A	Normal
8	Mortar elastic modulus Type N	11748 MPa	17.3	Appendix A	Normal
9	Mortar thickness	10 mm	9.11	CSA S304	Normal
10	Mortar poisson's ratio	LB: 0.05	UB: 0.25	H	Uniform

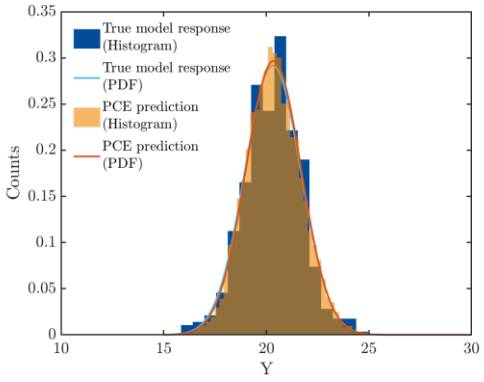

(a) 20 MPa nominal strength units and type N mortar

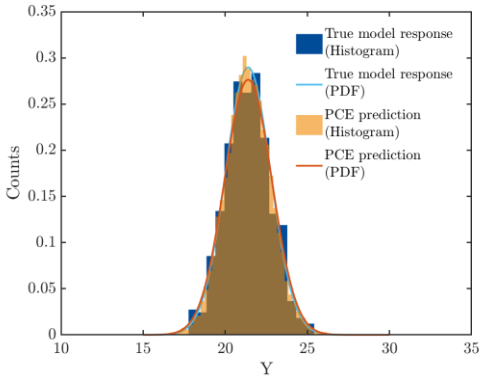

(b) 20 MPa nominal strength units and type S mortar

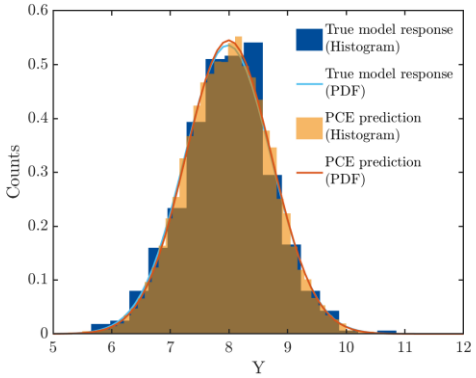

(c) 10 MPa nominal strength units and type N mortar

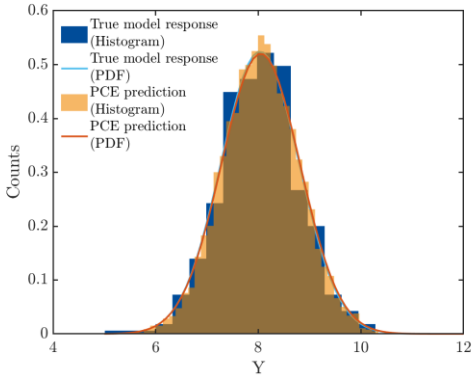

(d) 10 MPa nominal strength units and type S mortar

Figure 3-18: True model response & PCE prediction: (a) 20 MPa nominal strength units and type N mortar, (b) 20 MPa nominal strength units and type S mortar, (c) 10 MPa nominal strength units and type N mortar and (d) 10 MPa nominal strength units and type S mortar

It is shown in Figure 3-18 that the PCE model can well represent the true finite element model. The LOO errors are 0.0909, 0.0406, 0.0799 and 0.0668 for 20 MPa units with type N mortar, 20 MPa units with type S mortar, 10 MPa units with type N mortar and 10 MPa units with type S mortar, respectively.

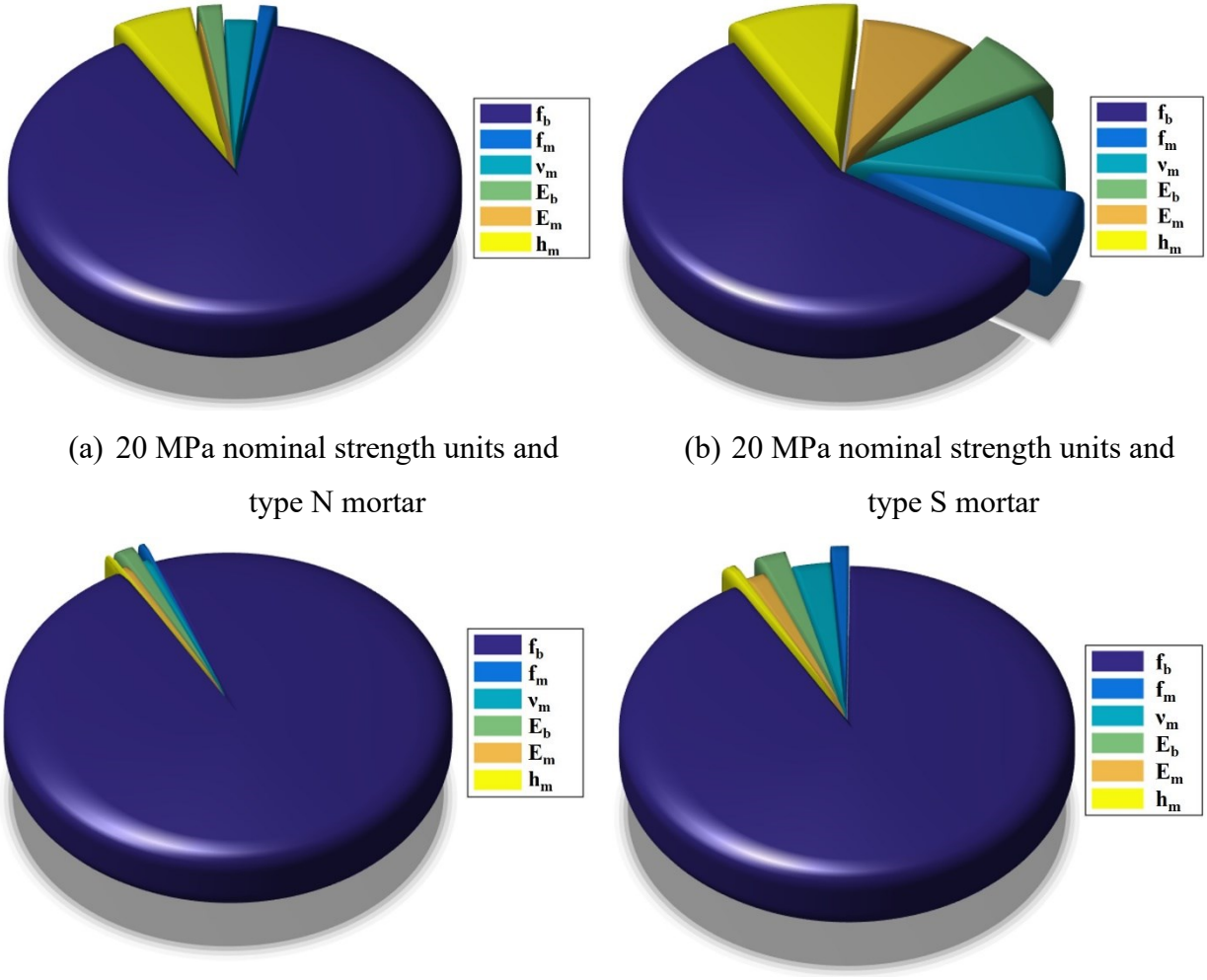

(a) 20 MPa nominal strength units and type N mortar

(b) 20 MPa nominal strength units and type S mortar

(c) 10 MPa nominal strength units and type N mortar

(d) 10 MPa nominal strength units and type S mortar

Figure 3-19: Total Sobol' indices: (a) 20 MPa nominal strength units and type N mortar, (b) 20 MPa nominal strength units and type S mortar, (c) 10 MPa nominal strength units and type N mortar and (d) 10 MPa nominal strength units and type S mortar

The total Sobol' indices are shown in Figure 3-19, where f_b, f_m, μ_m, E_b, E_m, h_m in the figures are compressive strength of concrete unit, compressive strength of mortar, Poisson's ratio of mortar, elastic modulus of concrete unit, elastic modulus of mortar and thickness of mortar layer, respectively. The values of total Sobol' indices, first order Sobol' indices and second order Sobol' indices for masonry compressive strength of the proposed FE model are presented in Table 3-9,

Table 3-10, Table 3-11 and Table 3-12, respectively. For all four combinations, the compressive strength of concrete units has the largest impact over the output variable masonry compressive strength. When units are stronger than mortar layers, the rest of the input variables have a more significant impact over the output variable. The total Sobol' indices of the thickness of mortar layer have the second highest values for prisms constructed with both type S and type N mortar. For prisms built using strong units and weak mortar layers, f_m, μ_m, E_b and E_m have a negligible impact over the output variable when type N mortar is adopted. While for prisms built with type S mortar, the value of total Sobol' indices of μ_m is larger than h_m and plays the second role. The other three input variables also have a significant impact over the output variable. When prisms are constructed using weak units and strong mortar layers, the variance of the output masonry compressive strength is mainly attributed to input f_b. Especially when type N mortar is adopted in this combination, the variance is solely attributed to f_b and E_b. As for the prisms constructed with type S mortar, μ_m and E_b have a larger impact comparing to type N mortar.

Table 3-9: Total Sobol' indices for masonry compressive strength of the proposed FE model

Material types	f_b	f_m	μ_m	E_b	E_m	h_m
Strong unit-weak mortar (20 MPa & Type N)	0.8990	0.0125	0.0233	0.0179	0.0007	0.0581
Strong unit-weak mortar (20 MPa & Type S)	0.8785	0.1050	0.1585	0.1057	0.1302	0.1477
Weak unit-strong mortar (10 MPa & Type N)	0.9853	0.0024	0.0054	0.0127	0.0060	0.0000
Weak unit-strong mortar (10 MPa & Type S)	0.9850	0.0142	0.0306	0.0231	0.0163	0.0076

Table 3-10: First order Sobol' indices for masonry compressive strength of the proposed FE model

Material types	f_b	f_m	μ_m	E_b	E_m	h_m
Strong unit-weak mortar (20 MPa & Type N)	0.8920	0.0109	0.0211	0.0159	0	0.0524
Strong unit-weak mortar (20 MPa & Type S)	0.7685	0.0119	0.0067	0.0179	0.0015	0.0196
Weak unit-strong mortar (10 MPa & Type N)	0.9820	0	0	0.0083	0	0
Weak unit-strong mortar (10 MPa & Type S)	0.9601	0	0	0.0082	0	0

Table 3-11: Second order Sobol' indices for masonry compressive strength of the proposed FE model

Material types	$f_b\mu_m$	f_bE_b	f_bE_m	f_bh_m	$f_m\mu_m$	f_mE_m
Strong unit-weak mortar (20 MPa & Type N)	-	0.0020	-	0.0026	-	-
Strong unit-weak mortar (20 MPa & Type S)	0.0015	-	0.0015	0.0012	-	-
Weak unit-strong mortar (10 MPa & Type N)	-	0.0014	-	-	0.0024	-
Weak unit-strong mortar (10 MPa & Type S)	-	-	-	-	-	0.0011

Table 3-12: Second order Sobol' indices for masonry compressive strength of the proposed FE model (continued)

Material types	μ_mE_b	μ_mE_m	μ_mh_m	E_bE_m	E_mh_m
Strong unit-weak mortar (20 MPa & Type N)	-	-	-	-	-
Strong unit-weak mortar (20 MPa & Type S)	0.0020	-	0.0024	-	0.0009
Weak unit-strong mortar (10 MPa & Type N)	-	0.0030	-	0.0010	-
Weak unit-strong mortar (10 MPa & Type S)	0.0012	-	-	-	-

Based on Table 3-9, the compressive strength of concrete unit alone has the main contribution to the masonry compressive variance. All six input variables have contributed to the output variance alone for strong unit-weak mortar prisms. While for weak unit-strong mortar prisms, only the two input variables: the compressive strength and the elastic modulus of concrete block unit has contribution to the output variance alone. When it comes to higher-order interaction indices, the Poisson's ratio of mortar has the main contribution to the output variance.

The results indicate that the compressive strength of masonry is more significantly affected by concrete unit compressive strength. When the prism is constructed using relatively stronger unit and relatively weaker mortar, thickness of mortar also has an unneglectable impact on masonry compressive strength. As for the prism constructed using relatively weaker unit and relatively stronger mortar, the thickness of mortar has a negligible influence over the output. It can be concluded that the empirical equations can be more accurate over the weak unit-strong mortar type prisms with type N mortar, and less accurate over the strong unit-weak mortar type prisms with type S mortar.

3.5 Chapter Summary and Conclusions

A 3D detailed micro finite element model is developed in this chapter to analyze the behavior of hollow concrete masonry prisms under compression load using commercial software ABAQUS. In this model, concrete damage plasticity (CDP), together with the uniaxial compressive behavior described by the modified Kent-Park model, is adopted for both concrete units and mortar layers. In addition, the tensile behavior is characterized using the concept of fracture energy.

The developed FE models are validated using the available experimental tests of concrete masonry prisms. Validation results proved that the proposed FE model is capable of accurately predicting the behavior of masonry under compression load. A series of parametric study is subsequently carried out. Results indicated that the compressive behavior of masonry prisms is more significantly affected by the physical material parameters and the mortar thickness, which shed lights on the importance of construction quality. Furthermore, the developed FE model is automated using Python and used to conduct a series of numerical prism tests. The results are compared with different numerical models including multiple international masonry design codes

and empirical formulas proposed by other researchers. The results indicate that the proposed FEM has the best prediction ability without a systematic bias comparing to varies masonry design codes and empirical formulas. The height-to-thickness correction factors are re-evaluated using the proposed FEM and the results indicate that the height-to-thickness correction factor stays at 1.0 when the height-to-thickness ratio of masonry prisms is equal to or greater than 4. Besides, a global sensitivity analysis is carried out and contribution of different input variables to the variance of the compressive strength of masonry is studied based on different concrete masonry units and mortar types. Six input parameters are taken into consideration in the GSA, and it can be reflected by the results that the compressive strength of masonry is mostly affected by the compressive strength of CMU. While the other input variables have different impact levels depending on the relationship between the compressive strength of CMU and mortar. The proposed FEM is proven to have an overall good prediction based on a large database and can be used in further sensitivity studies.

The proposed FEM can be adopted in varies ways for future studies. Workmanship study can be carried out by modifying the geometric parameters of mortar layers using the proposed FEM. Besides, similar sensitivity analysis and studies about the compressive behaviours of grouted masonry prisms can be carried out using the proposed FEM with some modifications to the material properties and contact definition.

CHAPTER 4:PREDICTION OF HOLLOW CONCRETE MASONRY PRISM COMPRESSIVE STRENGTH BASED ON GAUSSIAN PROCESS REGRESSION SURROGATE MODEL

4.1 Introduction

The popularity of masonry structures can be attributed to their attractive aesthetics, great durability, high thermal performance (ACI/TMS 122R-14 2014), and more importantly, great mechanical properties under compression. Among various masonry types, hollow concrete block masonry has been widely used in North America. The compressive strength of masonry is an essential mechanical property considering its important role in masonry structural design; its prediction accuracy and precision (i.e., uncertainty) affects the reliable and economic design of masonry walls.

In addition to physical prism testing, several numerical studies have been carried out on the behaviour of masonry prisms under compression (Drysdale and Guo 1991; Suwalski and Drysdale 1986; Pina-Henriques and Lourenço 2003 & 2006; Barbosa et al. 2009; Hamid and Chukwunenye 1986). In general, numerical models are complicated due to its requirements for a series of constitutive models and the corresponding model parameters in order to describe the failure mechanisms. In contrast, based on the data generated from prism tests, various empirical models have been proposed, which include the compressive strength determination methods proposed by different masonry design codes and other models proposed in the literature (Mann 1982; Guo 1991; Köksal et al. 2005; Fortes et al. 2015). However, the accuracy of these models is rarely evaluated with uncertainty quantified probabilistically. Furthermore, the empirical models developed by assuming the explicit parametric model form assumed in the empirical functions could be problematic in accuracy or generalization. Alternatively, as a new form of data-based modeling method, soft-computing techniques using artificial intelligence (AI) or machine learning (ML) can be used, especially non-parametric models.

In the past three decades, AI or ML methods have been increasingly adopted in civil engineering. Compared to the above-mentioned traditional methods (i.e., empirical formulas), AI or ML models have been proven to be more powerful. For example, Artificial Neural Networks (ANN) and Gaussian Process Regression (GPR) models have been commonly used, due to their great

flexibility in function approximations, in studying the mechanical properties of concrete, including compressive strength and elastic modulus of concrete (Tayfur et al. 2014; Ahmadi-Nedushan 2012; Duan et al. 2013; Asteris et al. 2021; Dao et al. 2020). When it comes to the specific problem of masonry compressive strength prediction, ANN is more widely adopted than GPR. The most commonly used ANN structure is the multilayered feed-forward perception network, which is consisted of neurons that are distributed into at least three layers. Typically, the layers include one input layer, one output layer and at least one hidden layer in-between. Zhou et al. (2016) adopted backpropagation (BP) algorithm based multilayered feed-forward networks for predicting the compressive strength of hollow concrete block masonry prisms. In that study, a total of 90 datasets, consisting of 308 prism specimens, were collected and used to develop predictive models based on three input variables (i.e., masonry unit compressive strength, mortar compressive strength, and prism height-to-thickness ratio). The network developed in this study is consisted of 3 neurons in the input layer, 12 neurons in the one hidden layer and 1 neuron in the output layer. Asteris et al. (2019) applied BP algorithm based multilayered feed-forward networks for predicting the compressive strength of masonry prisms with various brick materials, including earth bricks, clay bricks, concrete bricks, silicate bricks, based on a total of 232 specimens collected from the literature. The development of the proposed network is based on hidden layers ranging from 1 to 2 with the number of neurons ranging from 1 to 30 for each hidden layer. The results prove that the optimum network is consisted of 3 neurons in the input layer, two hidden layers with 8 and 28 neurons respectively and 1 output neuron. Lan et al. (2020) utilized three-layer BP neural network to predict the compressive strength of earth block masonry based on three input parameters: compressive strength of bocks, compressive strength of mortar, and prism height-to-thickness ratio, with a total of 72 groups of datasets (348 specimens). The model consists of 3 neurons in the input layer, one hidden layer with the number of neurons ranging from 3 to 12 and 1 output neuron. Garzón-Roca et al. (2013) also used three-layer BP algorithm to determine the compressive strength of clay brick masonry using the compressive strength of clay brick and cement mortar, based on a total of 19 experimental studies (96 specimens). A 2-n-1 feed-forward multilayer perception network is adopted in this study, which is consisted of 2 input neurons, 1 output neuron and one hidden layer with n neurons where n varies from 1 to 6. However, ANN model developments depend on the pre-selected configuration (e.g., number of layers and number of

nodes for multilayered feed-forward neural network) and typically requires a relatively large number of data samples for training. When the sample size of data collected is relatively small, it can potentially lead to overfitting and lack of generalization.

In contrast, GPR, as a nonparametric probabilistic ML algorithm, has the advantage of leveraging or integrating prior knowledge with data observed, which allows it to be less dependent on the data and thus more suitable when limited data exist. As such, GPR-based model can be continuously updated when more data is observed. Additionally, the prediction uncertainty or error can be provided after the model training process in GPR model development. GPR, also known as Kriging method, is constructed based on Gaussian processes to probabilistically represent an extensive variety of functions. GPR was first applied to geo-statistics as a spatial interpolation tool by Krige back in the 1950s (Krige 1951) and subsequently formalized by Matheron (1963). Later on, GPR was adopted as a form of surrogate modeling by Sacks et al. (1989), in which Gaussian Process modeling was used to replace the time-consuming computational model with an input-output mapping. For instance, Chisari et al. (2018) adopted GPR as the surrogate of the detailed FE model and carried out a sensitivity analysis of a brick-masonry mesoscale model. Moravej et al. (2019) used the modular Bayesian approach to replicate the undamaged to damaged states of real masonry structures, while Gaussian Process was adopted to reduce the calculation burden. Peng et al. (2020) proposed a new method based on GPR to calculate the reliability index for in-plane shear failure of unreinforced masonry walls, which indicated that the proposed GPR model was very efficient in probabilistic modeling. In a related research, Peng et al. (2019) used the deterministic shear model as the prior GPR model and then updated the prior model with the collected test results. The GPR models were proven to be very efficient and very convenient to be improved with the new data. Tubaldi et al. (2020) used GPR for global sensitivity analysis and uncertainty propagation. These studies have shown the great potential of GPR for masonry structures, but no relevant work has explored its potential for predicting the compressive strength of hollow concrete block masonry.

As such, this chapter aims to construct GPR models for the purpose of predicting the compressive strength of hollow concrete block masonry. GPR, the soft computing technique used for masonry strength prediction, will be briefly introduced and followed by sensitivity analysis using GPR. The

GPR models developed based on the database compiled is discussed, together with comparison of existing empirical models, including the deign code models. In particular, the prescribed values given by the current Canadian Masonry Design Standard CSA S304-2014 (2014) for masonry strength determination is re-evaluated with uncertainty quantified, considering that the tabulated values for hollow concrete masonry compressive strength and the height-to-thickness correction factors was based on outdated experimental studies (Maurenbrecher 1980, 1983, 1985, 1986).

4.2 Experimental Database

To develop a reliable and accurate surrogate model, a database is required for training and testing. The same database aforementioned in Chapter 3 is adopted here (Appendix A). The compiled database contains prims with concrete masonry units (CMUs) of a wide range of compressive strength (e.g., from 10 MPa to 40 MPa), mortars of types S and N. The histograms of the compressive strength of CMUs and mortars for prisms with type S and N mortar are shown in Figure 4-1 a to d. A good coverage of practical values is represented by the database compiled. Note that the compressive strength of concrete masonry unit (CMU), compressive strength or type of mortar are the most prominent variables in accordance with the masonry design standards (CSA S304-14, TMS 402/602/-16, European Standard 2005, Australian Standard 2017) and the commonly used empirical formulas (Mann 1982, Guo 1991, Köksal et al. 2005, Fortes et al. 2015). Additionally, another important variable is the prism height-to-thickness ratio (h/t), which is needed when prism testing data is used, and its histogram of the prisms in the database is shown in Figure 4-1 e and f. In this study, Gaussian Process models will be proposed to predict the output variable compressive strength of concrete block masonry based on these three input variables for masonry with type S and N mortar, respectively. Thus, the entire database is divided into two groups based on mortar type: type S mortar or type N mortar in accordance with the masonry design codes (CSA S304-14, TMS 402/602-16). Tests from 161 data points (a total of 781 prisms constructed with type N mortar) and 151 data points (646 prisms constructed with type S mortar) were analyzed, respectively. As mentioned in CSA S304-14, mortar with compressive strength of 5 – 12.5 MPa was classified as type N, and mortar with compressive strength of 12.5 – 17.6 MPa was classified as type S following the strength requirements from CSA A179. Note that according to TMS 602, mortar with compressive strength over 17.6 MPa was classified as type M. However,

it should be noted that since the latest revision of CSA has classified both type M and S together as type S mortar, the present study will follow suit.

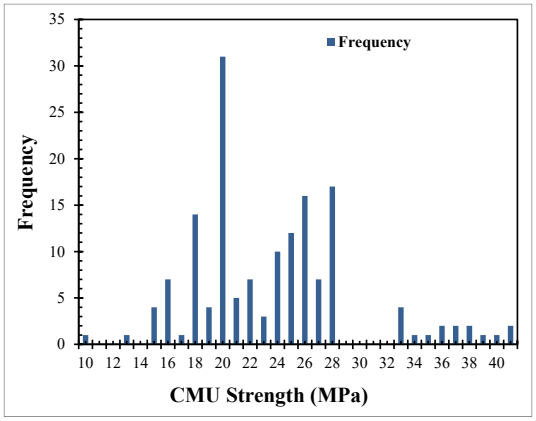

(a)

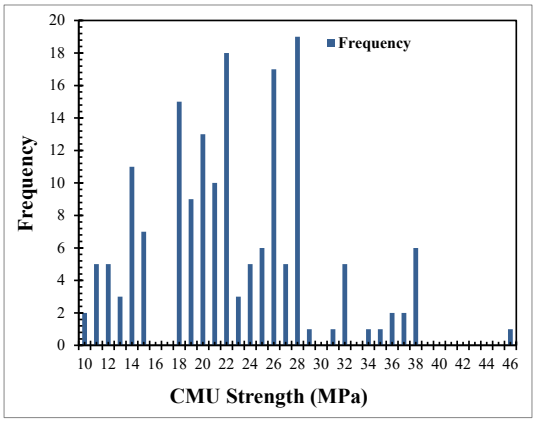

(b)

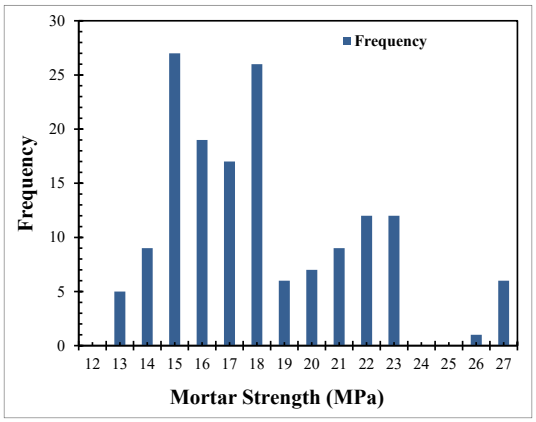

(c)

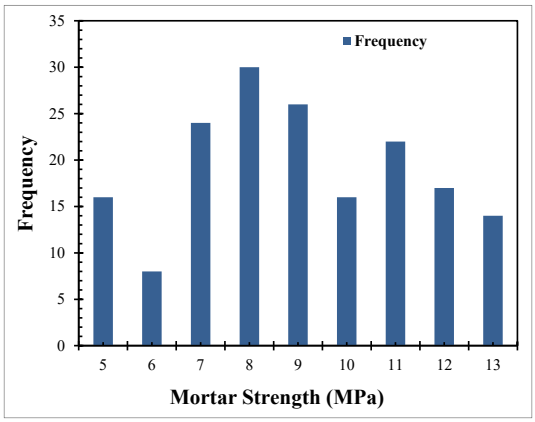

(d)

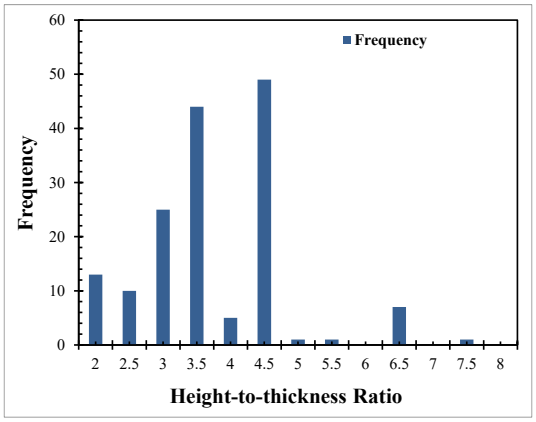

(e)

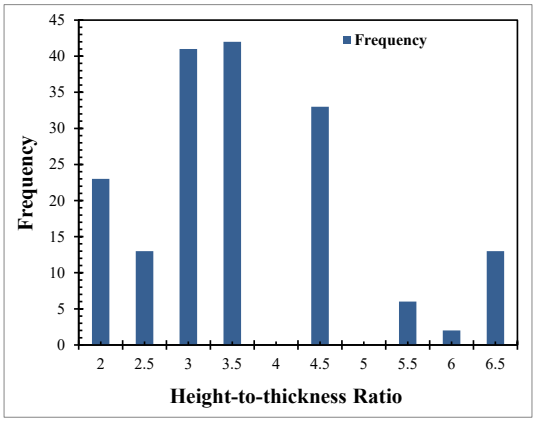

(f)

Figure 4-1: Histograms of input variables in the database: a) CMU compressive strength (prisms with type S mortar), b) CMU compressive strength (prisms with type N mortar), c) mortar compressive strength (prisms with type S mortar), d) mortar compressive strength (prisms with type N mortar), e) prism height-to-thickness ratio (prisms with type S mortar), f) prism height-to-thickness ratio (prisms with type N mortar)

The database compiled will be mainly used for three purposes in this study: (1) building GPR models to predict the compressive strength of masonry, (2) re-evaluating the currently prescribed values for masonry compressive strength, and (3) re-evaluating the currently used height-to-thickness correction factors in CSA S304-14. Note that (1) will be discussed in the following section 4.3 while (2) and (3) will be discussed in section 4.5.

4.3 Gaussian Process Regression (GPR) Modeling

The main purpose of using Gaussian Process Regression is to predict one or multiple certain outputs and uncertainty quantification. The graphical representation of the GPR model construction is presented in Figure 4-2.

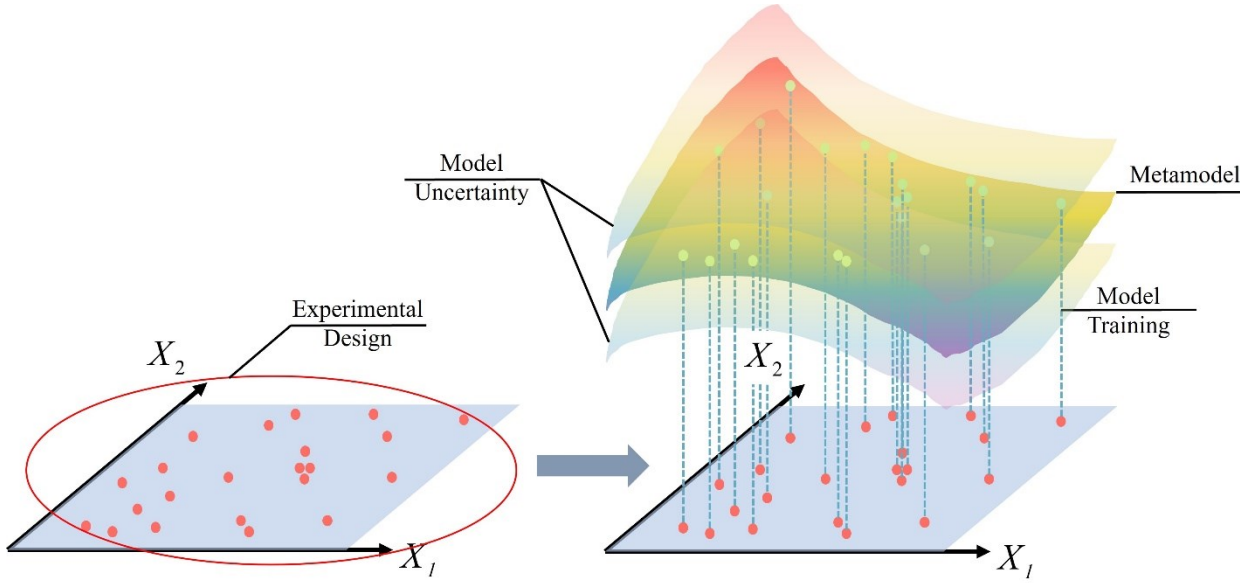

Figure 4-2: Graphical representation of the architecture GPR model metamodel construction

The construction process consists of three stages: experimental design, GPR model training and GPR model testing. The first step of the construction process is called the experimental design process, which is illustrated on the left side of Figure 4-2. The purpose of the experimental design

process is to gather information about the relationship between the input samples and the corresponding output responses generated using including chosen sampling methods (i.e., Monte Carlo sampling, Latin Hypercube sampling and Sobol' sequence sampling etc.), or through computational models (i.e., finite element models) or experimental testing. Note that only experimental testing data is used to construct GPR models in this study. After the input sample points and the corresponding outputs are gathered, part of the collected database (i.e., 80%) can be used as the training set. Then, the relationship between the input samples and the corresponding output response can be learned through the training process which is illustrated on the right side of Figure 4-2. After the GPR model is successfully trained, the testing process can be carried out based on the remaining dataset. Note that even deterministic models are adopted in the training process (i.e., FEM experimental design), the GPR output response includes uncertainties. Gaussian Process modeling is stochastic metamodeling technique which considers the output response as a realization of the modeling process. According to Santner et al. (2003), GPR is described by the following equation which is consisted of its two terms:

$$M^K(x) = \beta^{\mathrm{T}} f(\boldsymbol{x}) + \sigma^2 Z(\boldsymbol{x}, \omega) \qquad \text{(Eq. 4-1)}$$

where $\beta^T f(\boldsymbol{x})$ is the mean function (i.e., trend) of the Gaussian Process metamodel and $\sigma^2 Z(\boldsymbol{x}, \omega)$ is the correlation function (a.k.a. kernel function) of the Gaussian Process metamodel. The mean function is consisted of $\{f_j; j=1, \ldots, P\}$ and the unknown corresponding coefficients $\{\beta_j; j=1, \ldots, P\}$, where P is the total number of basic arbitrary functions. The correlation (kernel) function is consisted of σ^2, which is the constant variance of the Gaussian Process and a zero-mean, unit-variance, stationary Gaussian Process $Z(\boldsymbol{x}, \omega)$. Here ω represents the underlying probability space and its definition is based on an autocorrelation function R and its hyperparameters $\boldsymbol{\theta}$. The correlation between two output sample points is represented by the autocorrelation function (kernel function) $k = k(\boldsymbol{x}, \boldsymbol{x'}; \boldsymbol{\theta})$. In other words, the similarity between the output samples is defined by the autocorrelation function (Rasmussen 2003).

4.3.1 Mean function types

Different mean functions can be adopted in the Gaussian Process model. Namely the three types (Dubourg 2011) listed below: ordinary (constant) mean function, linear mean function and quadratic mean function.

In ordinary mean function, the mean function is an unknown constant. The function form is presented below, where $f_0(\boldsymbol{x}) = 1$:

$$\beta^{\mathrm{T}} f(\boldsymbol{x}) = \beta_0 f_0(\boldsymbol{x}) = \beta_0 \quad \text{(Eq. 4-2)}$$

In linear mean function, the mean function is assumed to be a linear combination of prescribed random functions:

$$\beta^{\mathrm{T}} f(\boldsymbol{x}) = \beta_0 + \sum_{i=1}^{M} \beta_i x_i \quad \text{(Eq. 4-3)}$$

Quadratic mean function:

$$\beta^{\mathrm{T}} f(\boldsymbol{x}) = \beta_0 + \sum_{i=1}^{M} \beta_i x_i + \sum_{i=1}^{M} \sum_{j=1}^{M} \beta_{ij} x_i x_j \quad \text{(Eq. 4-4)}$$

4.3.2 Correlation function types

Since the definition of the approximation function is included, the correlation function (also known as the kernel function or the covariance function) has a significant impact on the prediction ability of Gaussian Process models (Rasmussen 2003). Therefore, the kernel function is an extraordinarily important factor in Gaussian Process modeling. The main role of the kernel function is to describe the relationship between the training points and the new points, in other words, how similar the new points are to the training points with regard to the distance in between them. On this matter, the new points that are close to the training points should have similar responses.

Generally speaking, all the kernel functions mentioned here are stationary correlation functions. In this study, four different types of kernel functions (Rasmussen and Williams 2006) are adopted for masonry compressive strength prediction and the results are compared: squared exponential kernel (also called Gaussian kernel), exponential kernel, Matern 3/2 and Matern 5/2.

Squared exponential kernel is one of the most used kernel functions (Rasmussen and Williams 2006). The function is presented below:

$$k(x_i, x_j; \theta) = \sigma_f^2 \exp\left[-\frac{1}{2} \frac{(x_i - x_j)^T (x_i - x_j)}{\sigma_l^2} \right] \quad \text{(Eq. 4-5)}$$

where σ_f is the standard deviation of the signal and σ_l is the length scale which determines the distance in the input space that makes the function values uncorrelated.

Exponential kernel is defined as follows:

$$k(x_i, x_j; \theta) = \sigma_f^2 \exp\left[-\frac{r}{\sigma_l}\right] \quad \text{(Eq. 4-6)}$$

where $r = [(x_i-x_j)^T(x_i-x_j)]^{1/2}$.

The Matern functions are a series of kernel functions which have the same feature. Simplified forms can be used when computing the Matern functions, where the differentiable time (the ceiling value of v-1) of the corresponding Gaussian process are taken as p + ½ (p is a non-negative integer). The most commonly adopted v values are 3/2 and 5/2, for which the kernel functions are called Matern-3/2 and Matern-5/2, respectively. Matern-3/2 is defined as follow:

$$k(x_i, x_j; \theta) = \sigma_f^2 \left(1 + \frac{\sqrt{3}r}{\sigma_l}\right) \exp\left(-\frac{\sqrt{3}r}{\sigma_l}\right) \quad \text{(Eq. 4-7)}$$

Matern-5/2 is defined as follow:

$$k(x_i, x_j; \theta) = \sigma_f^2 \left(1 + \frac{\sqrt{5}r}{\sigma_l} + \frac{5r^2}{3\sigma_l^2}\right) \exp\left(-\frac{\sqrt{5}r}{\sigma_l}\right) \quad \text{(Eq. 4-8)}$$

4.3.3 Estimation methods

Different from model parameters, in machine learning, hyperparameters are configurations that are defined prior to the training process. According to Murray and Adams (2010), the hyperparameters $\boldsymbol{\theta}$ (i.e., free parameters) can be estimated using several methods. The most commonly used hyperparameter estimation methods include maximum-likelihood estimation method and cross-validation estimation method. The general cross-validation method, K-fold cross validation method (i.e., leave-one-out cross-validation) is adopted in this study. The whole database is divided into K exclusive subsets and the prediction results of the k-th subset is obtained evaluating the model based on all the other subsets. Leave-one-out (LOO) cross-validation is the special case of K-fold cross validation, in which the number of subsets K is equal to the number

of observations and subsequently only one observation is left out to be predicted. The objective of LOO cross-validation is to find the hyperparameters that minimize the overall LOO cross-validation error.

4.3.4 Quality assessment method

For the accuracy assessment and model reliability evaluation purposes, multiple performance metrics including the coefficient of determination R-squared (R^2), Root Mean Square Error (RMSE) and Mean Absolute Error (MAE) are adopted in this study.

The coefficient of determination R^2 is the measurement of the proportion of the variance between the model prediction and the true response. R^2 is a scale-free score, which means regardless of the prediction and the response values, the value of R^2 varies from 0 to 1. It can be said that there is a better correlation between the Gaussian model prediction and the true response when the value of R is close to 1, while the value of R is close to 0 indicates a poor performance of the Gaussian model. RMSE is the square root of the average of the squared difference between the true response and the Gaussian model predicted values. RMSE is the measurement of the standard deviation of residuals (Khosravi et al. 2019, Nguyen et al. 2019, Pham et al. 2018). MAE represents the average of the absolute difference between the true response and the Gaussian model predicted values. MAE is the measurement of the average of the residuals (Ly et al. 2019). Comparing to R^2 value, the lower the RMSE and MAE values are, the better the performance of the Gaussian model is. R value is used for explaining the ability of the independent variables in the regression model representing the variability in the dependent variables. As for RMSE, the advantage is that it is easy to calculate and differentiable. While MAE is more robust to data considering the outliers. Together, the above three performance metrics can reasonably evaluate the overall predictive ability of the Gaussian Process model.

Performance metrics R, RMSE and MAE are defined as follows:

$$R^2 = 1 - \frac{\sum_{i=1}^{N} (y_i - \hat{y})^2}{\sum_{i=1}^{N} (y_i - \bar{\hat{y}})^2} \qquad \text{(Eq. 4-9)}$$

$$RMSE = \sqrt{\frac{1}{N}\sum_{i=1}^{N}(y_i - \hat{y})^2} \quad \text{(Eq. 4-10)}$$

$$MAE = \frac{1}{N}\sum_{i=1}^{N}\left|y_i - \hat{y}\right| \quad \text{(Eq. 4-11)}$$

where N is the number of the sample points; y_i is the true output and $\hat{y}$ is the Gaussian model prediction output; $\overline{\hat{y}}$ is the mean value of the Gaussian model prediction output (Sarıdemir 2009).

4.4 GPR Model Structure Sensitivity Analysis

4.4.1 Parametric study based on different covariance functions

According to Rasmussen (2003), the covariance function is essential in the process of constructing a Gaussian Process model, while the mean function has insignificant influence over the performance of Gaussian Process Regression models. Thus, a parametric study based on different covariance functions is carried out with the most commonly used linear mean function adopted (Dubourg 2011). The comparison of prediction accuracy while using four different covariance functions is presented as follows. Three parameters contained in input vector $\boldsymbol{x}$: CMU compressive strength, mortar compressive and prism *h/t* ratio, are selected as the input variables and the output variable is the masonry prism strength.. The adopted covariance functions include squared exponential kernel, exponential kernel, Matern-3/2 and Matern-5/2. GPR-based model training and testing is carried out based on different mortar types: type S and type N. The proposed GPR models are trained over 80% of the data and validated over the remaining 20% of the data.

The statistical measurements of the GPR model based on different kernel functions are presented below in Table 4-1. Based on Table 4-1, for type S model, squared exponential kernel is selected due to its excellent performance over the testing dataset, considering the four kernel functions have very similar performance over the training dataset. For type N model, exponential kernel function has been selected due to its excellent performance over both training and testing datasets.

Table 4-1: Summary of statistical measurements of prediction error of Gaussian Process models based on different covariance functions

Statistical measurements	Training set (Type S)				Testing set (Type S)			
	Sq-Exp	Exp	Matern32	Matern52	Sq-Exp	Exp	Matern32	Matern52
R^2	0.9027	0.8964	0.9160	0.9233	0.8879	0.8556	0.8217	0.8532
RMSE	1.5322	1.5378	1.4770	1.3465	1.7560	2.1261	1.8650	2.5754
MAE	1.0778	1.0885	1.0011	0.8829	1.3867	1.6876	1.4234	2.1261
Mean	1.0094	1.0092	1.0085	1.0073	1.0033	1.0164	1.0001	0.9324
COV	8.52%	8.35%	8.19%	7.53%	10.20%	12.17%	10.55%	11.50%
	Training set (Type N)				Testing set (Type N)			
	Sq-Exp	Exp	Matern32	Matern52	Sq-Exp	Exp	Matern32	Matern52
R^2	0.9162	0.9571	0.9497	0.9493	0.8934	0.9073	0.8385	0.8584
RMSE	1.4884	1.1153	1.1903	1.1722	1.8371	1.5643	1.9595	1.9762
MAE	1.1260	0.8383	0.8688	0.8679	1.3888	1.1622	1.5458	1.3995
Mean	1.0142	1.0093	1.0095	1.0096	0.9912	1.0065	1.0245	1.0233
COV	10.86%	7.20%	8.18%	8.02%	11.37%	9.66%	12.08%	12.41%

4.4.2 Case study based on different number of input parameters

Based on engineering judgement, three input parameters including concrete masonry unit (CMU) compressive strength, mortar compressive strength and prism height-to-thickness ratio are investigated in this study. Specifically, four different cases of GPR model based on different numbers or different parameters included in the GPR structure are investigated, as shown in Table 4-2. Based on the parametric study conducted in the previous section, squared-exponential kernel function is selected for type S model and exponential kernel is selected for type N model in the subsequent work.

Table 4-2: Cases of Gaussian Process modeling architectures based on different number of input parameters

Case	Input parameters		
	CMU compressive strength	Mortar compressive strength	Prism height-to-thickness ratio
Ⅰ	√		
Ⅱ	√	√	
Ⅲ	√		√
Ⅳ	√	√	√

As shown in Table 4-2, case Ⅰ only includes one parameter: the compressive strength of concrete masonry units. Case Ⅱ and Ⅲ both include two parameters: the compressive strength of concrete masonry units and mortar, or the compressive strength of concrete masonry units and prism height-to-thickness ratio. Case Ⅳ includes all three parameters.

Table 4-3: Summary of statistical measurements of Gaussian Process models based on different number of input parameters

Statistical measurements	Training set (Type S)				Testing set (Type S)			
	I	II	III	IV	I	II	III	IV
R^2	0.8908	0.8926	0.8938	0.9027	0.6742	0.7861	0.7254	0.8879
RMSE	1.6426	1.6093	1.6438	1.5322	2.8977	2.3070	2.4097	1.7560
MAE	1.1730	1.0526	1.1534	1.0778	2.2853	1.7697	1.7368	1.3867
Mean	1.0105	1.0077	1.0097	1.0094	0.9852	1.0067	1.0148	1.0033
COV	8.50%	8.51%	8.62%	8.52%	14.30%	13.05%	14.55%	10.20%
	Training set (Type N)				Testing set (Type N)			
	I	II	III	IV	I	II	III	IV
R^2	0.9253	0.9376	0.9783	0.9571	0.7753	0.8396	0.8163	0.9073
RMSE	1.4306	1.2764	0.7786	1.1153	2.4732	2.2999	2.1172	1.5643
MAE	1.0632	0.9832	0.5402	0.8383	1.8725	1.7836	1.4259	1.1622
Mean	1.0129	1.0119	1.0048	1.0093	1.0067	1.0006	1.0294	1.0065
COV	9.33%	9.19%	4.79%	7.20%	15.82%	16.09%	13.26%	9.66%

Based on Table 4-3, GPR models with different input parameters have very different performances depending on mortar type. Different cases of input parameters only have minor effect over type S model, while more significant differences can be observed in type N models. For type N training model, case III with the compressive strength of CMU and prism height-to-thickness ratio as the input parameters has the best performance with a significantly lower COV (4.79%). This is due to the fact that type N mortar has lower compressive strength and has less impact over the masonry prism compressive strength. However, the extraordinary performance is due to model overfitting, therefore model performance (case III) decreased as observed for the testing dataset. For the testing dataset, case IV with three input parameters have the best performance for both type S and type N model with a much lower COV (type S: 10.2%; type N: 9.66%) and other prediction metrics compared to the other cases. It can be concluded that the prediction results are significantly affected by numbers of input parameters, meanwhile selecting the compressive strength of both concrete units and mortar and the prism height-to-thickness ratio can provide more reliable and accurate results. This is confirmed by the existing empirical models including the design code models. Note that height-to-thickness ratio of masonry prism needs to be one of the input variables for the proposed GPR models for masonry prim strength prediction; thus, the compressive strength of masonry needs to be corrected from masonry prism strength to consider the height-to-thickness ratio.

4.5 Masonry Prism Compressive Strength Prediction Based on the GPR Models

4.5.1 Prediction error quantification with comparison to masonry design codes

According to the current Canadian masonry design code CSA S304-14 and the Eurocode 6-2005, specified masonry compressive strength is prescribed based on the corresponding specified unit strength and mortar type. The specified compressive strength for masonry units shall be calculated based on a minimum of five masonry unit specimens. If fewer than ten units are tested, the coefficient of variation shall be the higher of the calculated value or 10%. The specified compressive strength for masonry shall also be calculated based on a minimum of five masonry prism specimens. The coefficient of variation shall be the higher of the calculated value or 10%. The specified compressive strength for masonry units or masonry prisms shall be calculated as follows:

$$f' = f_{av}(1-1.64\nu) = f_{av} - 1.64s \quad \text{(Eq. 4-12)}$$

where f' is the specified compressive strength; f_{av}, is the mean compressive strength; ν is the coefficient of variation; and s is the standard deviation, respectively. In contrast, the American code TMS 402/602-16 and the Australian code AS 3700-2017 provide the mean prediction. In the GPR model developed, both the mean prediction and 5th percentile prediction can be provided. Thus during accuracy evaluation and comparison, the 5th percentile value and the average value (mean) from the tests are used: namely the 5th percentile value for CSA S304.1-14 and Eurocode 6-2005, and the average value (mean) for TMS 402/602-16 and the Australian code AS 3700-2017.

Table 4-4 summarizes the prediction error represented by the prediction-to-test ratio, namely the compressive strength f_{exp} (the corresponding 5th percentile value for CSA S304.1-14 and Eurocode 6-2005, and the corresponding average value (mean) for TMS 402/602-16 and the Australian code AS 3700-2017) divided by the predicted compressive strength f_{pred} from GPR model or masonry design codes :

Table 4-4: Descriptive statistics values of prediction error f_{exp}/f_{pred} for international masonry design codes and the proposed GPR model

Test-to-prediction ratio	Mortar Type						Overall Database		
	Type S			Type N					
	Mean	STD.	COV (%)	Mean	STD.	COV (%)	Mean	STD.	COV (%)
CSA S304.1-14	1.24	0.20	16.2	1.36	0.32	23.2	1.30	0.27	21.1
Eurocode 6-2005	1.67	0.26	15.5	1.85	0.35	18.9	1.77	0.32	18.2
GPR (5th percentile)	1.26	0.14	10.9	1.22	0.14	11.4	1.24	0.14	11.2
TMS 402/602-16	1.13	0.21	18.6	1.11	0.28	25.1	1.12	0.25	22.2
AS 3700-2017	2.17	0.37	16.8	1.83	0.38	20.9	1.99	0.41	20.7
GPR (mean)	1.00	0.08	8.0	1.00	0.08	8.0	1.00	0.08	8.0

In order to visualize the prediction accuracy and reliability of the proposed GPR model, with comparison to the above-mentioned masonry design code methods, the compressive strength

prediction results for hollow concrete masonry prisms built with type S and N mortar are presented in terms of f_{exp}/f_{pred} in Figure 4-3 and Figure 4-4, respectively.

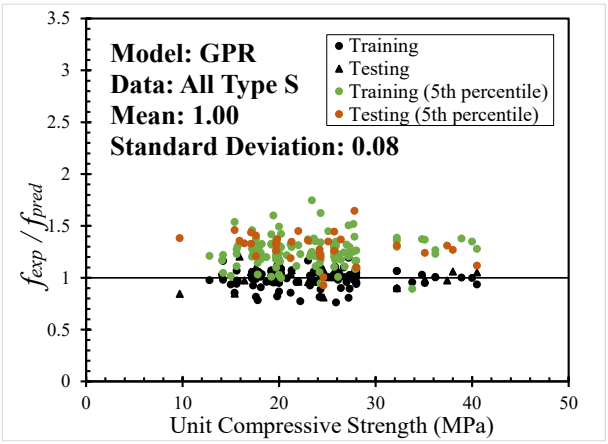

(a)

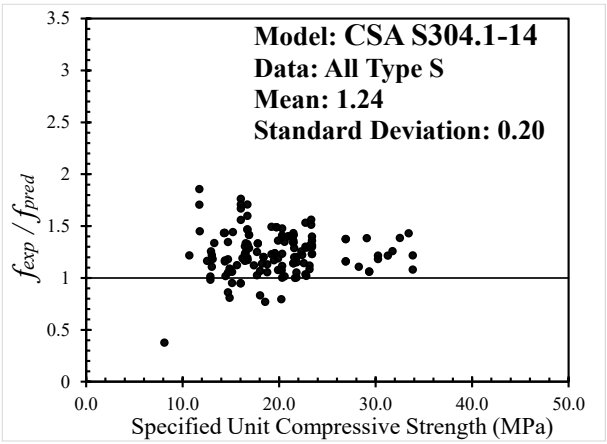

(b)

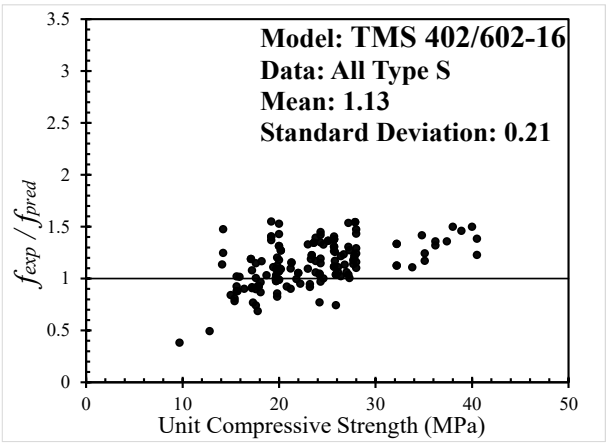

(c)

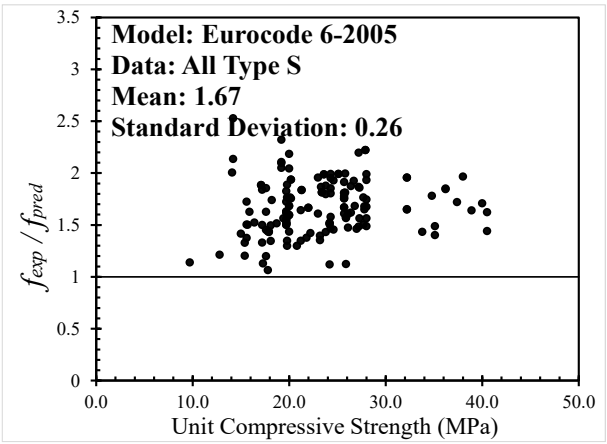

(d)

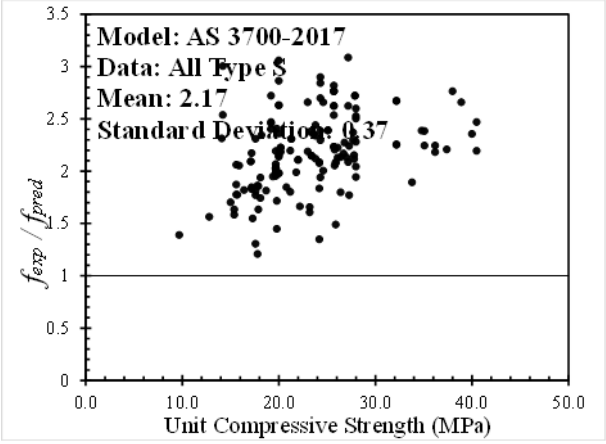

(e)

Figure 4-3: Comparison of prediction error of f_{exp}/f_{pred} for international masonry design codes and the proposed GPR model (type S): (a) GPR, (b) CSA S304-14, (c) TMS 402/602-16, (d) Eurocode 6-2005, (e) AS 3700-2017

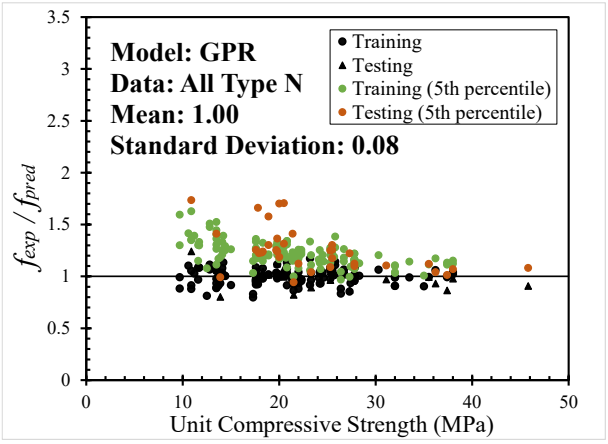

(a)

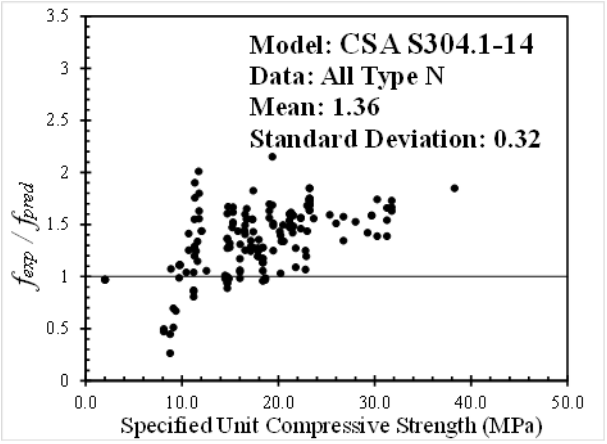

(b)

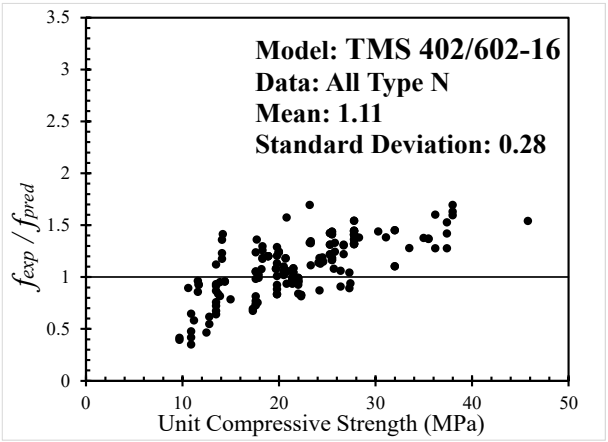

(c)

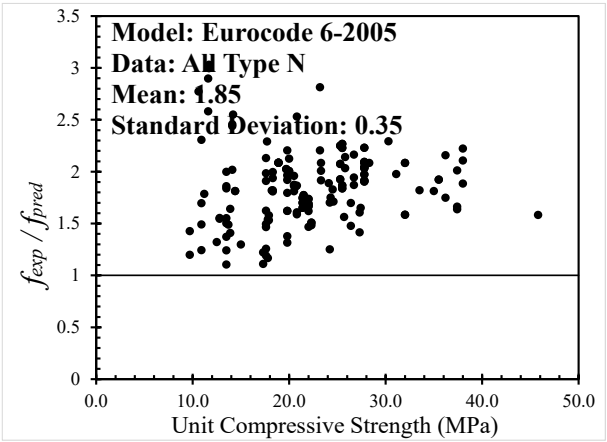

(d)

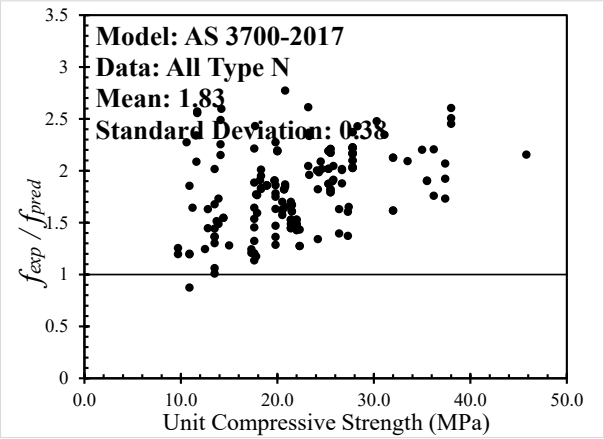

(e)

Figure 4-4: Comparison of prediction error of f_{exp}/f_{pred} for international masonry design codes and the proposed GPR model (type N): (a) GPR, (b) CSA S304-14, (c) TMS 402/602-16, (d) Eurocode 6-2005, (e) AS 3700-2017

Based on Table 4-4 and Figure 4-3/Figure 4-4, for mean strength prediction, the proposed GPR model has the lowest COV for both type S (8.0%) and type N mortar (8.0%) and the lowest prediction error (mean values for model prediction error are closest to 1), much lower compared to TMS 402/602-16 and the Australian code AS 3700-2017. For 5th percentile strength prediction, the proposed GPR model has the lowest COV for both type S (10.9%) and type N mortar (11.4%) and the lowest prediction error, much lower compared to CSA S304.1-14 and Eurocode 6-2005.

Overall, the two north American masonry design codes have relatively better estimation results compared to Eurocode 6 and Australian code AS 3700, which both largely underestimated the compressive strength of masonry. It is shown that Eurocode 6 is relatively more over-conservative about type N mortar while Australian code AS 3700 is relatively more over-conservative about type S mortar. As for CSA S304 and TMS 402/602, it is shown in Table 4-4 that both masonry design codes have lower COV for type S mortar. Specifically, CSA S304 has more accurate prediction for type S mortar with an average prediction error of 1.24 while for type N mortar the average prediction error is higher (1.36, further from 1). Comparing to CSA S304, TMS 402/602 has an overall more accurate and more reliable prediction with the average prediction errors for type S and type N mortar as 1.13 and 1.11, respectively.

To summarize, the masonry design code methods evaluated here are all shown to be over conservative. Among different design codes, European code and Australian code are proven to be overly conservative. The two north American codes are relatively better while still conservative, and their prediction error (e.g., measured by COV) are shown to be higher than the proposed GPR model. The proposed GPR model, on the other hand, can provide overall accurate and reliable masonry compressive strength with very low variance or systematic bias for both the mean and 5th percentile strength values.

4.5.2 Prediction error quantification with comparison to empirical-formula methods

Furthermore, the proposed GPR model is compared to other analytical formulas available in literature. Different empirical formulas have been proposed for the estimation of the compressive strength of masonry. The most commonly considered predictors in the empirical formulas include the compressive strength of masonry and the compressive strength of mortar. While only a few research shed light on the prism height-to-thickness ratio (Sarhat and Sherwood 2014). In this section, the most representative empirical formulas (see Table 3-4) from literature for hollow concrete masonry are selected and compared to the proposed GPR model in order to further show the accuracy and reliability of the proposed GPR model. In order to compare with the test results for the compressive strength of masonry prisms, the calculated values for the compressive strength of masonry based on empirical formulas should be converted to the masonry prism strength, by dividing the masonry strength with the corresponding correction factor for a certain height-to-thickness ratio (h/t) (see Table 3-3 (CSA S304-14)). Note that linear interpolation is used for other values of h/t.

Table 4-4 summarizes the prediction error represented by the prediction-to-test ratio, namely the compressive strength f_{exp} (the corresponding mean) divided by the predicted compressive strength f_{pred} from GPR model or empirical formulas (corrected by height-to-thickness correction factors).

Table 4-5: Descriptive statistics values of prediction error f_{exp}/f_{pred} for different empirical formulas and the proposed GPR model

Test-to-prediction ratio	Mortar Type						Overall Database		
	Type S			Type N					
	Mean	STD.	COV (%)	Mean	STD.	COV (%)	Mean	STD.	COV (%)
Mann (1982)	1.81	0.28	15.6	1.82	0.32	17.6	1.82	0.30	16.7
Guo (1991)	1.21	0.20	16.2	1.15	0.21	17.9	1.18	0.20	17.2
Köksal et al. (2005)	0.91	0.15	15.9	0.85	0.15	17.9	0.88	0.15	17.2
Fortes et al. (2015)	1.01	0.17	17.3	0.93	0.22	24.0	0.97	0.21	21.1
GPR	1.00	0.08	8.0	1.00	0.08	8.0	1.00	0.08	8.0

In order to visualize the prediction accuracy and reliability of the proposed GPR model, with comparison to the above-mentioned empirical formulas, the compressive strength prediction results for hollow concrete masonry prisms built with type S and N mortar are presented in terms of f_{exp}/f_{pred} in Figure 4-5 and Figure 4-6, respectively.

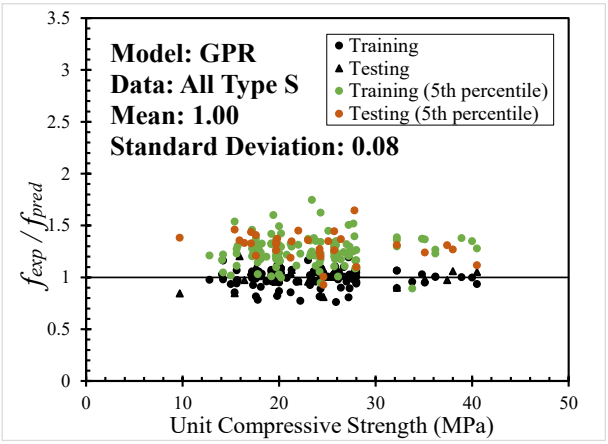

(a)

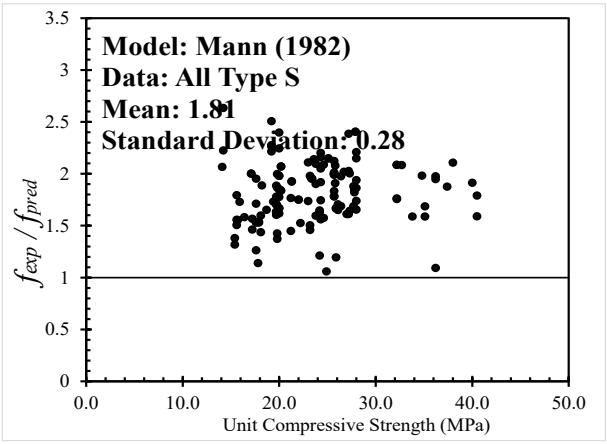

(b)

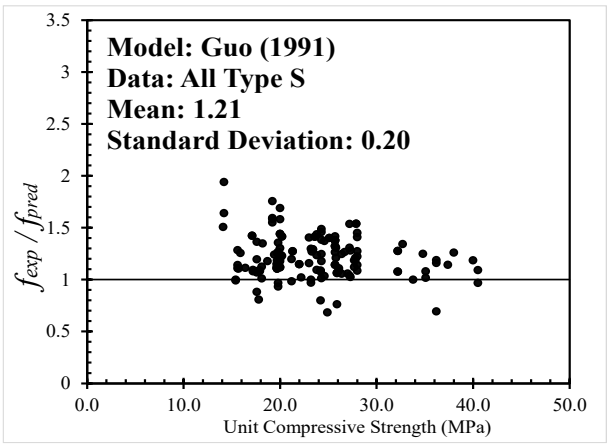

(c)

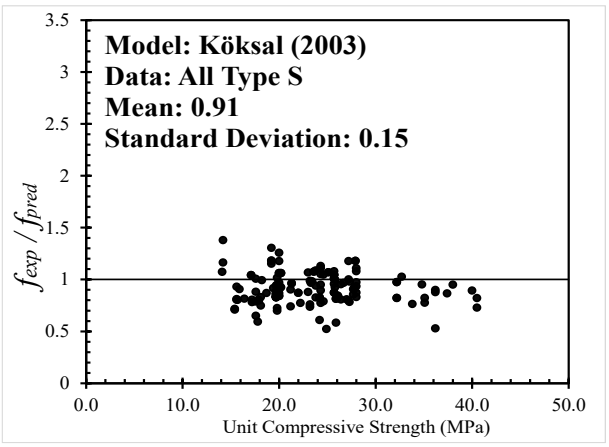

(d)

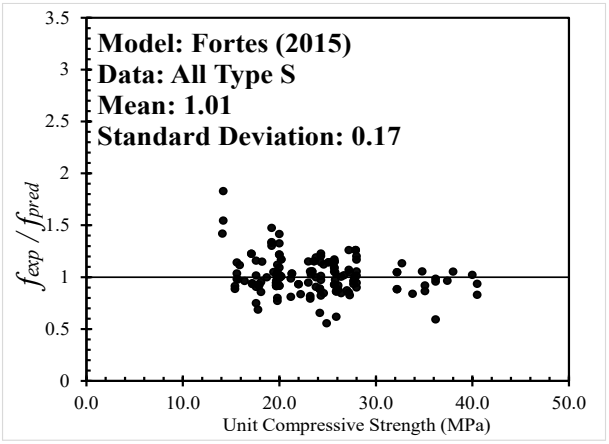

(e)

Figure 4-5: Comparison of prediction error of f_{exp}/f_{pred} for empirical formulas and the proposed GPR model (type S): (a) GPR, (b) Mann (1982), (c) Guo (1990), (d) Köksal et al. (2005), (e) Fortes et al. (2015)

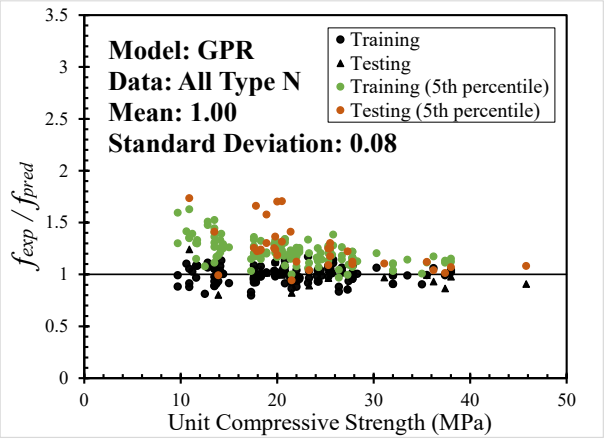
Model: GPR
Data: All Type N
Mean: 1.00
Standard Deviation: 0.08
Training
Testing
Training (5th percentile)
Testing (5th percentile)
f_{exp} / f_{pred}
Unit Compressive Strength (MPa)

(a)

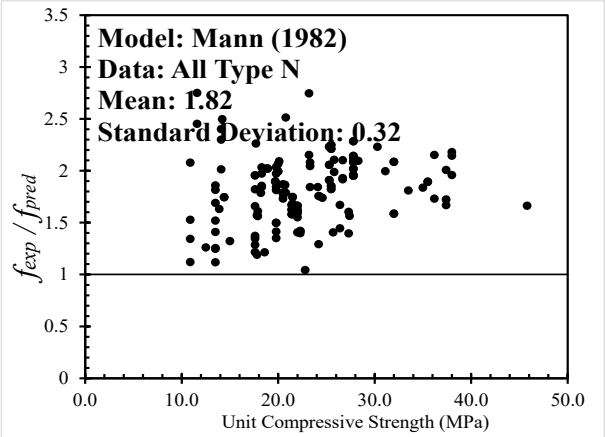
Model: Mann (1982)
Data: All Type N
Mean: 1.82
Standard Deviation: 0.32
f_{exp} / f_{pred}
Unit Compressive Strength (MPa)

(b)

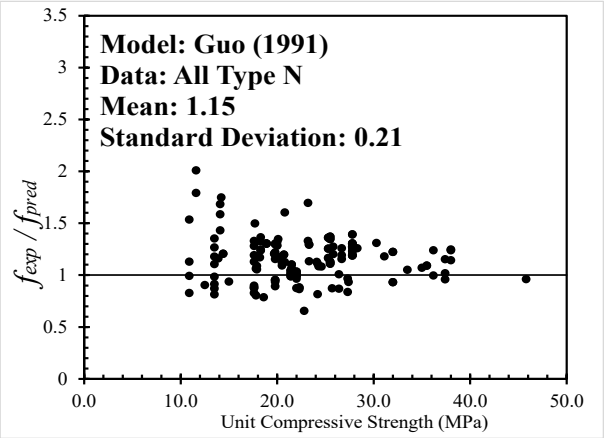
Model: Guo (1991)
Data: All Type N
Mean: 1.15
Standard Deviation: 0.21
f_{exp} / f_{pred}
Unit Compressive Strength (MPa)

(c)

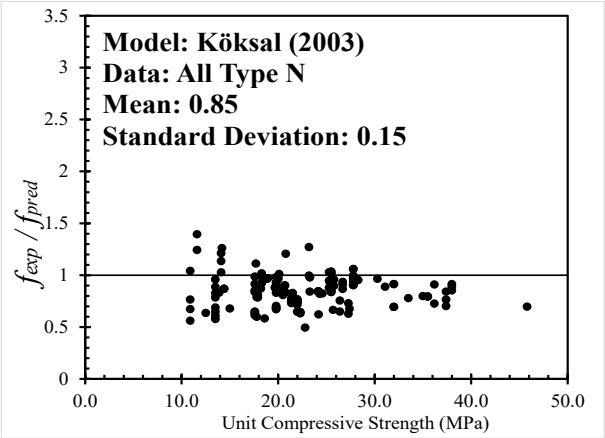
Model: Köksal (2003)
Data: All Type N
Mean: 0.85
Standard Deviation: 0.15
f_{exp} / f_{pred}
Unit Compressive Strength (MPa)

(d)

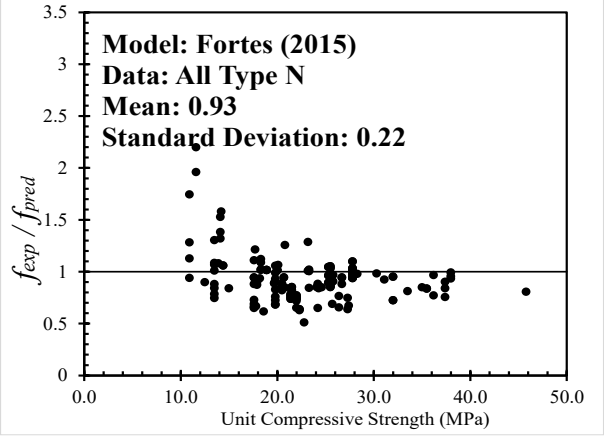
Model: Fortes (2015)
Data: All Type N
Mean: 0.93
Standard Deviation: 0.22
f_{exp} / f_{pred}
Unit Compressive Strength (MPa)

(e)

Figure 4-6: Comparison of prediction error of f_{exp}/f_{pred} for empirical formulas and the proposed GPR model (type N): (a) GPR, (b) Mann (1982), (c) Guo (1990), (d) Köksal et al. (2005), (e) Fortes et al. (2015)

Based on Table 4-4, Figure 4-5and Figure 4-6, the other empirical formulas are most systematically biased. For type S model, the models proposed by Mann (1982) and Guo (1991) both over-estimates the compressive strength to different degrees. Even for the models (Köksal et al. 2005, Fortes et al. 2015) that have relatively less biased prediction results with mean values of prediction error as 0.91 and 1.01, the variances of the prediction results are higher than the proposed GPR model. As for prediction of masonry strength with type N model mortar, models proposed by Mann (1982) over-estimates the compressive strength while the model proposed by Guo (1991) provides a less biased prediction with the mean value of the prediction error as 1.15. However, the models (Köksal et al. 2005, Fortes et al. 2015) that have less biased prediction for type S underestimates the compressive strength with higher variances as (COV as 17.9% and 24.0%, respectively) compared to models for masonry with type S mortar. In contrast, the proposed GPR model provides an overall good prediction without a systematic bias. The mean value of the prediction error of the proposed GPR model for type S and N are both 1.00.

4.5.3 Prescribed compressive strength values in CSA S304-14 re-evaluation

In order to get more representative values for masonry compressive strength, a lower bound approach was adopted in order to obtain the specified values. For every specified unit compressive strength in the Table 4 in CSA S304-14, the proposed value is the corresponding specified masonry compressive strength (i.e., 5^{th} percentile) predicted by the proposed GPR models with the course number = 5. The proposed values are plotted along with values from current Table 4 in CSA S304-14 for comparison. The results confirm the suspected conservatism in the prescribed masonry compressive strength values in the Canadian standard CSA S304-14 particularly for prisms constructed with type N mortar. The summary of masonry compressive strength based on the proposed GPR model is presented in Table 4-6:

Table 4-6: Summary of masonry compressive strength based on the proposed GPR model

Specified compressive strength of unit (MPa)	GPR re-evaluated masonry compressive strength							
	Type S				Type N			
	Mean (MPa)	STD. (MPa)	COV (%)	5th per. (MPa)	Mean (MPa)	STD. (MPa)	COV (%)	5th per. (MPa)
10	10.01	1.32	13.19	7.85	9.38	1.06	11.30	7.64
15	12.49	1.14	9.13	10.61	12.13	1.05	8.66	10.41
20	16.34	1.33	8.14	14.15	14.92	1.06	7.10	13.18
30	22.85	1.45	6.35	20.47	20.45	1.06	5.18	18.71

According to the 5th percentile (5th per.) values in Table 4-6, specified values for masonry compressive strength based on GPR is proposed. The comparison of the proposed masonry specified strength to the prescribed masonry compressive strength for ungrouted hollow concrete units in CSA S304-14 is presented in Table 4-7 as a re-evaluation:

Table 4-7: Comparison of the proposed specified masonry compressive strength to the prescribed masonry compressive strength for ungrouted hollow concrete units in CSA S304-14

Net area specified compressive strength of unit (MPa)	Specified concrete masonry compressive strength (MPa)			
	Type S Mortar		Type N Mortar	
	CSA	GPR proposed	CSA	GPR proposed
10	6.5	7.5	6	7.5
15	10	10.5	8	10
20	13	14	10	13
30 or more	17.5	20	12	18.5

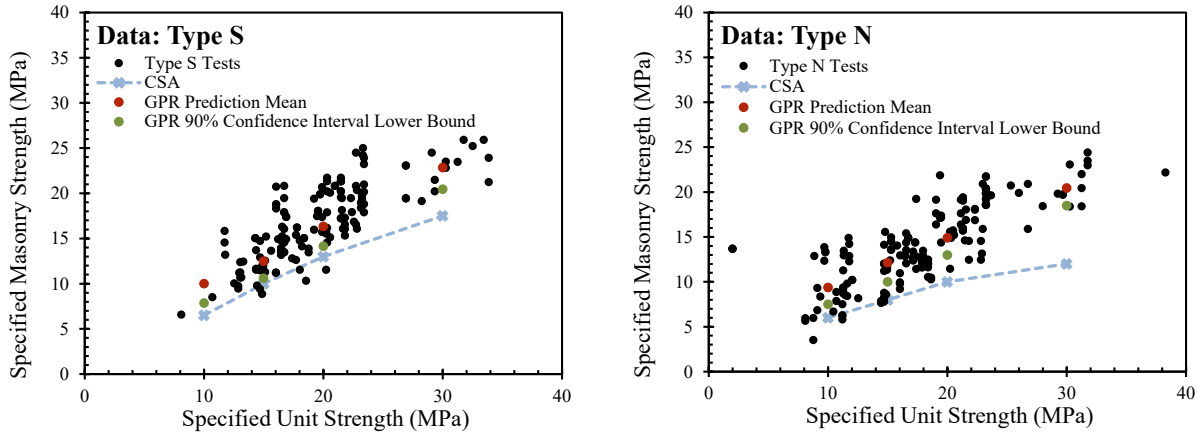

(a) (b)

Figure 4-7: Comparison of the specified value for CSA S304 and the proposed GPR model: (a) type S mortar, (b) type N mortar

Based on the proposed GPR model, the specified compressive strength of masonry is re-evaluated. It is shown in Figure 4-7 and Table 4-7 that the current prescribed values are over-conservative, especially for masonry constructed with type N mortar. The re-evaluated values by the proposed GPR model for type S mortar are 5% - 15.4% higher than the current prescribed values. For type N mortar, the re-evaluated values are 25% - 54.2% higher than the current prescribed values.

4.5.4 Results and discussion

A Gaussian Process Regression model is developed in this section to predict the compressive strength of hollow concrete block masonry. The proposed model is compared to empirical models and masonry design code models to validate the effectiveness of GPR models in the ability to predict the compressive strength of masonry, in a reliable and comprehensive manner. The results showed that the proposed GPR model can give out accurate and reliable prediction for masonry compressive strength.

After the proposed GPR model is validated through its comparison with other models, prescribed masonry compressive strength values are re-evaluated. The results indicated that the current prescribed values are overly conservative and need to be updated.

4.6 Chapter Summary and Conclusions

A Gaussian Process Regression model is developed in this chapter to predict the compressive strength of hollow concrete block masonry or masonry prisms. The proposed model is built based on an extensive database, which consisted of 312 groups of hollow concrete masonry prisms including 1427 individual prism specimens collected from 40 literatures. The whole database is divided into two groups based on mortar type and GPR models are built upon each type.

A parametric study based on different covariance functions is carried out and the results show that squared exponential kernel is the most suitable for type S mortar, while exponential is the most suitable for type N mortar. Case study based on different number of input parameters is also carried out and the results show that the optimum model is that of case IV, which corresponds to GPR architecture with three input parameters: the compressive strength of CMU, the compressive strength of mortar, and prism height-to-thickness ratio.

The proposed model is compared to empirical models and masonry design code models to evaluate the effectiveness of GPR models in predicting the compressive strength of masonry or masonry prisms, in a reliable and comprehensive manner. The results showed that the proposed GPR model can give out an accurate and reliable prediction for masonry compressive strength, compared to existing design code models.

After the proposed GPR model is validated, prescribed masonry compressive strength values in CSA are re-evaluated. The results indicated that the current prescribed values are overly conservative.

CHAPTER 5: CONCLUSIONS AND RECOMMENDATIONS

5.1 Summary

Both HC (FE model) and SC (GPR model) techniques are adopted in this study to construct prediction models for the compressive strength of hollow concrete masonry and masonry prisms. To be specific, a 3D detailed micro-FE model is developed in this work to analyze the behaviour of hollow concrete masonry prisms under compression load using commercial software ABAQUS. An automatic numerical prism testing apparatus is developed. The accuracy of the prediction is assessed using experimental testing data and compared to other existing models used in the design codes and literature. Furthermore, Gaussian Process Regression (GPR) models are developed in this work to predict the compressive strength of hollow concrete block masonry. The proposed model is built based on an extensive experimental database, which is divided into two groups based on mortar type. Similarly, the accuracy of the prediction is assessed using experimental testing data, and compared to other existing models used in the design standards/codes and literature.

5.2 Conclusions

Both FE model and GPR model are validated and are proven to have good prediction abilities. The model validation, accuracy assessment & comparison, and its applications leads to the following findings in this research:

FE model development with automatic numerical prism testing tool:

(1) The developed FE model is validated using the available experimental tests of concrete masonry prisms. Validation results prove that the proposed FE model is capable of accurately predicting the behavior of masonry under compression load.

(2) A series of parametric study is subsequently conducted. Results indicate that the compressive behavior of masonry prisms is more significantly affected by the physical material parameters and the mortar thickness, which shed lights on the importance of construction quality.

(3) The developed FE model is automated using Python and used as a masonry compressive strength prediction tool. The results indicate that the tool is more effective and accurate in predicting the compressive strength of masonry, with the mean prediction error values

f_{exp}/f_{pred} of 1.01 and 1.02 for type S and N mortar, respectively. Compared to other empirical models, the results of the developed FE model have the best prediction ability without a systematic bias.

(4) The height-to-thickness correction factors are re-evaluated using the proposed FE model and the results indicate that the height-to-thickness correction factor stays at 1.0 when the height-to-thickness ratio of masonry prisms is equal to or greater than 4.0, and the correction factors used in CSA are sufficiently accurate.

(5) A global sensitivity analysis is carried out using the proposed FE model and the contribution of different input variables to the variance of the compressive strength of masonry is studied based on different concrete masonry units and mortar types. The results show that the compressive strength of masonry is mostly affected by the compressive strength of CMU, while the other input variables have much lower influence, depending on the relationship between the compressive strengths of CMU and mortar.

GPR model development:

(1) For the GPR model, parametric study based on different covariance functions is carried out and the results show that the most suitable covariance functions for different mortar types are different. The optimum GPR architecture in this study is proven to be the one with three input parameters: the compressive strength of CMU, the compressive strength of mortar, and prism height-to-thickness ratio.

(2) The proposed GPR model is used as a masonry prism compressive strength prediction tool over the collected database and the results are compared with different empirical models, including various international masonry design standards and codes and empirical formulas proposed by previous researchers. The values of the mean prediction error f_{exp}/f_{pred} are 1.00 for both type S and N mortar, which indicate that the proposed GPR model can provide a more accurate and reliable prediction for masonry prism compressive strength.

(3) Through the comparisons with the current Canadian masonry design standard CSA S304-14, a high degree of conservatism exists in the current prescribed HCB masonry compressive strength and thus based on such re-evaluation, a set of new prescribed values are proposed. The proposed values based on the GPR models for type S mortar are 5% -

15.4% higher than the current prescribed values. For type N mortar, the proposed values are 25% - 54.2% higher than the current prescribed values.

5.3 Limitations and Recommendations for Future Work

The presented study has limitations in the following aspects, therefore, recommendations for future work are listed as follows:

(1) Workmanship study is recommended for future study using the proposed FE model, considering geometric imperfection by modifying the geometric parameters of mortar layers.
(2) Only hollow concrete masonry prisms are studied in the presented work. Therefore, studies about the compressive behaviours of grouted masonry prisms are recommended using the proposed FE model with some modifications to the material properties and contact definition or the proposed GPR model with different input parameters.
(3) Studies about clay brick masonry prisms using the proposed FE and GPR model are recommended.

REFERENCES

ABAQUS (2014). User's Manual, Version 6.14, Hibbitt, Karlsson & Sorensen, Inc., Pawtucket, Rhode Island, USA.

Abasi, A.; Hassanli, R.; Vincent, T. and Manalo, A. (2020). "Influence of prism geometry on the compressive strength of concrete masonry." *Construction and Building Materials*, 264 (2020) 120182.

ACI/TMS 122R-14: *Guide to Thermal Properties of Concrete and Masonry Systems*. ACI/TMS Committee 122, December 2014.

Aguila, V., Sandoval, C., Adam, J. M., Garzón-Roca, J. and Valdebenito, G. (2016). "Prediction of the shear strength of reinforced masonry walls using a large experimental database and artificial neural networks." *Structure and Infrastructure Engineering*. 2016, 12:12, 1661-1674.

Ahmadi-Nedushan, B. (2012). "Prediction of elastic modulus of normal and high strength concrete using ANFIS and optimal nonlinear regression models." *Construction and Building Materials*. 2012, 36: 665–673.

Álvarez-Pérez, J; Chávez-Gómez, J. H.; Terán-Torres, B. T.; Mesa-Lavista, M. and Balandrano-Vázquez, R. (2020). "Multifactorial behavior of the elastic modulus and compressive strength in masonry prisms of hollow concrete blocks." *Construction and Building Materials*, 241 (2020) 118002.

Arıoglu, N.; Girgin, Z. C. and Arıoglu, E. (2006). "Evaluation of ratio between splitting tensile strength and compressive strength for concretes up to 120 MPa and its application in strength criterion." *ACI Materials Journal*, (2006) 103(1):18–25.

Asteris, P. G., Argyropoulos, I., Cavaleri, L., Rodrigues, H., Varum, H., Thomas, J. and Lourenço, P. B. (2019). "Masonry compressive strength prediction using Artificial Neural Networks." *Springer Nature Switzerland* AG 2019, CCIS 962: 200–224.

Asteris, P. G., Skentou, A. D., Bardhan, A., Samui, P., Pilakoutas, K. (2021). "Predicting concrete compressive strength using hybrid ensembling of surrogate machine learning models." *Cement and Concrete Research*. 2021, 145:106449.

Australian Standard (2017). *AS 3700-2017: Masonry Structures*, Standards Australia Limited,

Sydney, Australia.

Barbosa, C.; Lourenço, P. B. and Hanai, J. B. (2009). "On the compressive strength prediction for concrete masonry prisms." *Mater Struct*, 43, 331–344 (2010).

Birtel, V. and Mark, P. (2006). "Parameterised finite element modelling of RC beam shear failure." 2006 ABAQUS User's Conference,

Bolhassani, M.; Hamid, A. A.; Lau, A. C. W. and Moon, F. (2015). "Simplified micro modeling of partially grouted masonry assemblages." *Construction and Building Materials*, (2015) 83:159–173.

British Standards Institution (2011). *BS EN 772-1-2011: Methods of test for Masonry Units – Part 1: Determination of Compressive Strength*. BSI, London, United Kingdom.

CEB-FIP, Model Code 2010, London: Thomas Telford; 2010.

Chahine, G. N. (1989). "Behaviour Characteristics of Face Shell Mortared Block Masonry under Axial Compression." M.Eng. Thesis, McMaster University. Hamilton, Ontario.

Chaudhari, S.V. and Chakrabarti, M.A. (2012). "Modeling of concrete for nonlinear analysis Using Finite Element Code ABAQUS." *International Journal of Computer Applications*, (2012) 44 (7):0975–8887.

Cheema, T. S. and Klingner, R. E. (1984). "Compressive strength of concrete masonry prisms." *American Concrete Institute Journal*. 1984, Nov./Dec., 88-97.

Chisari, C., Macorini, L., Amadio, C. and Izzuddin, B. A. (2018). "Identification of mesoscale model parameters for brick-masonry." *International Journal of Solids and Structures*. 2018, 146: 224–240.

CSA (2014). *S304-14 Design of Masonry Structures*. Canadian Standards Association, Mississauga, Ontario, Canada.

Dao, D. V., Adeli, H., Ly, H., Le, L. M., Le, V. M., Le, T. and Pham, B. T. (2020). "A sensitivity and robustness analysis of GPR and ANN for high-performance concrete compressive strength prediction using a Monte Carlo simulation." *Sustainability*. 2020, 12: 830.

Dassault Systemes (2017). Abaqus.

Drosopoulos, G. A. and Stavroulakis, G. E. (2020). "Data-driven computational homogenization using Neural Networks: FE^2-NN application on damaged masonry."

ACM Journal on Computing and Cultural Heritage. 2020, (14) 1.

Drougkas, A; Roca, P and Molins, C. (2015). "Numerical prediction of the behaviour, strength and elasticity of masonry in compression." *Engineering Structures*, 90 (2015): 15-28.

Drysdale, R. G. and Hamid, A. A. (1979). "Behavior of concrete block masonry under axial compression." *American Concrete Institute Journal*. 1979, June, 707-721.

Drysdale, R. G., Guo, P. (1990). "Compressive strength for concrete block masonry based on the properties of constituent materials."

Duan, Z.H., Kou, S.C., Poon, C.S. (2013). "Using artificial neural networks for predicting the elastic modulus of recycled aggregate concrete." *Construction and Building Materials*. 2013, 44: 524–532.

Dubourg, V. (2011). Adaptive surrogate models for reliability analysis and reliability-based design optimization. Ph. D. thesis, Universit´e Blaise Pascal, Clermont-Ferrand, France. 3, 6, 11, 13

Dymiotis, C. and Gutlederer, B.M. (2002). "Allowing for uncertainties in the modelling of masonry compressive strength." *Constr. Build. Mater*. (2002)16: 443–452.

Engesser, F. (1907). "Über weitgespannte wölbbrücken." *Z. Architekt. Ing.-wesen.* (1907) 53: 403–440.

European Standard (2005). *EN 1996-1-1:2005: Eurocode 6 – Design of Masonry Structures*. European Committee for Standardization, Brussels, Belgium.

Fahmy, E. H. and Ghoneim, T. G. M. (1994). "Behaviour of concrete block masonry prisms under axial compression." *Can. J. Civ. Eng.* 22: 898-915 (1995).

Ferguson, W. A. (1995). "A comparison between the compressive strength of mortar obtained from 70.7 mm mortar cubes and 40 mm × 40 mm × 160 mm prisms." Report to Masonry Research Advisory Committee.

Fortes, E. S., Parsekian, G. A. and Fonseca, F. S. (2015). "Relationship between the compressive strength of concrete masonry and the compressive strength of concrete masonry units." *Journal of Materials in Civil Engineering*, 2015, 27(9): 04014238.

Ganesan, T. P. and Ramamurthy, K. (1992). "Behaviour of concrete hollow-block masonry prisms under axial compression." *J. Struct. Eng.*, 1992, 118(7): 1751-1769.

García-Macías, E., Venanzi, I. and Ubertini, F. (2020). "Metamodel-based pattern recognition approach for real-time identification of earthquake-induced damage in historic masonry structures." *Automation in Construction.* 2020, 120: 103389.

Garzón-Roca, J., Marco, C. O. and Adam, J. M. (2013). "Compressive strength of masonry made of clay bricks and cement mortar: Estimation based on Neural Networks and Fuzzy Logic." *Engineering Structures.* 2013, 48: 21–27.

Gayed, M.; Korany, Y. and Gary, S. (2012). "Examination of the prescribed concrete block masonry compressive strengths in the Canadian Masonry Design Standard, CSA S304.1-2004." *Proceedings of the Fifteenth International Brick and Block Masonry Conference*, Florianopolis, Brazil.

Guo, P. (1991). "Investigation and modelling of the mechanical properties of masonry." Ph.D. Thesis, McMaster University, Hamilton, Ontario, Canada.

Hamid, A. A. and Chukwunenye, A. O. (1986). "Compression behavior of concrete masonry prisms." *Journal of Structural Engineering*, (1986) 112(3):605–613.

Harsh, S., Shen, Z. and Darwin, D. (1990). "Strain-rate sensitive behavior of cement paste and mortar in compression." *ACI Materials Journal*. V. 87, No. 5, September-October 1990.

Hendry, A.W. and Malek, M.H. (1986). "Characteristic compressive strength of brickwork walls from collected test results." *Mason. Int*. (1986) 7, 15–24.

Ip, F. (1999) Compressive Strength and Modulus of Elasticity of Masonry Prisms. M. Sc. Thesis, Carlton University, 147 pp.

Jia, G. and Taflanidis, A. A. (2013). "Kriging metamodeling for approximation of high-dimensional wave and surge responses in real-time storm/hurricane risk assessment." *Computer Methods in Applied Mechanics and Engineering*. 2013, 261: 24–38.

Kersaudy, P., B. Sudret, N. Varsier, O. Picon, and J. Wiart (2015). "A new surrogate modeling technique combining Kriging and polynomial chaos expansions – Application to uncertainty analysis in computational dosimetry." *Journal of Computational Physics*. 286, 103–117. 2.

Khalaf F. M., Hendry A. W., Fairbairn D. R. (1994). "Study of the compressive strength of blockwork masonry." ACI Struct J 1994; 91(4):367–76.

Khalaf, F. M. (1996). "Factors influencing compressive strength of concrete masonry prisms."

Magazine of Concrete Research. 1996, 48(174): 95-101.

Khosravi, K.; Daggupati, P.; Alami, M.T.; Awadh, S.M.; Ghareb, M.I.; Panahi, M.; Pham, B.T.; Rezaie, F.; Qi, C.; Yaseen, Z.M. "Meteorological data mining and hybrid data-intelligence models for reference evaporation simulation: A case study in Iraq." *Comput. Electron. Agric.* 2019, 167, 105041.

Korany, Y. and Glanville, J. (2005) Comparing Masonry Compressive Strength in Various Codes. Concrete International, vol. 27, no. 1, pp. 35- 39.

Köksal, H. O., Karakoç, C., and Yildirim, H. (2005). "Compressive behavior and failure mechanisms of concrete maosnry prisms," *Journal of Materials in Civil Engineering*. 2005, 17(1): 107-115.

Krige, D. G. (1951). "A statistical approach to some mine valuation and allied problems on the Witwatersrand." Master's thesis, University of the Witwatersrand, South Africa.

Lan, G., Wang, Y., Zeng, G. and Zhang, J. (2020). "Compressive strength of earth block masonry: Estimation based on neural networks and adaptive network-based fuzzy inference system." *Composite Structures*. 2020, 235: 111731.

Lee, J. and Fenves, G. L. (1998). "Plastic-damage model for cyclic loading of concrete structures." *Journal of Engineering Mechanics*, (1998) 124(8):892–900.

Liu, J. (2012). "The effect of height-to-thickness ratio on the compressive strength of concrete masonry." (2012). Electronic Theses and Dissertations. 4827.

Liu, W., Wu, X., Zhang, L., A. M. ASCE, Zheng, J. and Teng, J. (2017). "Global Sensitivity Analysis of Tunnel-Induced Building Movements by a Precise Metamodel." *Journal of Computing in Civil Engineering*. 2017, 31(5): 04017037.

Lubliner, J.; Oliver, J; Oller, S. and Oñate, E. (1989). "A plastic-damage model for concrete." *International Journal pf Solids and Structures*. (1989) 25:299–329.

Ly, H.-B.; Le, L.M.; Duong, H.T.; Nguyen, T.C.; Pham, T.A.; Le, T.-T.; Le, V.M.; Nguyen-Ngoc, L.; Pham, B.T. "Hybrid Artificial Intelligence Approaches for Predicting Critical Buckling Load of Structural Members under Compression Considering the Influence of Initial Geometric Imperfections." *Appl. Sci*. 2019, 9, 2258.

Mann. W. (1982). "Statistical evaluation of tests on masonry by potential functions." Proceedings of the Sixth International Brick Masonry Conference, Rome, Italy, May

1982, pp. 86–98.

Marelli, S. and Sudret, B. (2014). *UQLab: A framework for uncertainty quantification in Matlab*, Proc. 2nd Int. Conf. on Vulnerability, Risk Analysis and Management (ICVRAM2014), Liverpool, United Kingdom, 2014, 2554-2563.

Marelli, S.; Lamas, C.; Konakli, K.; Mylonas, C; Wiederkehr, P and Sudret, B. (2021). *UQLab user manual – Sensitivity analysis*, Report UQLab-V1.4-106, Chair of Risk, Safety and Uncertainty Quantification, ETH Zurich, Switzerland.

Martin, J. L.; Darwin, D. and Terry, R. E. (1991). "Cement paste, mortar and concrete under monotonic, sustained and cyclic loading." Research Report Sponsored by The National Science Foundation, University of Kansas, Lawrence, Kansas, USA.

Matheron, G. (1963). "Principles of geostatistics." Economic Geology 58(2), 1246–1266.

Maurenbrecher, A. H. P. (1983). Compressive Strength of Eccentrically Loaded Masonry Prisms. Third Canadian Masonry Symposium. Edmonton, Alberta, Canada, 10-1 to 10-13.

Maurenbrecher, A. H. P. (1985). Axial compression tests on masonry walls and prisms. In: Third North American masonry conference, University of Texas at Arlington; 1985. p. 1901–14.

Maurenbrecher, A. H. P. (1980) Effect of test procedures on compressive strength of masonry prisms. In: Proceedings, 2nd Canadian masonry symposium, Carleton University, Ottawa, June 1980. p. 119–32.

Maurenbrecher, A. H. P. (1986). "Compressive strength of hollow concrete blockwork." *Proceedings of the Fourth Canadian Masonry Symposium*, University of New Brunswick, Fredericton, New Brunswick, Canada. (1986) 2:997–1009.

Mishra, M., Bhatia, A. S. and Maity, D. (2019). "Support vector machine for determining the compressive strength of brick-mortar masonry using NDT data fusion (case study: Kharagpur, India)." *Spring Nature Applied Sciences.* (2019) 1:564.

Mohamad, G., Lourenco, P. and Roman, H.R. (2005). "Mechanical behavior assessment of concrete block masonry prisms under compression." Proceedings of International Conference on Concrete for Structures.

Mohamad, G., Lourenço, P.B., Roman, H.R. (2007). "Mechanics of hollow concrete block

masonry prisms under compression: review and prospects." *Cem. Concr. Compos*. 29 (3) (2007) 181–192.

Mohamad, G.; Fonseca, F. S.; Vermeltfoort, A. T.; Martens, D. R. W. and Lourenço, P. B. (2017). "Strength, behavior, and failure mode of hollow concrete masonry constructed with mortars of different strengths." *Construction and Building Materials*, 134 (2017) 489–496.

Mohsin, E. (2005). "Support stiffness effect on tall load bearing masonry walls." The University of Alberta.

Moradabadi, E.; Laefer, D. F.; Clarke, J. A. and Lourenço, P. B. (2015). "A semi-random field finite element method to predict the maximum eccentric compressive load for masonry prisms." *Construction and Building Materials*, (2015) 77:489-500.

Moravej, H., Chan, T. H., Nguyen, K. and Jesus, A. (2019). "Vibration-based Bayesian model updating of civil engineering structures applying Gaussian process metamodel." *Advances in Structural Engineering.* 2019, 22(16) 3487–3502.

Murray, I.; Adams, R.P. Slice sampling covariance hyperparameters of latent Gaussian models. In Advances in Neural Information Processing Systems; NIPS Proceedings; Hyatt Regency: Vancouver, BC, Canada, 2010; pp. 1732–1740.

National Concrete Masonry Association (2008). "NCMA Unit Strength Method Research." Technical Report, National Concrete Masonry Association, Herndon, USA, 10 pp.

National Concrete Masonry Association (2012). "Recalibration of the unit strength method for verifying compliance with the specified compressive strength of concrete masonry." NCMA, Herndon, Virginia, USA, 98 pp.

Nguyen, H.-L.; Pham, B.T.; Son, L.H.; Thang, N.T.; Ly, H.-B.; Le, T.-T.; Ho, L.S.; Le, T.-H.; Tien Bui, D. "Adaptive Network Based Fuzzy Inference System with Meta-Heuristic Optimizations for International Roughness Index Prediction." *Appl. Sci*. 2019, 9, 4715.

Obaidat, A. M. (2017). "Compressive behavior of C-shaped confined masonry boundary elements." Ph.D. Thesis, Concordia University, Montréal, Québec, Canada.

Oden, J. T. and Martins, J. A. C. (1985). "Models and Computational Methods for Dynamic Friction Phenomena," *Computer Methods in Applied Mechanics and Engineering*, 1985, vol. 52, pp. 527–634.

Peng, B., Wang, D. D., Zong, G. and Wei, S. D. (2020). “Calculation of reliability index for in-plane shear failure of unreinforced masonry walls based on Gaussian process model.” *European Journal of Environmental and Civil Engineering*. 2020. DOI: 10.1080/19648189.2019.1708467.

Peng, B., Wei, S., Zong, G. and Wang, D. (2019). “Shear resistance estimation for unreinforced masonry walls based on Gaussian process models.” *Structure and Infrastructure Engineering.* 2020, 16(2): 328–345.

Pham, B.T.; Son, L.H.; Hoang, T.-A.; Nguyen, D.-M.; Tien Bui, D. “Prediction of shear strength of soft soil using machine learning methods.” CATENA 2018, 166, 181–191.

Pina-Henriques, J. and Lourenço, P. B. (2003). “Testing and modelling of masonry creep and damage in uniaxial compression.” *Transaction on the Built Environment*, (2003) 66:151–160.

Pina-Henriques, J. and Lourenço, P. B. (2006). “Validation of analytical and continuum numerical methods for estimating the compressive strength of masonry.” *Computers and Structures*, (2006) 84:1977–1989.

Queipo, N., Haftka, R., Shyy, W., Goel, T., Vaidyanathan, R., and Tucker, P. K. (2005). “Surrogate-based analysis and optimization.” *Progress in Aerospace Sciences*. 2005, 41(1): 1–28.

Ramamurthy, K., Sathish, V., and Ambalavanan, R. (2000). “Compressive Strength Prediction of Hollow Concrete Block Masonry Prisms.” ACI Structural Journal, 97(1), 61-67.

Rasmussen, C. and C. Williams (2006). Gaussian processes for machine learning. Adaptive computation and machine learning. Cambridge, Massachusetts: MIT Press. 1, 5, 10, 11, 14

Rasmussen, C.E. Gaussian Processes in Machine Learning. In Advanced Lectures on Machine Learning; Lecture Notes in Computer Science; Springer: Berlin/Heidelberg, Germany, 2003; Volume 3176.

Ross, M. D. (2013). “Recalibration of the unit strength method for determining the compressive strength of grouted concrete masonry.” Master of Science Thesis, University of Alberta, Edmonton, Alberta, Canada. 2013.

Sacks, J., Welch, W. J., Mitchell, T. J. and Wynn, H. P. (1989). “Design and analysis of computer experiments.” *Statistical Science* 4, 409–435. 1, 11

Santner, T., B. Williams, and W. Notz (2003). “The design and analysis of computer experiments.” *Springer series in Statistics*. Springer. 1, 2, 3, 13, 15

Santos, C. F. R., Alvarenga, R. C. S. S., Ribeiro, J. C. L., Castro, L. O., Silva, R. M., Santos, A. A. R. and Nalon, G. H. (2017). “Numerical and experimental evaluation of masonry prisms by finite element method.” *Structures and Materials Journal*, 2017, vol 10: 478-492.

Sarangapani, G.; Venkatarama Reddy, B. V. and Jagadish, K. S. (2005). “Brick-mortar bond and masonry compressive strength.” *Journal of Materials in Civil Engineering*, (2005) 17(2):229–237.

Sarhat, S.R., Sherwood, E.G. (2014). “The prediction of compressive strength of ungrouted hollow concrete block masonry.” *Constr. Build. Mater*. 58 (2014): 111–121

Sarıdemir, M. “Predicting the compressive strength of mortars containing metakaolin by artificial neural networks and fuzzy logic.” *Adv. Eng. Softw*. 40 (9) (2009) 920–927.

Schobi, R., B. Sudret, and J. Wiart (2015). “Polynomial-chaos-based Kriging.” *International Journal for Uncertainty Quantification* 5(2), 171–193. 2.

Schobi, R., B. Sudret, and S. Marelli (2016). “Rare event estimation using Polynomial-Chaos-¨ Kriging.” *ASCE-ASME Journal of Risk and Uncertainty in Engineering Systems*, Part A: Civil Engineering, D4016002. 2.

Sharafati, A., Asadollah, S. B. H. S., Al-Ansari, Nadhir. (2021). “Application of bagging ensemble model for predicting compressive strength of hollow concrete masonry prism.” Ain Shams Engineering Journal, https://doi.org/10.1016/j.asej.2021.03.028.

Spiridonakos, M.D. and Chatzi, E.N. (2015). “Metamodeling of dynamic nonlinear structural systems through polynomial chaos NARX models.” *Computers and Structures*. 2015, 157: 99-113.

Suwalski, P. and Drysdale R. (1986). “Influence of slenderness on the capacity of concrete block walls.” Proceedings of the Fourth Canadian Masonry Symposium, University of New Brunswick, Fredericton, New Brunswick, Canada. (1986) p. 122–35.

Tao, Y. and Chen, J. F. (2015). “Concrete damage plasticity model for modeling FRP-to-

Concrete bond behavior." *Journal of Composites for Construction*, (2015) 9 (1).

Tayfur, G., Erdem, T.K., Kirca, Ö. (2014). "Strength prediction of high-strength concrete by fuzzy logic and artificial neural networks." *Journal of Materials in Civil Engineering*. 2014, 26 (11): 04014079,

The European Union (2009). *BS EN 1996-1-1:2005: UK National Annex to Eurocode 6 – Part 1-1: General rules for reinforced and unreinforced masonry structures*. BSI, London, United Kingdom.

TMS (2016). *402/602-16 Building Code Requirements and Specification for Masonry Structures*. The Masonry Society, Longmont, Colorado, USA.

Towashiraporn, P. (2004). "Building seismic fragilities using response surface metamodels." PhD Thesis. Georgia Institute of Technology. August 2004.

Tubaldia, E., Macorini, L. and Izzuddin, B. A. (2020). "Identification of critical mechanical parameters for advanced analysis of masonry arch bridges." *Structure and Infrastructure Engineering.* 2020, 16(2): 328–345.

Vindhyashree, Prema Kumar W. P., Rahamath, A. and Prathap Kumar M. T. (2015). "Numerical simulation of masonry prism test using ANSYS and ABAQUS." *International Journal of Engineering Research & Technology (IJERT)*, ISSN: 2278-0181 Vol. 4 Issue 07, July-2015.

Xiu, D. and G. E. Karniadakis (2002). "The Wiener-Askey polynomial chaos for stochastic differential equations." *SIAM Journal of Scientific Computing*. 2002, 24(2), 619–644. 2.

Zahra, T. and Dhanasekar, M. (2016). "Prediction of maonsry compressive behaviour using a damage mechanics inspired modelling method." *Construction and Building Materials*, 109 (2016):128-138.

Zhou, Q., Wang, F. and Zhu, F. (2016). "Estimation of compressive strength of hollow concrete masonry prisms using artificial neural networks and adaptive neuro-fuzzy inference systems." *Construction and Building Materials*. 2016, 125: 417-426.

Zhu, F.; Zhou, Q.; Wang, F. and Yang, X. (2017). "Spatial variability and sensitivity analysis on the compressive strength of hollow concrete block masonry wallettes." *Construction and Building Materials*, 140 (2017):129-138.

APPENDIX A – EXPERIMENTAL DATABASE WITH FE PREDICTIONS

Experimental database with FE predictions (type S mortar)

Nr.	CMU						Mortar			Prism				FEM Pred	Ref.
	l_{cu} (mm)	t_{cu} (mm)	h_{cu} (mm)	n	f_{cu} (MPa)	E_{cu} (MPa)	h_{mr} (mm)	f_{mr} (MPa)	E_{mr} (MPa)	Full:0 FS:1	Void (%)	f'_m (MPa)	COV (%)	(MPa)	
1	195	140	190	3	22	25703	9.5	14.2	16595	0	30	18		21.07	[5]
2	390	190	189	3	14.2	20650	10.0	15.4	17517	0	43.7	17.4	5.2	21.92	[19]
3	397	194	194	3	24.2	26958	4.0	17.7	19221	1	48.4	18.77		17.76	[12]
4	397	194	194	3	24.2	26958	4.0	17.7	19221	0	48.4	18.68		24.70	[12]
5	190	190	190	3	25.7	27781	9.5	20.2	20990	0	43.7	24.2		17.57	[18]
6	390	190	190	3	24.3	27014	10.0	21.2	21678	0	43.7	20.6	13.1	24.96	[18]
7	390	143	194	3	32.2	31096	9.5	14.2	16595	0	42	27.6	4.9	28.27	[5]
8	195	140	190	3	32.2	31096	9.5	14.2	16595	0	42	23.24		24.29	[5]
9	195	240	190	3	23.4	26509	10.0	17.0	18711	1	47	21.6	8.9	16.37	[6]
10	390	140	190	5	23.2	26395	10.0	17.3	18930	1	53.2	16.6	3.7	18.87	[17]
11	390	190	190	3	26.7	28316	9.5	13.2	15807	1	48.3	23.3		22.69	[24]
12	397	101	194	2	21.2	25232	10.0	17.5	19076	0	26	18.4		21.07	[34]
13	390	190	193	3	24.3	27014	5.0	21.2	21678	0	43.7	24.2	2.9	24.97	[18]
14	390	190	190	3	20	24507	9.5	26.5	25155	0	43.7	21.4		18.57	[18]
15	390	143	194	3	19.7	24323	9.5	14.7	16982	0	41	16.4	3.6	18.76	[5]
16	390	200	190	3	17.6	22990	10.0	15.6	17669	0	40	13.8	10.3	19.52	[31]
17	190	190	190	3	25.7	27781	9.5	26.5	25155	0	43.7	25.5		21.60	[18]
18	397	194	192	2	25.9	27889	12.7	14.9	17136	0	48	13.8	3.3	18.08	[3]
19	396	194	203	4	33.8	31859	10.0	19.2	20292	1	48.5	22.9	9.6	22.75	[8]
20	195	140	190	3	23.6	26622	10.0	17	18711	1	47	23.8		16.21	[6]
21	195	140	190	3	19.7	24323	9.5	17.2	18857	0	41	15.93		17.08	[5]
22	397	92	194	2	23	26281	10	17.5	19076	0	26	23.2		17.55	[34]
23	390	190	190	4	40	34659	17.3	19.8	20712	1	44	31		28.43	[38]
24	397	194	194	2	28	28997	1.0	21	21541	1	48	28.6		22.01	[4]
25	195	140	190	3	32.2	31096	9.5	14.2	16595	0	42	27.58		19.49	[5]
26	190	190	190	3	25.7	27781	9.5	15.4	17517	0	43.7	20.6		16.28	[18]
27	390	190	190	3	24.3	27014	10.0	15.4	17517	0	43.7	17.4	5.2	17.77	[18]
28	195	140	190	3	20.2	24630	9.5	14.2	16595	0	36	17.86		13.39	[5]
29	397	194	194	2	25.9	27889	9.5	14.9	17136	0	48	19.3	14.3	25.15	[3]
30	390	140	190	3	18.2	23378	9.5	19.9	20782	0	42	18.2		22.13	[25]
31	390	190	190	6	20	24507	10.0	26.6	25218	0	43.7	17.5		19.23	[18]
32	397	194	194	5	28	28997	5.0	21	21541	1	48	21.4		24.91	[4]
33	397	94	194	2	17.2	22727	10.0	22.8	22755	0	26	13.93		18.12	[32]
34	390	200	190	3	19.8	24384	10.0	15.6	17669	1	41	13.4	9.3	16.52	[31]
35	390	190	190	3	26.4	28157	10.0	13.8	16282	1	40	22.8	20	19.52	[11]
36	190	190	190	2	25.7	27781	18.0	21.2	21678	0	43.7	26		25.09	[18]
37	390	143	194	3	19.7	24323	9.5	15.1	17289	0	41	15.8	4.2	13.99	[5]

Nr.	CMU						Mortar			Prism				FEM Pred (MPa)	Ref.
	l_{cu} (mm)	t_{cu} (mm)	h_{cu} (mm)	n	f_{cu} (MPa)	E_{cu} (MPa)	h_{mr} (mm)	f_{mr} (MPa)	E_{mr} (MPa)	Full:0 FS:1	Void (%)	f'_m (MPa)	COV (%)		
38	390	143	194	3	19.7	24323	9.5	17.3	18930	0	41	15.9	3.3	17.08	[5]
39	390	190	190	3	27.3	28633	9.5	16.3	18193	1	48.3	24.35		19.66	[24]
40	390	190	190	3	36.2	32971	10	12.7	15405	1	40	27.3	8	24.16	[11]
41	390	190	190	2	25.9	27889	10.0	14.9	17136	0	48	19.24		25.01	[3]
42	447	220	194	2	18.1	23314	10.0	17.5	19076	0	26	15		19.78	[34]
43	195	140	190	3	19.7	24323	9.5	14.7	16982	0	41	16.4		15.11	[5]
44	390	190	189	3	14.2	20650	10.0	15.4	17517	0	43.7	20.6	14.1	13.83	[19]
45	390	143	194	3	19.7	24323	9.5	16.7	18490	0	41	16.0	7.5	19.77	[5]
46	195	140	190	3	19.7	24323	9.5	15.1	17289	0	41	15.8		13.35	[5]
47	397	194	194	4	28	28997	4.3	21	21541	0	48	24.1		28.09	[4]
48	195	190	190	3	20.2	24630	10.0	17.0	18711	1	47	20.8	1.5	14.41	[6]
49	397	194	192	3	24.2	26958	10.0	17.7	19221	1	48.4	13.8	7.4	17.57	[12]
50	190	190	190	3	25.7	27781	14.0	25.5	24518	0	43.7	25.5		21.70	[19]
51	397	194	194	3	17.9	23185	4.0	17.7	19221	1	49.6	14.38		13.68	[12]
52	195	190	190	3	25.1	27455	10.0	17	18711	1	47	24.9		20.16	[6]
53	447	220	194	2	18.1	23314	10.0	17.5	19076	0	26	13.5		19.78	[34]
54	390	143	187	3	32.2	31096	19.1	14.2	16595	0	42	23.3	1.1	24.42	[5]
55	390	190	190	3	36.2	32971	10.0	13.8	16282	1	40	28.1	7	24.47	[11]
56	390	194	190	2	19.2	24012	10.0	18.8	20009	1	49	24.8		15.64	[7]
57	390	190	190	4	27.8	28894	17.3	19.8	20712	1	44	23.6		18.93	[38]
58	178	143	194	3	19.7	24323	9.5	14.5	16828	0	41	16.4	3.6	19.41	[14]
59	195	140	190	3	19.7	24323	9.5	18.2	19581	0	41	16.28		13.39	[5]
60	390	143	194	3	19.7	24323	9.5	12.8	15486	0	41	16.7	1.1	17.73	[5]
61	397	194	192	3	17.8	23120	10.0	17.7	19221	1	49.6	10.6	6.1	13.69	[12]
62	390	200	190	3	17.6	22990	10.0	15.6	17669	1	41	11.4	10.7	10.32	[31]
63	390	190	190	2	19.4	24137	10.0	22.9	22821	1	44	17.85		15.83	[15]
64	390	190	190	2	20	24507	209.0	21.2	21678	0	43.7	24.9		17.92	[18]
65	390	140	190	3	32.7	26392	9.5	22.2	22354	0	53.2	30.18		22.49	[4]
66	195	140	190	3	21.3	25291	9.5	14.2	16595	0	31	19.38		23.63	[5]
67	195	190	190	3	17.1	22661	10.0	17.0	18711	1	47	18.0	7.3	20.84	[6]
68	397	194	194	2	28	28997	1.0	21	21541	1	48	27.8		22.01	[4]
69	390	140	190	3	36.2	27104	10.0	22.2	22354	0	53.2	16.9	3.9	22.58	[4]
70	195	190	190	3	17.1	22661	10.0	17	18711	1	47	18		21.07	[6]
71	390	200	190	3	19.8	24384	10.0	15.6	17669	0	40	13.9	11.7	14.20	[31]
72	195	190	190	3	22.2	25820	10.0	17.0	18711	1	47	16.3	22.4	15.57	[6]
73	390	140	190	3	23.2	26395	10.0	17.3	18930	1	53.2	16.1	8.1	14.92	[17]
74	390	190	190	3	27.3	28633	9.5	13.2	15807	1	48.3	19.23		19.34	[24]
75	397	143	194	2	15.4	21505	10.0	14.8	17059	0	44	11.31		16.20	[32]
76	390	190	190	4	27.8	28894	17.3	19.8	20712	1	44	23.2		23.63	[38]
77	397	194	194	2	15.6	21644	10.0	14.8	17059	0	46	14.82		16.60	[32]
78	195	190	190	3	20.2	24630	10.0	17	18711	1	47	20.8		14.41	[6]

Nr.	CMU						Mortar			Prism				FEM Pred (MPa)	Ref.
	l_{cu} (mm)	t_{cu} (mm)	h_{cu} (mm)	n	f_{cu} (MPa)	E_{cu} (MPa)	h_{mr} (mm)	f_{mr} (MPa)	E_{mr} (MPa)	Full:0 FS:1	Void (%)	f'_m (MPa)	COV (%)		
79	190	190	190	6	25.7	27781	10.0	26.6	25218	0	43.7	23.4		21.24	[18]
80	397	194	194	4	28	28997	4.3	21	21541	1	48	22.5		19.32	[4]
81	397	194	194	2	15.6	21644	10.0	22.8	22755	0	46	13.45		16.42	[32]
82	390	200	190	3	19.8	24384	9.5	15.6	17669	1	41	18.22		14.83	[31]
83	195	240	190	3	23.4	26509	10.0	17	18711	1	47	21.6		18.38	[6]
84	390	143	194	3	20.0	24507	9.5	14.2	16595	0	26	16.1	6.9	19.56	[5]
85	397	143	194	2	24.6	27180	10.0	17.5	19076	0	43	24		24.86	[34]
86	397	143	194	2	27.2	28580	10.0	17.5	19076	0	43	19.8		16.31	[34]
87	190	190	190	3	25.7	27781	14.0	20.2	20990	0	43.7	24.2		17.55	[19]
88	195	190	190	3	27.9	28946	10.0	17	18711	1	47	29.9		19.17	[6]
89	219	194	194	2	23.3	26452	1.0	14	16439	0	48	20.9		17.44	[26]
90	397	101	194	2	15.9	21851	10.0	17.5	19076	0	26	14.9		16.85	[34]
91	178	143	194	3	19.7	24323	9.5	18.2	19581	0	42	16.3	3.3	20.06	[14]
92	390	190	190	3	24.3	27014	20.0	21.2	21678	0	43.7	25.5	1.6	26.37	[18]
93	397	143	194	2	40.5	34875	10.0	17.5	19076	0	43	28.6		22.10	[34]
94	390	190	190	3	20	24507	14.0	26.5	25155	0	43.7	21.4		21.29	[19]
95	195	140	190	3	20	24507	9.5	14.2	16595	0	26	16.14		15.12	[5]
96	390	143	194	3	16.4	22192	9.5	14.2	16595	0	40	13.4	4.0	13.67	[5]
97	219	194	194	2	14.1	20577	1.0	14	16439	0	48	15.8		13.83	[26]
98	390	190	190	3	20	24507	9.5	21.2	21678	0	43.7	19.2		22.69	[18]
99	390	190	190	3	20	24507	9.5	21.2	21678	0	43.7	23.3		17.92	[18]
100	397	143	194	2	15.4	21505	10.0	22.8	22755	0	44	11.66		16.71	[32]
101	190	190	190	3	25.7	27781	9.5	26.5	25155	0	43.7	25.5		21.60	[18]
102	390	190	190	2	18.7	23697	10.0	20.5	21198	1	44	16.31		13.39	[39]
103	390	140	190	3	23.2	26395	9.5	15.5	17593	0	53.2	21.43		25.44	[1]
104	397	94	194	2	26.1	27996	10.0	22.8	22755	0	26	20.69		27.50	[32]
105	397	194	192	3	24.2	26958	10.0	17.7	19221	0	48.4	18.6	5.4	24.61	[12]
106	390	240	190	2	23.8	26734	10.0	22.9	22821	1	44	24.75		19.12	[15]
107	397	94	194	2	17.2	22727	10.0	14.8	17059	0	26	13.8		17.90	[32]
108	397	101	194	2	21.2	25232	10.0	17.5	19076	0	26	15.1		22.40	[34]
109	397	92	194	2	23	26281	10.0	17.5	19076	0	26	19.1		16.15	[34]
110	397	194	194	3	35.1	32466	1.0	22.8	22755	0	48	24.2		34.74	[37]
111	190	190	190	3	25.7	27781	14.0	15.4	17517	0	43.7	20.6		16.31	[19]
112	397	143	194	2	24.6	27180	10	17.5	19076	0	43	18.1		24.86	[34]
113	195	190	190	2	24.3	27014	10.0	21.2	21678	0	43.7	26.0	1.5	23.65	[18]
114	390	143	194	3	21.3	25291	9.5	14.2	16595	0	31	19.4	1.5	20.52	[5]
115	397	194	194	2	27.7	28842	10.0	22.8	22755	0	46	22		28.15	[32]
116	390	140	190	3	24.9	27345	10.0	15.5	17593	0	53.2	12.0	4.8	15.59	[1]
117	195	140	190	3	23.6	26622	10.0	17.0	18711	1	47	23.8	3.6	16.21	[6]
118	390	190	190	4	34.8	32327	17.3	19.8	20712	1	44	29.3		36.56	[38]
119	390	143	194	3	22.0	25703	9.5	14.2	16595	0	30	18.0	1.7	12.29	[5]

Nr.	CMU						Mortar			Prism				FEM Pred (MPa)	Ref.
	l_{cu} (mm)	t_{cu} (mm)	h_{cu} (mm)	n	f_{cu} (MPa)	E_{cu} (MPa)	h_{mr} (mm)	f_{mr} (MPa)	E_{mr} (MPa)	Full:0 FS:1	Void (%)	f'_m (MPa)	COV (%)		
120	397	194	194	3	28	28997	3.5	21	21541	1	48	25.1		20.95	[4]
121	397	194	194	2	35.1	32466	2.0	22.8	22755	0	48	25.7		34.05	[37]
122	397	94	194	2	26.1	27996	10.0	14.8	17059	0	26	19.79		24.31	[32]
123	390	190	190	3	25.8	27835	10	12.7	15405	1	40	23.3	3	18.78	[11]
124	390	200	190	3	19.8	24384	9.5	15.6	17669	0	40	19.49		20.57	[31]
125	390	200	190	3	17.6	22990	9.5	15.6	17669	0	40	17.63		17.97	[31]
126	397	143	194	2	27.2	28580	10.0	17.5	19076	0	43	24.9		26.80	[34]
127	390	190	190	3	26.4	28157	10	12.7	15405	1	40	19.2	10	18.28	[11]
128	219	194	194	2	38	33781	1.0	14	16439	0	48	31		26.36	[26]
129	397	143	194	2	27.2	28580	10.0	17.5	19076	0	43	29.3		26.80	[34]
130	397	143	194	2	23.8	26734	10.0	14.8	17059	0	44	20.76		23.27	[32]
131	397	194	194	3	17.9	23185	4.0	17.7	19221	0	49.6	14.29		19.14	[12]
132	195	190	190	3	27.9	28946	10.0	17.0	18711	1	47	29.9	11.6	26.80	[6]
133	397	143	194	2	40.5	34875	10.0	17.5	19076	0	43	25.4		36.56	[34]
134	195	140	190	3	19.7	24323	9.5	16.7	18490	0	41	16		19.77	[5]
135	195	140	190	3	15.6	21644	9.5	14.2	16595	0	39	12.76		9.97	[5]
136	397	194	194	2	27.7	28842	10.0	14.8	17059	0	46	22.69		26.38	[32]
137	390	143	194	3	19.7	24323	9.5	12.8	15486	0	41	17.7	4.6	18.87	[5]
138	390	194	190	5	19.2	24012	16.5	18.8	20009	1	49	22.4		15.18	[7]
139	390	190	190	3	24.3	27014	10.0	15.4	17517	0	43.7	21.4	1.9	23.75	[18]
140	390	140	190	3	27	28475	9.5	19.9	20782	0	42	20.17		27.87	[25]
141	397	194	192	3	17.8	23120	10.0	17.7	19221	0	49.6	14.3	4.0	18.45	[12]
142	195	190	190	3	25.1	27455	10.0	17.0	18711	1	47	24.9	6.8	20.33	[6]
143	397	143	194	2	23.8	26734	10.0	22.8	22755	0	44	18.82		20.01	[32]
144	390	143	194	3	20.1	24568	9.5	14.2	16595	0	36	17.9	5.1	19.72	[5]
145	390	190	190	3	20	24507	14.0	15.4	17517	0	43.7	17.4		23.75	[19]
146	390	200	190	3	17.6	22990	9.5	15.6	17669	1	41	15.45		13.34	[31]
147	390	194	190	3	19.2	24012	9.5	18.8	20009	1	49	21.9		14.72	[7]
148	390	194	190	4	19.2	24012	17.3	18.8	20009	1	49	22.5		13.39	[7]
149	390	190	190	3	37.4	33513	9.5	16.3	18193	1	48.3	28.09		25.73	[24]
150	390	190	190	3	25.8	27835	10.0	13.8	16282	1	40	21.7	8	18.30	[11]
151	390	143	194	3	15.7	21714	9.5	14.2	16595	0	39	12.8	8.4	15.93	[5]

Experimental database with FE predictions (type N mortar)

Nr.	CMU						Mortar			Prism				FEM Pred (MPa)	Ref.
	l_{cu} (mm)	t_{cu} (mm)	h_{cu} (mm)	n	f_{cu} (MPa)	E_{cu} (MPa)	h_{mr} (mm)	f_{mr} (MPa)	E_{mr} (MPa)	Full:0 FS:1	Void (%)	f'_m (MPa)	COV (%)		
1	390	140	190	3	20.1	24568	9.5	9.4	12605	0	53.2	18.81		20.77	[1]
2	99	48	44	2	30.3	30165	10.0	6.76	10118	0	40	24.8	6.5	15.63	[13]
3	390	190	190	2	25.5	27673	10.0	8.4	11694	1	46.2	23.2	2.4	19.09	[2]
4	390	190	190	3	27.8	28894	9.5	10.6	13656	1	48	23		21.51	[40]
5	390	190	190	4	25.5	27673	10.0	8.4	11694	1	46.2	19.1	1.6	18.17	[2]
6	195	140	190	3	19.7	24323	9.5	5.7	9030	0	41	15.38		13.14	[5]
7	390	190	190	3	26.7	28316	9.5	11.4	14335	1	48.3	21.67		20.92	[24]
8	390	140	190	3	12.5	19375	9.5	7.7	11035	0	42	8		7.08	[35]
9	390	200	190	3	13.5	20135	9.5	12.2	14998	1	41	11.02		14.56	[31]
10	219	194	194	2	14.1	20577	1.0	6.7	10058	0	48	15.4		15.62	[26]
11	400	200	195	2	18.9	23824	10.0	7.6	10939	1	50.8	16.8	11.3	13.42	[28]
12	390	200	190	3	19.8	24384	10	5.0	8275	1	46.2	11.9	13.8	11.77	[31]
13	390	140	190	2	20.5	24812	10.0	6.6	9957	1	38	14.8		13.14	[22]
14	390	190	190	3	26.4	28157	10.0	7.8	11131	1	40	17.4	2	17.36	[11]
15	390	200	190	3	13.5	20135	9.5	5	8275	1	41	10.43		9.21	[31]
16	390	200	190	3	13.5	20135	10.0	12.2	14998	1	46.2	8.1	14.4	11.69	[31]
17	390	190	190	3	26.7	28316	9.5	6.9	10257	1	48.3	21.56		17.58	[24]
18	390	190	190	3	23.2	26395	9.5	7.6	10939	1	44	26.15		15.63	[36]
19	390	190	190	2	25.5	27673	10.0	8.4	11694	1	46.2	22.8	4.4	18.33	[2]
20	390	200	190	3	13.5	20135	10.0	5.0	8275	0	41.5	8.7	17.0	11.14	[31]
21	390	190	190	2	32.0	31000	10.0	8.4	11694	1	46.2	25.0	4.1	19.09	[2]
22	390	190	190	3	25.8	27835	10.0	7.4	10747	1	40	20.2	9	17.00	[11]
23	219	194	194	2	20.8	24993	1.0	9.1	12335	0	48	23		22.99	[26]
24	390	190	190	4	25.3	27564	9.7	8.4	11694	1	46.2	19.6		18.71	[2]
25	219	194	194	2	38	33781	1.0	9.1	12335	0	48	29.2		28.07	[26]
26	397	143	194	2	24.6	27180	10.0	10.4	13484	0	43	18.2		25.36	[34]
27	397	194	194	2	22	25703	10.0	6.6	9957	1	45	13.9		15.09	[20]
28	390	190	190	5	27.8	28894	10.0	10.6	13656	1	48	22.3		20.31	[40]
29	178	143	194	3	19.7	24323	9.5	5.7	9030	0	41	15.4	5.5	15.88	[5]
30	99	48	44	2	20.8	24993	10.0	6.76	10118	0	40	15.5	5.4	13.16	[13]
31	390	200	190	3	13.5	20135	9.5	5	8275	0	40	11.21		12.16	[31]
32	390	200	190	3	19.8	24384	10.0	12.2	14998	0	41.5	13.2	10.3	15.20	[31]
33	390	140	190	2	21.4	25351	10.0	6.6	9957	1	44	14.7	4.8	13.60	[20]
34	390	140	190	2	20.5	24812	10.0	6.6	9957	1	38	16		14.58	[22]
35	390	200	190	3	19.8	24384	9.5	12.2	14998	1	41	17.2		19.84	[31]
36	390	140	190	3	35.5	32651	9.5	7.1	10454	1	42	23.56		22.04	[35]
37	390	190	190	3	37.4	33513	9.5	8.1	11414	1	48.3	22.01		24.24	[24]
38	390	190	190	2	21.5	25410	10.0	8.4	11694	1	46.2	16.1	4.2	16.34	[2]

Nr.	CMU						Mortar			Prism				FEM Pred (MPa)	Ref.
	l_{cu} (mm)	t_{cu} (mm)	h_{cu} (mm)	n	f_{cu} (MPa)	E_{cu} (MPa)	h_{mr} (mm)	f_{mr} (MPa)	E_{mr} (MPa)	Full:0 FS:1	Void (%)	f'_m (MPa)	COV (%)		
39	397	194	194	3	22	25703	10.0	6.6	9957	1	45	14.5		14.55	[20]
40	390	190	190	4	25.5	27673	9.7	8.4	11694	1	46.2	19.1		18.84	[2]
41	390	190	190	3	27.8	28894	9.5	10.6	13656	1	48	24.4		21.51	[40]
42	390	200	190	3	17.6	22990	10.0	12.2	14998	0	41.5	11.1	18.1	14.21	[31]
43	390	190	190	3	27.8	28894	10.0	10.6	13656	1	48	23.0	10.0	21.93	[40]
44	397	194	194	3	17.9	23185	4.0	11.9	14751	0	49.6	13.58		15.20	[12]
45	390	190	190	5	27.8	28894	10.0	10.6	13656	1	48	22.3	10.0	20.31	[40]
46	219	194	194	2	38	33781	1.0	10.8	13827	0	48	27.5		34.87	[26]
47	390	200	190	3	10.9	18092	9.5	5	8275	1	41	8.19		7.67	[31]
48	390	140	190	2	20.5	24812	10.0	6.6	9957	1	38	15.3		13.14	[22]
49	390	190	190	4	32.0	31000	10	8.4	11694	1	46.2	19.0	8.4	20.66	[2]
50	397	194	194	3	17.9	23185	4.0	11.9	14751	1	49.6	14		15.24	[12]
51	390	190	190	3	18.3	23443	9.5	11.7	14585	1	48	16.21		15.28	[16]
52	390	190	190	2	25.3	27564	18.0	8.4	11694	1	46.2	21.1		17.13	[2]
53	390	190	190	3	27.8	28894	10.0	10.6	13656	1	48	26.0	1.0	21.93	[40]
54	219	194	194	2	38	33781	1.0	6.7	10058	0	48	28.1		27.39	[26]
55	390	140	190	3	14.4	20795	9.5	7.9	11225	1	42	12.2		9.08	[35]
56	397	140	188	4	21.4	25351	10.0	6.6	9957	1	44	13.9		13.77	[20]
57	390	190	190	3	27.8	28894	10.0	10.6	13656	1	48	24.3	2.0	21.93	[40]
58	390	190	190	3	36.2	32971	10.0	7.4	10747	1	40	22.0	9	23.17	[11]
59	390	200	190	3	17.6	22990	9.5	5	8275	0	40	14.39		15.16	[31]
60	219	194	194	2	23.3	26452	1.0	10.8	13827	0	48	20.8		25.87	[26]
61	390	190	190	3	37.4	33513	9.5	12.1	14916	1	48.3	24.44		28.57	[24]
62	390	190	190	2	22.0	25703	10.0	6.6	9957	1	45	14.9	3.6	15.21	[20]
63	390	200	190	3	17.6	22990	10	5.0	8275	1	46.2	9.9	9.9	11.65	[31]
64	390	190	190	2	25.5	27673	18.0	8.4	11694	1	46.2	22.8		19.13	[2]
65	390	190	190	4	32	31000	9.7	8.4	11694	1	46.2	19		22.99	[2]
66	390	190	190	3	27.8	28894	9.5	10.6	13656	1	48	23.8		21.51	[40]
67	390	140	190	3	14.4	20795	10.0	7.9	11225	1	42	12.2	10.0	9.76	[35]
68	390	190	190	2	32	31000	18.0	8.4	11694	1	46.2	25		19.74	[2]
69	390	140	190	3	20	24507	9.5	7.7	11035	0	53.2	17.86		17.68	[1]
70	390	190	190	3	27.8	28894	9.5	10.6	13656	1	48	26		21.51	[40]
71	390	200	190	3	19.8	24384	10	5.0	8275	0	41.5	11.9	7.7	13.67	[31]
72	390	190	190	2	25.3	27564	10.0	8.4	11694	1	46.2	22.9	1.8	18.64	[2]
73	400	197	197	6	25.7	27781	10.0	11.1	14082	0	37	15.32		19.28	[33]
74	397	194	194	5	22	25703	10.0	6.6	9957	1	45	14.3		13.83	[20]
75	390	200	190	3	10.9	18092	10.0	5.0	8275	1	46.2	6.0	25.1	7.25	[31]
76	397	140	188	2	21.4	25351	10.0	6.6	9957	1	44	14.7		13.83	[20]
77	390	190	190	3	36.2	32971	10.0	7.8	11131	1	40	27.6	7	23.32	[11]
78	390	190	190	3	27.3	28633	9.5	7.87	11197	1	48.3	14.89		17.97	[24]
79	397	194	194	2	22	25703	10.0	6.6	9957	1	45	14.9		17.28	[20]

Nr.	CMU						Mortar			Prism				FEM Pred (MPa)	Ref.
	l_{cu} (mm)	t_{cu} (mm)	h_{cu} (mm)	n	f_{cu} (MPa)	E_{cu} (MPa)	h_{mr} (mm)	f_{mr} (MPa)	E_{mr} (MPa)	Full:0 FS:1	Void (%)	f'_m (MPa)	COV (%)		
80	390	190	190	2	25.3	27564	18.0	8.4	11694	1	46.2	22.9		18.95	[2]
81	390	200	190	3	10.9	18092	9.5	5	8275	0	40	11.14		10.04	[10]
82	390	190	190	3	27.3	28633	9.5	8.7	11971	1	48.3	17.42		21.16	[24]
83	219	194	194	2	35	32420	1.0	9.1	12335	0	48	23.7		28.96	[26]
84	400	200	195	2	18.9	23824	10.0	7.6	10939	1	50.8	16.8	11.3	13.20	[28]
85	390	190	190	3	26.7	28316	9.5	7.9	11225	1	48.3	20.17		17.67	[24]
86	219	194	194	2	17.7	23055	1.0	9.1	12335	0	48	18.6		19.81	[26]
87	390	140	190	3	20.7	24932	9.5	9.8	12960	1	42	17.23		16.77	[35]
88	390	200	190	3	13.5	20135	10.0	5.0	8275	1	46.2	7.7	14.9	6.25	[31]
89	397	194	192	3	17.8	23120	10.0	11.9	14751	0	49.6	13.6	3.1	19.32	[12]
90	400	200	195	2	18.9	23824	10.0	7.6	10939	1	50.8	16.8	11.3	13.20	[28]
91	390	200	190	3	13.5	20135	9.5	12.2	14998	0	40	13.48		13.03	[31]
92	390	200	190	3	19.8	24384	9.5	5	8275	0	40	14.42		16.88	[31]
93	390	190	190	3	23.2	26395	9.5	7.6	10939	1	44	20.49		15.63	[36]
94	390	190	190	3	24.3	27014	10.0	9.2	12425	0	43.7	17.8	6.2	19.30	[18]
95	219	194	194	2	23.3	26452	1.0	9.1	12335	0	48	20.5		25.93	[26]
96	390	200	190	3	19.8	24384	9.5	5	8275	1	41	16.18		13.22	[31]
97	390	190	190	4	25.3	27564	10.0	8.4	11694	1	46.2	19.6	3.0	15.87	[2]
98	390	190	190	3	18.3	23443	9.5	11.7	14585	1	48	17.35		15.28	[16]
99	390	140	190	3	35.5	32651	10.0	7.1	10454	1	42	23.6	10.0	22.48	[35]
100	390	190	190	5	22.0	25703	10.0	6.6	9957	1	45	14.3	3.9	13.79	[20]
101	390	190	190	3	18.3	23443	9.5	11.7	14585	1	48	16.31		15.45	[16]
102	390	140	190	2	22.3	25878	10.0	5.7	9030	1	40.4	12.5		13.93	[21]
103	390	140	190	2	20.5	24812	10.0	6.6	9957	1	38	15.2		13.14	[22]
104	390	190	190	3	11.6	18664	9.5	7.6	10939	1	44	14.77		13.06	[36]
105	397	194	194	3	24.2	26958	4.0	11.9	14751	1	48.4	18.63		20.19	[12]
106	390	190	190	3	27.8	28894	9.5	10.6	13656	1	48	24.3		21.51	[40]
107	390	190	190	3	27.8	28894	9.5	10.6	13656	1	48	23.7		21.51	[40]
108	390	140	190	3	27.4	28685	9.5	5.6	8924	0	42	15.73		22.62	[9]
109	390	190	190	3	26.4	28157	10.0	7.4	10747	1	40	14.9	7	15.09	[11]
110	390	190	190	4	25.5	27673	10.0	8.4	11694	1	46.2	18.8	4.8	16.85	[2]
111	390	200	190	3	19.8	24384	10.0	12.2	14998	1	46.2	12.6	13.6	16.40	[31]
112	390	200	190	3	17.6	22990	10.0	12.2	14998	1	46.2	10.5	9.4	14.92	[31]
113	400	197	197	6	45.8	37086	10.0	11.1	14082	0	37	26.53		30.55	[33]
114	390	140	190	3	24.1	26902	9.5	7.4	10747	0	42	17.89		18.90	[35]
115	390	190	190	3	15.0	21224	10.0	12.4	15161	1	40	10.3	12.6	11.74	[30]
116	390	140	190	2	22.3	25878	10.0	5.7	9030	0	40.4	12.3		18.90	[21]
117	390	190	190	3	25.8	27835	10.0	7.8	11131	1	40	21.6	10.0	17.34	[11]
118	390	190	190	4	21.5	25410	9.7	8.4	11694	1	46.2	15.5		16.28	[2]
119	390	190	190	3	37.4	33513	9.5	7.8	11131	1	48.3	26.31		24.19	[24]
120	390	190	189	3	14.2	20650	10.0	9.2	12425	0	43.7	17.8	6.2	15.49	[19]

Nr.	CMU						Mortar			Prism				FEM Pred (MPa)	Ref.
	l_{cu} (mm)	t_{cu} (mm)	h_{cu} (mm)	n	f_{cu} (MPa)	E_{cu} (MPa)	h_{mr} (mm)	f_{mr} (MPa)	E_{mr} (MPa)	Full:0 FS:1	Void (%)	f'_m (MPa)	COV (%)		
121	390	190	190	4	21.5	25410	10	8.4	11694	1	46.2	15.5	6.4	16.54	[2]
122	219	194	194	2	23.3	26452	1.0	6.7	10058	0	48	17.2		18.41	[26]
123	390	200	190	3	19.8	24384	9.5	12.2	14998	0	40	18.41		16.25	[31]
124	390	190	190	2	13.9	20431	209.0	10.5	13570	0	44	11.74		12.75	[27]
125	390	140	190	2	22.3	25878	10.0	5.7	9030	1	40.4	12.5		13.93	[21]
126	219	194	194	2	28.3	29152	1.0	9.1	12335	0	48	23.5		27.18	[26]
127	219	194	194	2	31.1	30561	1.0	9.1	12335	0	48	23.8		27.15	[26]
128	390	200	190	3	10.9	18092	10.0	5.0	8275	0	41.5	7.2	10.4	8.13	[31]
129	390	190	190	3	20	24507	9.5	9.2	12425	0	43.7	17.8		20.67	[18]
130	390	140	190	3	21.4	25351	10.0	6.6	9957	1	44	14.3	3.0	13.33	[20]
131	390	140	190	3	22.8	26167	10.0	9.4	12605	0	53.2	10.2	1.9	15.90	[1]
132	397	140	188	3	21.4	25351	10.0	6.6	9957	0	44	14.3		18.77	[20]
133	390	140	190	3	20.7	24932	10.0	9.8	12960	1	42	17.2	10.0	16.93	[35]
134	390	190	190	3	11.6	18664	9.5	7.6	10939	1	44	16.57		15.02	[36]
135	390	190	190	3	20	24507	14.0	9.2	12425	0	43.7	17.8		19.67	[19]
136	390	190	190	3	22.0	25703	10.0	6.6	9957	1	45	14.5	5.4	14.76	[20]
137	390	200	190	3	13.5	20135	10.0	12.2	14998	0	41.5	9.1	10.7	12.29	[31]
138	390	200	190	3	17.6	22990	9.5	12.3	15080	0	40	16.9		20.84	[31]
139	390	190	190	2	21.5	25410	18.0	8.4	11694	1	46.2	16.1		16.96	[2]
140	390	140	190	4	21.4	25351	10.0	6.6	9957	1	44	13.9	4.3	12.37	[20]
141	390	190	190	2	25.3	27564	10.0	8.4	11694	1	46.2	21.1	3.7	16.49	[2]
142	390	140	190	3	18.6	23634	10.0	7.7	11035	0	53.2	10.0	3.7	9.00	[1]
143	390	140	190	3	18.2	23378	9.5	8.63	11907	0	42	14.82		19.01	[25]
144	397	194	194	2	22	25703	10.0	6.6	9957	0	45	12.6		19.30	[20]
145	390	190	190	2	25.5	27673	18.0	8.4	11694	1	46.2	23.2		19.09	[2]
146	390	190	190	3	27.8	28894	10.0	10.6	13656	1	48	23.8	4.0	21.93	[40]
147	397	194	192	3	17.8	23120	10.0	11.9	14751	1	49.6	10.3	4.2	15.02	[12]
148	390	200	190	3	17.6	22990	9.5	5	8275	1	41	13.4		11.67	[31]
149	390	190	190	5	27.8	28894	10.0	10.6	13656	1	48	22.2		20.31	[40]
150	390	200	190	3	17.6	22990	9.5	12.2	14998	1	41	14.33		12.98	[31]
151	390	190	190	4	25.5	27673	9.7	8.4	11694	1	46.2	18.8		18.84	[2]
152	390	190	190	3	27.8	28894	10.0	10.6	13656	1	48	24.4	2.0	21.93	[40]
153	390	140	190	3	33.5	31718	9.5	7.8	11131	0	42	22.04		20.46	[35]
154	397	194	192	3	24.2	26958	10.0	11.9	14751	1	48.4	13.7	4.9	19.23	[12]
155	390	200	190	3	17.6	22990	10	5.0	8275	0	41.5	10.1	11.4	13.06	[31]
156	219	194	194	2	14.1	20577	1.0	9.1	12335	0	48	17		15.78	[26]
157	400	200	200	2	18.9	23824	0.0	7.6	10939	1	50.8	16.8		13.20	[28]
158	390	190	190	3	27.8	28894	10.0	10.6	13656	1	48	23.7	10.0	21.93	[40]
159	390	190	190	5	27.8	28894	10.0	10.6	13656	1	48	22.2	10.0	20.31	[40]
160	219	194	194	2	14.1	20577	1.0	10.8	13827	0	48	14.7		15.84	[26]
161	390	190	190	3	18.3	23443	9.5	11.7	14585	1	48	17.88		15.28	[16]

[1] Barbosa, C.; Lourenço, P. B. and Hanai, J. B. (2009). “On the compressive strength prediction for concrete masonry prisms.” Mater Struct, 43, 331–344 (2010).

[2] Chahine, G. N., & Drysdale, R. G. (1989). Influence of Test Conditions on the Compressive Strength and Behaviour of Face Shell Mortar bedded Concrete Block Prisms. 5Th Canadian Masonry Symposium, Vancouver, B.C., Canada. 2 651-660.

[3] Cheema, T. S. and Klingner, R. E. (1984). “Compressive strength of concrete masonry prisms.” American Concrete Institute Journal. 1984, Nov./Dec., 88-97.

[4] Das S, Liu J, El Sayed M, Sturgeon G. Effect of height-to-thickness ratio on compressive strength of hollow concrete masonry. In: 12th Canadian masonry symposium, Vancouver, BC; 2013

[5] Drysdale RG, Hamid AA. Behavior of concrete block masonry under axial compression. ACI J 1979;76(6):707–21.

[6] Drysdale RG, Hamid AA. Capacity of concrete block masonry prisms under eccentric compressive loading. ACI J 1983;80(2):102–8.

[7] Wong HE, Drysdale RG. “Compression characteristics of concrete block masonry prisms.” Masonry, research, application, and problems. ASTM STP 871; 1985. p. 167–177.

[8] Duncan, L. J. (2008). Effect of Block Face Shell Geometry and Grouting on the Compressive Strength of Concrete Block Masonry. MSc. Thesis to the Faculty of Graduate Studies, University of Windsor.

[9] Fonseca, F. S., Roman, H. R., Mohamad, G., Mendes, R. J. K., and Romagna, R. H. (2014). “Compressive capacity and behaviour of concrete and ceramic masonry prisms.” 9th International Masonry Conference, Guimarães 2014.

[10] Ganesan, T. P. and Ramamurthy, K. (1992). “Behaviour of concrete hollow-block masonry prisms under axial compression.” *J. Struct. Eng.*, 1992, 118(7): 1751-1769.

[11] Gayed M, Korany Y. Concrete compressive strength using the unit strength method. Masonry chair report No. 102, May 2011. 22pp.

[12] Gaynor, P., Woodward, K., Scribner, C. (1987). Influence of Mortar Bedding on Masonry Prism Behavior. U.S. Department of Commernce, National Bureau of Standards, Report NBSIR 86-3467.

[13] Hamid, A. A., & Abboud, B. E. (1986). Effect of Block Geometry on the Compressive Strength of Concrete Block Masonry. 4th Canadian Masonry Symposium, University of New Brunswick, 1 290-298.

[14] Hamid, A.A., Drysdale, R.G., Heidebrecht, A.C. (1978). Effect of Grouting on the Strength Characteristics of Concrete Block Masonry. Proceedings of the North American Masonry Conference, Boulder, Colorado, 11-1 to 11-17.

[15] Hawk SW, Mclean DL, Young TC. Compressive behavior of insulated concrete masonry prisms. TMS J 1997;15(2):53–60.

[16] Hegmier GA, Krishnmoorthy G, Nunn RO, Moorthy TV. Prism tests for the compressive strength of concrete masonry. Report No. AMES-NSF-77-1, University of California, San Diego; 1977. 100pp.

[17] Hou, J. (2006). Strain Gradient Effect on the Behaviour and Strength of Masonry Prisms. Master of Applied Science, Dalhousie University.

[18] Khalaf FM. Factors influencing compressive strength of concrete masonry prisms. Mag Concr Res 1996;48(175):95–101.

[19] Khalaf FM, Hendry AW, Fairbairn DR. Study of the compressive strength of blockwork masonry. ACI Struct J 1994;91(4):367–76.

[20] Maurenbrecher AHP. Effect of test procedures on compressive strength of masonry prisms. In: Proceedings, 2nd Canadian masonry symposium, Carleton University, Ottawa, June 1980. p. 119–32.

[21] Mauenbrecher, A.H.P. (1983). Compressive Strength of Eccentrically Loaded Masonry Prisms. Third Canadian Masonry Symposium. Edmonton, Alberta, Canada, 10-1 to 10-13.

[22] Maurenbrecher AHP. Axial compression tests on masonry walls and prisms. In: Third North American masonry conference, University of Texas at Arlington; 1985. p. 1901–14.

[23] Maurenbrecher AHP. Compressive strength of hollow concrete blockwork. In: 4Th Canadian masonry symposium, Fredericton, NB, Canada;1986. p. 997–1009.

[24] Gayed M, Korany Y, Sturgeon G. Examination of the prescribed concrete block masonry compressive strengths in the Canadian masonry design standard, CSA S304.1-2004. In: 15th International brick and block masonry conference, Florianopolis, Brazil; 2012.

[25] Mohamad G, Lourenco PB, Humberto Roman R. Mechanics of hollow concrete block masonry prisms under compression: review and prospects. Cem Concr Compos 2007;29(3):181–92.

[26] National Concrete Masonry Association. Recalibration of the unit strength method for verifying compliance with the specified compressive strength of concrete masonry. Report No. MR37; 2012. 98pp.

[27] Olatunji TM, Warwaruk J, Longworth J. Behaviour and strength of masonry wall/slab joints. Report No. 139, University of Alberta; 1986. 228pp.

[28] Page AW, Shrive NG. Concentrated loads on hollow concrete masonry. ACI Struct J 1990;87(4):436–44.

[29] Page, A. W. and Kleeman, P. W. (1991). "A Study of the Compressive Behaviour of Hollow Masonry", Research Report No. 060.02.1991, Department of Civil Engineering and Surveying, The University of Newcastle, April 1991.

[30] Paturova, A. (2006). The Influence of Vertical Reinforcement and Lateral Confinement on the Axial Capacity of Masonry Block Walls. MSc. Thesis to the Faculty of Graduate Studies, University of Saskatchewan.

[31] Ramamurthy, K., Sathish, V., & Ambalavanan, R. (2000). Compressive Strength Prediction of Hollow Concrete Block Masonry Prisms. ACI Structural Journal, 97(1), 61-67.

[32] Redmond TB, Allen MH. Compressive strength of composite brick and concrete masonry walls. Masonry: past and present. ASTM STP 589; 1975. p. 195–232.

[33] Richart FE, Moorman RB, Woodworth PM. Strength and stability of concrete masonry walls. University of Illinois, Bulletin 251; 1932. 38pp

[34] Roberts JJ. The effect of different test procedures upon the indicated strength of concrete blocks in compression. Mag Concr Res 1973;25(83):87–98.

[35] Romagna RH, Roman HR. Compressive strength of grouted and ungrouted concrete block masonry. Proc Br Masonry Soc 2002;9:399–404.

[36] Scrivener JC, Baker LR. Factors influencing grouted masonry prism compressive strength. Brick Block Masonry 1988;2:874–83.

[37] Self MW. Structural properties of load bearing concrete masonry. Masonry: past and present. ASTM STP 589; 1975. p. 233–54.

[38] Steadman M, Drysdale RG, Khattab MM. Influence of block geometry and grout type on compressive strength of block masonry. In: 7th Canadian masonry symposium, Hamilton, Canada, June 1995. p. 1116–27.

[39] Thomas RD, Scolforo MJ. Evaluation of the compressive strength of masonry by prism sampling. TMS J 1995;13(2):56–67.

[40] Xie H, Page AW, Kleeman PW. An investigation of the compressive failure mechanism for face-shell bedded hollow masonry. In: 6th Canadian masonry symposium, Saskatoon, SK, Canada; 1992. p. 97–108.

APPENDIX B – AUTOMATIC PRISM GENERATOR INSTRUCTION

Procedures to construct multiple prisms (contact the author to request the files):

1. Save the attached 7 files including 4 .py files, two .txt files and one .xlxs file in one same folder.
2. Open each of the .py files using NotePad (or whatever software prefered) and change file_path to the folder path where all the files are saved.
3. Also change the text saving path in "Compression_Hardening_Generation.py" to the folder path where all the files are saved.
4. Open "Input_Variables_Defination.xlsx" file, input all the parameters following the headers provided. Each row represents a single model.
5. After done with all the input, copy all the input data (do not copy the headers) to "Input_Variables.txt" file. Select all the existing content and replace them.
6. Save and close "Input_Variables.txt" file. The file can also be left opened but save it after all the data is pasted.
7. Then, generate the compression hardening curves for both unit and mortar. Open "Compression_Hardening_Generation.py" file in whatever python environment preferred, run it and 4 text files under the same path as before: "CDP_PE.txt", "CDP_PE_m.txt", "CDP_PS.txt", "CDP_PS_m.txt" should be generated.
8. Open Abaqus and click on "run script" tab, go to the path where all the files are saved and run "Prism_Generation.py" file.
9. Abaqus should be able to generate all the models defined and the related jobs.

10. Check all the models, go run "Submit_Jobs.py" file also using "run script" if everything went as expected. All the jobs will be submitted and run one by one till finished (maybe overnight or longer).
11. Once all the models are finished running, run the "Strain_Stress_Extraction.py" scripts. These scripts create Excel files in the "temp" folder.